Modulation of Human Small Heat Shock Proteins via Changes in Quasi-ordered Networks of Interactions

Christopher N. Woods

A dissertation

submitted in partial fulfillment of the

requirements for the degree of

Doctor of Philosophy

University of Washington

2022

Reading Committee:

Rachel Klevit, Chair

Abhinav Nath

Dana Miller

Program Authorized to Offer Degree:

Biochemistry

University of Washington

Abstract

Modulation of Human Small Heat Shock Proteins via Changes in Quasi-ordered Networks of Interactions

Christopher N. Woods

Chair of the Supervisory Committee:
Rachel Klevit
Department of Biochemistry

Small heat shock proteins (sHSPs) are molecular chaperones found in all domains of life that directly interact with client proteins to maintain them in a soluble and functional state. sHSPs are among the earliest responders to cellular stress events associated with client destabilization, and failure to fully or properly respond leads to client protein aggregation. Protein aggregation is a hallmark of several known disease states, including fibrillar aggregation associated with neurodegenerative diseases and amorphous aggregation in the eye lens that causes cataract. sHSPs are finely tuned to the cellular environment and are modulated by conditions that are associated with stress, such as pH acidosis or change in redox state. While we understand that modulation of sHSPs' chaperone activity and expression level occurs, the molecular details that underlie mechanisms of chaperone activity remain enigmatic, largely because sHSPs' properties defy conventional structural analysis. Recent development of new methods and experimental approaches are beginning to shed light on this crucially important, yet poorly understood family of chaperones. This dissertation reveals how primary sequence changes in the two most highly-

related human sHSPs, HSPB4 and HSPB5, affect their structure and dynamics, interactions, and ability to delay aggregation of lens client γD-crystallin. Chapter 2 reveals the molecular changes caused by two single-site mutations in HSPB5 that are associated with autosomal dominant inheritance of cataract and myopathy in human patients. Chapter 3 describes how sequence differences in the N-terminal region of human HSPB4 and HSPB5 affects their structure, dynamics, interactions, and ability to productively interact with γD-crystallin.

TABLE OF CONTENTS

LIST OF FIGURES

ACKNOWLEDGEMENTS

I have been lucky to meet many scientists, without whom, this work would not have been possible. First, I want to thank my mentor Rachel Klevit for her years of support. She has always pushed me to improve myself and has been a constant source of inspiration. Whenever I had new data or ideas, Rachel was there to share in the journey and provide useful feedback. I feel fortunate to have joined Rachel's group, as I have met many great individuals over the years. I especially want to thank Amanda Clouser for encouraging me to study small heat shock proteins. All members of the small heat shock protein sub-group have contributed to my development, and I want to thank Hannah Baughman, Scott Delbecq, Natalie Stone, Maria Janowska, and Ponni Rajagopal for being great teammates. I also want to thank my thesis committee members, Abhinav Nath, David Veesler, Dana Miller, and Matt Bush for their advice, as well as my undergraduate mentor at the University of Wisconsin - La Crosse, Todd Weaver, for giving me the opportunity to work in his group, allowing my excitement for protein science to flourish. Without him, I would not be here today. Finally, thank you to Miklos Guttman, Edgar Hodge, Mark Benhaim, and Michael Watson for their assistance with HDX-MS studies.

My education has benefited tremendously from being a part of the Biological Physics, Structure and Design Ph.D. program and the Molecular Biophysics Training Program. Both affiliations have exposed me to diverse research from departments across the University of Washington, and this has inspired some of my own approaches that have advanced the small heat shock protein field.

Finally, thank you to my family and friends for always supporting and encouraging me along the way.

Chapter 1. INTRODUCTION

1.1 PROTEIN CHAPERONES IN HUMAN HEALTH AND DISEASE

All cell types that make up the human body require precise cellular conditions for healthy functioning. These conditions are maintained through regulated processes collectively called homeostasis (Billman, 2020). Maintenance of proteins, the molecular machines of the cell, is carried out through a process called protein homeostasis and has important implications in human health and disease (Goloubinof, 2016). Proteins are exquisitely sensitive to small changes in cellular conditions typically associated with stress, such as pH acidification and changes in redox state, and can aggregate or become dysfunctional under these conditions (Goloubinof, 2016). One method that cells employ for protein homeostasis is the expression of molecular chaperone proteins that directly interact with "client" proteins under normal and stress-associated cellular conditions to promote their proper functioning (Goloubinof, 2016). The role of chaperones in preventing aggregation in the cell under stress-associated conditions is well appreciated, while the significance of chaperone-client interactions under normal conditions is not as well understood (Jolly, 2000; Ma and Hendershot, 2004; Voth and Jakob, 2017).

Multiple types of chaperones co-exist within the cell and function as a network to maintain destabilized and/or misfolded clients in a soluble state for refolding or degradation (Rosenzweig et al., 2019; Reinle et al., 2022). Among the earliest chaperone responders to cellular stress events are small heat shock proteins (sHSPs), which form dynamic ensembles of oligomers that directly interact with client proteins and are the focus of this work. All tissue types express sHSPs, and they are especially abundant in neurons, eye lens, and myocytes (Carra et al., 2017). sHSPs' chaperone activity has been colloquially described as "holdase", as they possess no ability to refold

destabilized clients and instead hold them in a refolding-competent state (Delbecq and Klevit, 2013). Molecular chaperones from the Hsp70 and Hsp100 families accept misfolded clients from sHSPs and use energy gained from ATP hydrolysis to attempt to refold them (Żwirowski et al., 2017; Ungelenk et al., 2016). If refolding is unsuccessful, clients will generally be degraded through the ubiquitin proteasome system or lysosome-autophagy pathway and replaced via *de novo* protein synthesis (Takalo et al., 2013; Lamark and Johansen, 2012; Ciechanover and Kwon, 2015). While degradation pathways exist in most cell types, proteinaceous aggregates do form and persist within cells and tissues, and this has implications for human health.

Failure of chaperones to prevent aggregation is associated with various types of diseases in humans. Two prominent examples with high incidence include aggregation of proteins in the brain associated with neurodegeneration and aggregation of proteins in the eye lens called cataract, causing blindness. sHSPs interact with client proteins in both of these tissues and are expected to play an important role in disease outcomes (Webster et al., 2019; Clark et al., 2012). Interactions between sHSPs and neuronal clients are among the most well studied, as clients tau, amyloid beta, and α-synuclein aggregate readily under relevant conditions on timescales that are experimentally tractable (Baughman et al., 2018; Hochberg et al., 2014; Scheidt et al., 2021). In contrast, wild-type (WT) lens clients are highly stable and only aggregate when exposed to high temperatures (i.e. 50-60 °C; Horwitz, 1992). The work presented in this thesis uses a newly-developed assay to reveal how two human sHSPs found in eye lens, HSPB4 and HSPB5 (αA-crystallin and αB-crystallin), interact with lens client γD-crystallin, a protein found in cataractous aggregates.

1.2 CATARACT BLINDNESS AND THE ROLE OF SMALL HEAT SHOCK PROTEINS

Cataract is a leading cause of blindness worldwide and is caused by protein aggregation in the eye lens (Hashemi et al., 2020). Cataractous aggregates scatter light, preventing it from reaching

the retina (Shiels and Heitmancik, 2019). Cataracts can be age- or disease-related or caused by environmental exposure, and risk of cataract development can be genetically inherited (Shiels and Heitmancik, 2019). Regardless of the mechanism of onset, the varieties of cataract are similar in protein aggregate composition (Schmid et al., 2021; Su et al., 2011; Ueda et al., 2002; MacCoss et al., 2002). The eye lens is a unique tissue, composed primarily of eye lens fiber cells that express very high concentrations of proteins (300+ mg/mL; Bloemendal et al., 2004; Takemoto and Sorensen, 2008). Lens proteins have abnormally high dN/dC values (change in refractive index with concentration), meaning they bend incident light more strongly than most proteins, and there is a refractive index gradient from the nucleus to the cortex of the lens that helps focus light on the retina (Vérétout and Tardieu, 1989). Clearance of all organelles in lens fiber cells during development further allows proper light transmission to the retina for clear vision by reducing light scattering (Bassnett, 2002; Moreau and King, 2012b; Bassnett, 2009). The consequence of organelle clearance is that all but the youngest lens fiber cells lack the ability to synthesize new proteins (Lynnerup et al., 2008). This means that the lens proteins an individual is born with must remain properly folded and functional throughout a lifetime (~80 years), while most proteins in other cell types have half-lives of hours to days (Chen et al., 2016; Pierce et al., 2010). The eye lens is nearly constantly exposed to light, including high energy forms that can damage and modify proteins (Lampi et al., 2014). Many modifications have been described which destabilize lens proteins and can influence their stability and aggregation, and the effect is cumulative over a lifetime (Michiel et al., 2010; Srivastava et al., 2017). It is believed that age-related modifications contribute to cataract formation in otherwise healthy individuals (Bloemendal et al., 2004). To our current knowledge, the primary mechanism used to prevent protein aggregation in lens is high

expression of molecular chaperones from the sHSP family (HSPB4 and HSPB5; ~150 mg/mL in total).

As in other tissues, HSPB4 and HSPB5 interact directly with client proteins in lens to prevent their aggregation. HSPB4 and HSPB5 form mixed oligomeric assemblies in the eye lens in a 3:1 ratio and are considered a single entity (α-crystallin; Horwitz et al., 1999). This ratio has been shown to be optimal for stabilizing the assembly from temperature-induced structural changes in vitro (Horwitz et al., 1999). Both HSPB4 and HSPB5 are expressed outside the lens, but high expression of HSPB4 is limited to lens, while HSPB5 is also expressed in high abundance in muscle tissue and neurons (Bartelt-Kirbach et al., 2017; Dimauro et al., 2018). Lens is the only tissue where both HSPB4 and HSPB5 are both expressed in high abundance and, outside of the lens, HSPB5 can form mixed oligomers with other sHSPs (Mymrikov et al., 2020; Zantema et al., 1992; Kato et al., 1992). It should be noted that the pH of the eye lens is neutral to mildly acidic, and these conditions are associated with heightened chaperone activity of HSPB5 *in vitro* (Rajagopal et al., 2015). Outside of lens, pH values are slightly above neutral and can become mildly acidic during cellular stress events, so HSPB5 experiences a range of pH conditions depending on cellular context (Chesler, 2003; Street et al., 2001). Importantly, age-related photodamage in lens also directly modifies HSPB4 and HSPB5 and these changes are expected to affect chaperone activity and influence cataract development (Derham and Harding, 2002; Weinreb et al., 2000).

The major clients of α-crystallin in lens are the β/γ-crystallins, a superfamily of highly-abundant proteins that share a common domain structure and vary in oligomeric state from monomers up to octamers (Serebryany and King, 2014; Slingsby et al., 2013; Chan et al., 2008). β/γ-crystallins are highly stable and are rich in cysteine residues but have no known biochemical

function. The role of β/γ-crystallins in lens has been historically viewed as contributing to lens optical quality (clarity) by densely packing together without aggregation or crystallization (Moreau and King, 2012b). Recent investigations have shown that γD-crystallin can quench incident UV light, which is expected to reduce photodamage, and that cysteine residues of γD-crystallin participate in disulfide exchange which might constitute a biological redox buffer (Chen et al., 2009; Serebryany et al., 2018). Interaction of α-crystallin and β/γ-crystallins leads to long-lived, soluble co-complex formation which eventually results in co-aggregation (i.e. cataract; Horwitz et al., 1999), leading to the belief that finite chaperone capacity of α-crystallin in lens can eventually be overwhelmed.

Point mutations associated with cataract development have been identified in many lens proteins including the α-crystallins HSPB4 and HSPB5 and the β/γ-crystallins, and disease is generally inherited in an autosomal dominant manner (Datskevich et al., 2012; Jiaox et al., 2015). Truncation and frame shift variants have also been identified in the α-, β-, and γ-crystallins and are associated with dominant or recessive inheritance of cataract (ClinVar). The expected result of sequence changes is modification of chaperone-client interactions. Additionally, the eye lens has high spatial order and expression of various cataract-associated crystallin mutants in mice causes similar changes in the proteome regardless of which crystallin is mutated, suggesting there is a delicate balance of interactions in lens that is disrupted in cataract (Schmid et al., 2021; Horwitz et al., 1999). Some cataract-associated β/γ-crystallin mutations cause protein crystallization within the lens, while others seem to escape the chaperone activity of α-crystallin (Pande et al., 2001; Michiel et al., 2010; Moreau and King, 2012). Cataract-associated mutations in α-crystallin are found throughout the sequence and have been the focus of many investigations (Muranova et al., 2020; Huang et al., 2009; Ghahramani et al., 2020). Most appear to be dominant negative in living

systems, but other than promoting premature aggregation, the molecular consequences of these mutations remain poorly understood (Perng et al., 2004; Wang et al., 2001; Wu et al., 2018; Mishra et al., 2018). Chapter 2 of this work focuses on two single-site mutations in HSPB5 associated with autosomal dominant cataract and myopathy development in humans.

1.3 Modulation of structure, dynamics, and productive interactions between HSPB4 or HSPB5 and beta/gamma-crystallins

The focus of this thesis work is on the human versions of the molecular chaperones HSPB4 and HSPB5 from the sHSP family (α-crystallin). In general, sHSPs are extraordinarily challenging to study in vitro because, while their polypeptide chains are relatively short (~180 amino acids), they assemble into large, polydisperse oligomeric ensembles that exchange subunits among oligomers (Delbecq and Klevit, 2013). This has been best described for HSPB5, which forms an ensemble of oligomers with ~10-40 subunits under normal cellular conditions and is modulated by changes in conditions (Hochberg and Benesch, 2014; Rajagopal et al., 2015). The properties of HSPB4 are similar (Kaiser et al., 2019). Many groups have sought to correlate changes in oligomeric properties, such as average size or subunit exchange rate, with chaperone activity, but no trend is evident (Janowska et al., 2019). Recalcitrance of sHSPs to investigation by traditional structural methods and lack of standard assay conditions has resulted in an overall rudimentary understanding of sHSPs and conflicting information. For example, solution acidification from pH 7.5 to 6.5 is known to modulate HSPB5 oligomeric assemblies towards larger sizes and is associated with increased chaperone activity against model client proteins (Rajagopal et al., 2015a). For some model clients, sHSP oligomers dissociate under these conditions (Rajagopal et al., 2015a). However, glutaraldehyde crosslinking of α-crystallin oligomers increased chaperone activity against WT β-crystallin at high temperature relative to unmodified α-crystallin, suggesting

subunit dissociation is not necessarily required for high activity (Augusteyn, 2004). This is consistent with recent experiments that show HSPB5 oligomers do not dissociate upon interaction with γD-crystallin *in vitro* (this work) and is in contrast with the finding that α-crystallin dissociates upon interaction with UV-damaged βL-crystallin *in vitro* (Muranov et al., 2019). The role of subunit dissociation may differ for different clients but cannot be tested directly because the heterogeneity of sHSPs means that no single property (subunit exchange, oligomer size, local structure/dynamics etc.) can ever be affected in isolation. Furthermore, we expect that all of these properties are interrelated and depend on interactions formed by sHSPs' dynamic terminal regions.

All sHSPs have three domains, consisting of a central, structurally-conserved domain (α-crystallin domain, ACD) that defines the family, and disordered N- and C-terminal regions (NTR and CTR) that are relatively poorly conserved among sHSPs. The ACD forms an anti-parallel dimer with a dynamic interface that can adopt multiple inter-chain orientations and is considered the building block of oligomers (Clark et al., 2011; Bagnéris et al., 2009). Sequence differences in the NTR and CTR are thought to reflect differences in client preferences and to influence mixed oligomer formation. The NTR contributes to formation of very large oligomers (Bova et al., 2000) and is required for productive interactions between HSPB1 and client protein Tau (Baughman et al., 2020) and HSPB5 and model client protein lysozyme (Mainz et al., 2015) or γD-crystallin (this work). High heterogeneity in the NTR that prevents structural analysis, in addition to the inability to study the NTR in isolation, has hampered the field's understanding of this important region until recently.

Techniques that can address NTR interactions have shown that it interacts with other NTRs and with the structured core ACD in HSPB1, HSPB2/3, HSPB5, and HSPB6 (Clouser et al., 2019; Clark et al., 2018; this work; Sluchanko et al., 2017). The nature of these interactions is similar

among sHSPs and presents an emerging theme of modulation of productive client binding by the NTR via networks of NTR interactions. Two sub-regions of the NTR have been observed or inferred to form similar interactions with the ACD in multiple sHSPs. In HSPB1, HSPB2/3, HSPB5, and HSPB6, the most N-terminal portion of the NTR (residues 1-13 in HSPB5) interacts with a region of the ACD called the edge groove (formed by the β4 and β8 strands, Figure 1.1; Clouser et al., 2019; Clark et al., 2018; this work; Sluchanko et al., 2017). In HSPB1, HSPB5, and HSPB6 a region of the NTR with highly-conserved sequence (Conserved NTR; residues 22-30 in HSPB5) interacts with the ACD central groove (formed by the dimer interface; Clouser et al., 2019; this work; Sluchanko et al., 2017). In the case of NTR interactions with the ACD in HSPB1 and HSPB5, which have been studied in greater detail, there are more NTR interactors than there are binding sites on the ACD (Clouser et al., 2019; this work). This establishes the formal possibility of competitive binding and results in a property that has been termed "quasi-order", arising from specific and relatively long-lived competitive interactions formed by the disordered NTR (Clouser et al., 2019). A similar situation exists for NTR to NTR interactions in HSPB5, where any single sub-region interacts with all other sub-regions and the state of each sub-region is likely interdependent on others (this work). Consistent with this hypothesis, NTR mutations in HSPB1 and HSPB4 or HSPB5 affect structure and/or dynamics of other NTR sub-regions that have interactions in common with the mutated site (Clouser et al., 2019; this work). These interactions provide new context with which to interpret results of chaperone activity assays and site-directed mutations.

Beyond NTR interactions, little is known about structure formation in the NTR of sHSPs. There is experimental evidence of secondary structure formation in the NTR for only one sHSP. Based on solid-state Nuclear Magnetic Resonance spectroscopy (ssNMR) data, two portions of

HSPB5 NTR can form secondary structure (Jehle et al., 2011). First, the central portion of the NTR, which contains the only conserved stretch of NTR sequence among sHSPs (Conserved Sequence; residues 20-29 in HSPB5), can form an α-helix. Based on available structures of the ACD, helical structure in the central NTR is expected to be incompatible with binding to the ACD central groove. This suggests that NTR structure may also affect the NTR to ACD interactions which are hypothesized to affect NTR availability for client interactions, therefore affecting chaperone activity. The NTR was not resolved in electron microscopy data for HSPB4 or HSPB5, suggesting it is dynamic and/or exists in multiple states (Peschek et al., 2009; Jehle et al., 2011; Peschek et al., 2013; Kaiser et al., 2019). In a crystal structure of full-length HSPB6, the central NTR sequence from HSPB6 interacts with its ACD in an extended conformation, further suggesting the central NTR can adopt a range of states from ordered to disordered depending on context and that α-helix formation may be incompatible with ACD binding (Sluchanko et al., 2017). Additionally, the C-terminal portion of the HSPB5 NTR can form an anti-parallel β-hairpin that associates with the first ACD β-strand and can be considered a continuation of the ACD structure ("β1", Figure 1.1; Jehle et al., 2011). ssNMR revealed evidence of more than five distinct states for a methionine in this region (Jehle et al., 2009). Such structural heterogeneity within the NTR of HSPB5, and likely other sHSPs, confounds interpretation of the role of structure, dynamics, and interactions on modulation of NTR availability for productive client interactions.

High stability of wild-type (WT) eye lens client proteins has precluded their use in sHSP chaperone activity assays at physiological temperature, preventing investigation of these important interactions under relevant conditions on experimentally-accessible timescales. The recent development of a mutant model of lens client protein γD-crystallin that spontaneously aggregates (γD-W130E) has enabled the investigation of these interactions at physiological temperature and

pH (Serebryany et al., 2016). γD-crystallin is a known client of HSPB4 and HSPB5 in lens (Andley et al., 2014; Su et al., 2011) and the W130E mutation mimics photodamage that occurs in WT γD-crystallin following exposure to UV light in vitro (Moran et al., 2013). Two other assays involving lens client have been developed, which utilized UV-damaged γD- or βL-crystallin as client, a mixture of low molecular weight β-crystallins (Muranov et al., 2019; Li). The new assay with γD-W130E offers a more homogenous client pool for in vitro experiments and improves the field's ability to investigate sHSP-lens client interactions with the γ-crystallin family.

1.4 SCOPE OF THESIS

The purpose of this work was to determine how the human sHSPs HSPB4 and HSPB5 are affected by sequence changes, with the goal of gaining new mechanistic insight into modulation of sHSPs in general and how changes in HSPB4 and HSPB5 interactions with lens client γD-crystallin might influence cataract development.

Chapter two describes changes in structure/dynamics, interactions, and chaperone activity of two cataract- and myopathy-associated HSPB5 mutations located in the structurally-conserved ACD (D109H and R120G). HSPB5 R120G was among the first sHSP mutations to be associated with disease development and has been a focus of numerous studies in vitro and in living systems (Vicart et al., 1998; Perng et al., 2004; Wang et al., 2001; Delbecq and Klevit, 2019), while relatively little is known about changes associated with the D109H mutation (Sacconi et al., 2012; Ghahramani et al., 2020). Residues R120 and D109 are highly conserved and can form an ionic interaction across the ACD dimer interface that has been observed in structures of multiple sHSP ACDs (Clark et al., 2011). Both HSPB5 ACD mutations have long-range effects that decrease structure and/or increase dynamics throughout the NTR and ACD. These molecular changes are associated with increased chaperone activity against γD-W130E relative to HSPB5 WT and result

in oligomers that bind γD-W130E under conditions that HSPB5 WT does not. Investigation of NTR interactions in HSPB5 WT using NMR spectroscopy and cross-linking mass spectrometry revealed novel NTR to NTR and NTR to ACD interactions that we hypothesize can modulate availability of the NTR for productive client binding, expanding our understanding of connections between sHSP domains and their potential importance for chaperone activity.

Chapter three compares chaperone activity of the two most highly related sHSPs, HSPB4 and HSPB5, against lens client protein γD-W130E. To our knowledge, this is the first ever in vitro investigation of productive interactions between both sHSPs and any member of the γ-crystallin family under physiologically relevant conditions. HSPB4 is far less active than HSPB5 and high HSPB5 chaperone activity is suppressed in mixed oligomers as found in lens. Chimeric constructs revealed the difference in activity is encoded by a short ~10 residue stretch in the NTR (Critical sequence; HSPB5 residues 31 to 42). The Critical sequence is somewhat conserved between HSPB4 and HSPB5 and is highly divergent in other sHSPs. Swapping the HSPB4 Critical sequence into otherwise HSPB5 yields oligomers with more β-structure and low chaperone activity that is nearly identical to HSPB4, while swapping the HSPB5 Critical sequence into otherwise HSPB4 yields oligomers with less β-structure and high chaperone activity that is most similar to HSPB5. Biophysical and spectroscopic studies indicate that the Critical sequence modulates structure and/or dynamics of the entire NTR and parts of the ACD and suggest that this region may play an important role in modulating client interactions in other sHSPs. This work improves our understanding of the role of sHSP NTR sequences on overall structure and dynamics and productive client interactions.

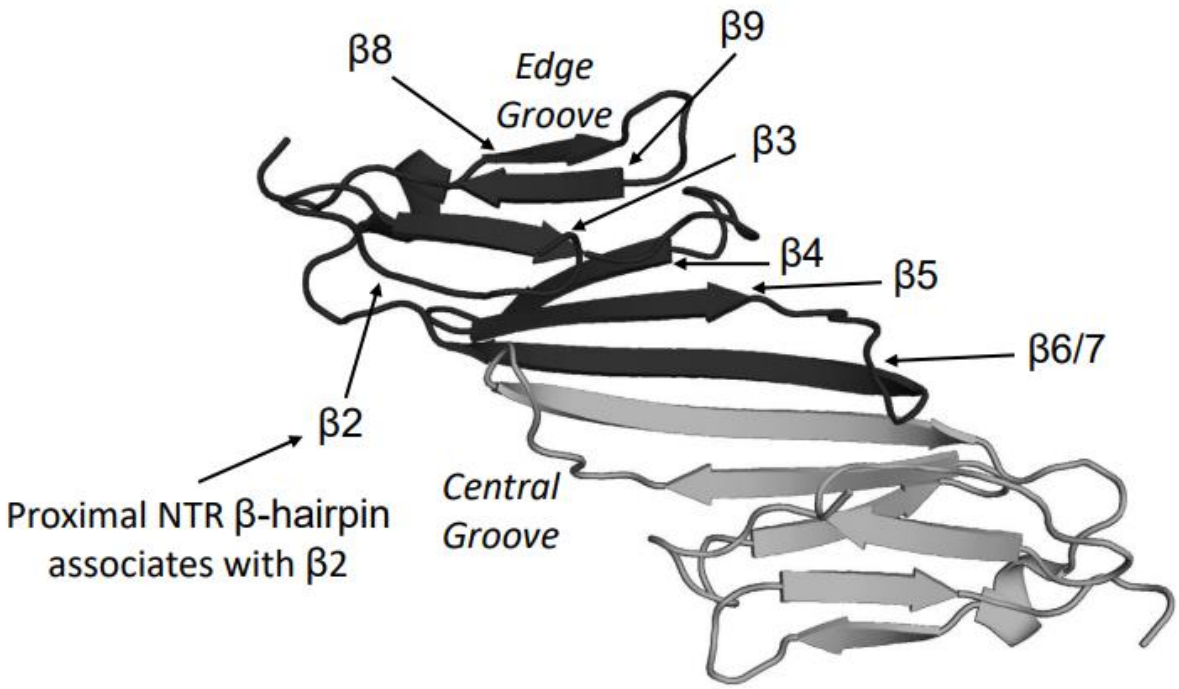

Figure 1.1. Structure of the HSPB5 ACD-only dimer (PDB: 2N0K) with all β-strands and the edge and central grooves labeled.

Chapter 2. HSPB5 DISEASE-ASSOCIATED MUTATIONS HAVE LONG-RANGE EFFECTS ON STRUCTURE AND DYNAMICS THROUGH NETWORKS OF QUASI-ORDERED INTERACTIONS

[Adapted from Woods, Ulmer, Janowska, Stone, James, Guttman, Bush, and Klevit (2022) "HSPB5 disease-associated mutations have long-range effects on structure and dynamics through networks of quasi-ordered interactions" (under review)]

Abstract:

Small heat shock proteins (sHSPs) are chaperones whose importance in protein homeostasis is exemplified by dozens of missense mutations associated with tissue-specific disease states. Despite decades of studies, the structure, dynamics, and mechanism of chaperone activity remain unclear. Here we show that the human sHSP HSPB5 distinguishes native lens protein γD-crystallin from damaged γD-crystallin even though the mutant/damaged client is folded. The disordered N-terminal region of HSPB5 (NTR) is essential for its chaperone activity, whereas the structured domain (ACD) has no intrinsic activity. Nevertheless, two sHSP mutational hotspots associated with disease, D109 and R120, are located in the ACD. Our studies on wild-type HSPB5 oligomers reveal that distinct regions within the NTR interact with specific grooves presented on the ACD dimer and/or with other NTR sub-regions and that the number of binding partners is greater than the number of binding sites, leading to a large, but finite number of potential combinations of interactions at any given time. The ACD mutations result in increased dynamics and accessibility of the disordered NTR and enhanced chaperone activity in vitro. Our findings reveal that HSPB5 quasi-order is delicately balanced and that perturbations arising from mutations within the

structured core cause alterations that contribute to misbalance in eye lens protein homeostasis that lead to cataract formation.

2.1 INTRODUCTION

Protein aggregation is a natural consequence of aging and must be controlled to maintain cellular health. Protein aggregates are a hallmark of multiple disease states in diverse tissues, including fibrillar aggregates associated with neurodegeneration and amorphous aggregates associated with cataract (Pedersen and Heegaard, 2013; Boatz et al., 2017). Small heat shock proteins (sHSPs) are a family of proteins whose ATP-independent chaperone activity contributes to protein homeostasis and inhibits protein aggregation (Horwitz, 1992). Although sHSPs were first discovered over 40 years ago (Ignolia and Craig, 1982), how the ten human sHSPs interact with diverse client proteins and how their chaperone activity is modulated remain poorly understood.

Previous studies have sought to gain insight into sHSP mechanisms by studying disease-associated mutations. Mutations identified in human sHSPs are primarily associated with autosomal dominant inheritance of tissue-specific diseases that include neuropathy, cataract, and myopathy (Datskevich et al., 2012). Among the first discovered and most extensively studied disease-associated mutations is substitution of Arginine 120 with Glycine in the ubiquitously expressed sHSP HSPB5, also known as αB-crystallin (Vicart et al., 1998; Fardeau et al., 1978). HSPB5 R120G is associated with autosomal dominant inheritance of desmin-related myopathy and cataract in patients (Vicart et al., 1998). Mutations at the R120-equivalent residue in other human sHSPs are also associated with autosomal dominant inheritance of tissue-specific diseases, implying a common critical role for the residue (Datskevich et al., 2012). Arginine 120 is located in the conserved core domain that defines the sHSP family, called the α-Crystallin domain (ACD).

The ACD is stably structured and forms a homodimer with a second copy of an ACD via long anti-parallel β-strands (Bagnéris et al., 2009). Arginine 120 is at the ACD dimer interface, where it can form an ionic interaction with Aspartate 109 (D109) across the dimer interface (Figure 2.1 A). Intriguingly, patient mutations of HSPB5 D109 (D109H, D109A, D109G) are associated with similar phenotypes as R120G (Sacconi et al., 2012; Fichna et al., 2017; Brodehl et al., 2017). Expression of HSPB5 R120G in cells or animals is associated with formation of aggregates and/or eye lens defects, leading to the widely held belief that it is a less effective chaperone (Wu et al., 2018; Andley et al., 2011; Perng et al., 2004; Wang et al., 2001). In vitro characterizations have revealed that HSPB5 R120G has more exposed hydrophobic surfaces than WT, has faster subunit exchange dynamics (Liang and Liu, 2006), and is less effective at maintaining solubility of model client proteins under destabilizing conditions (Bova et al., 1999; Treweek et al., 2005). But the molecular details that underpin the deleterious consequences of the HSPB5 R120G mutation remain undefined.

The tissue-specificity of sHSP disease phenotypes implies that certain mutations are particularly deleterious under some conditions or toward some clients. To date, investigations of sHSP mutants suggest they form abnormal interactions with clients (Koteiche and Mchourab, 2006; Delbecq and Klevit, 2019). In light of the cataract-associated phenotype of HSPB5 R120G and D109H, we focused on one of the main eye lens client proteins, γD-crystallin. Mature lens fiber cells lack the ability to synthesize or degrade proteins, so lens proteins can accumulate damage over an individual's lifetime (Lynnerup et al., 2008). Failure to prevent aggregation of damaged proteins, including γD-crystallin and β/γ-crystallins, results in cataract, a leading cause of blindness worldwide (Foster, 2000). Lens cells are highly enriched in sHSP content where the

total concentration of the two major lens sHSPs, HSPB4 and HSPB5 is roughly 150 mg/mL, corresponding to a subunit concentration of 7.5 millimolar.

Inherent properties of human sHSPs pose a major impediment to understanding their mechanisms. While sHSP protomers are small (~20 kDa), they assemble into large, structurally heterogenous and polydisperse ensembles of oligomers containing ~10-40 subunits that undergo dynamic subunit exchange among oligomers (Baldwin et al., 2011). There is high sequence conservation in the ACD (Figure 2.4), the only stably structured region (Figure 2.1 A). ACDs form dimers that present grooves into which short sequences from termini can bind (Clouser et al., 2019; Sluchanko et al., 2017; Clark et al., 2018; Klevit, 2020). The N-and C-terminal regions (NTR and CTR) are highly variable in sequence and length and are thought to support differences in client preferences and, possibly, mechanisms of activation.

We sought to identify determinants of HSPB5 chaperone activity by assessing changes caused by disease-associated mutations R120G and D109H. We compared the interactions, structure and dynamics, and chaperone activity of WT and mutant HSPB5 using hydrogen deuterium exchange coupled with mass spectrometry (HDX-MS) and biochemical assays and investigated interactions of the heterogenous NTR by Nuclear Magnetic Resonance Spectroscopy (NMR) and site-specific crosslinking. Paradoxically, the disease mutants associated with cataract and myopathy display gain-of-function properties, as they are more effective chaperones of a damaged lens client and associate with client protein under conditions where the wild-type (WT) HSPB5 does not. Our results identify novel HSPB5 interactions that modulate binding to γD-crystallin and suggest a mechanism for premature cataract formation in patients with inherited mutations.

2.2 RESULTS

2.2.1 *Disease mutants of HSPB5 are activated chaperones of γD-crystallin, a major client in eye lens*

Regions within HSPB5 responsible for its chaperone activity have not been determined for any physiological client. We sought this information for γD-crystallin ("GammaD"), a major client of HSPB5 in eye lens (Andley et al., 2014). In lens, pH values range from ~7 to ~6.5 and while non-lenticular tissues that express HSPB5 tend to have a pH of ~7.5, values can drop as low as 6.5 (Bassnett and Duncan, 1985; Mathias et al., 1991; Leem at al., 1999). HSPB5 is highly sensitive to pH in this range (Rajagopal et al., 2015a), so we investigated its capacity to delay aggregation of GammaD at the two extremes. WT, unmodified GammaD does not aggregate at 37 °C, so we used GammaD W130E, an oxidation-mimicking missense mutant that remains folded but spontaneously aggregates at 37 °C (Serebryany et al., 2016). At pH 6.5 and 37 °C, GammaD W130E aggregates over time as evidenced by increasing absorbance at 360 nm; the presence of HSPB5 WT delays the onset of aggregation by over two hours under assay conditions, even when GammaD W130E is present at 5-fold molar excess over HSPB5 (Figure 2.1 B). To identify regions within HSPB5 that are required for the observed chaperone activity, we compared the activity of full-length HSPB5 to truncated versions that lack the NTR (HSPB5 ACD-CTR) or lack both the NTR and CTR (HSPB5 ACD-only). The results clearly demonstrate that the HSPB5 NTR is required, as neither the ACD-CTR construct nor the ACD-only construct have a detectable effect on the aggregation curve (Figure 2.1 B). HSPB5 chaperone activity towards GammaD is greatly reduced at pH 7.5, providing only a short delay in aggregation onset at an identical molar ratio as the experiment conducted at pH 6.5 (Figure 2.1 C). Co-incubation of HSPB5 WT and GammaD W130E at 37 °C under assay conditions resulted in soluble complexes that co-elute early on size

exclusion chromatography (SEC), whereas no detectable complex was observed in the presence of GammaD WT (Figure 2.1 D and Figure 2.3). Similar observations of activated chaperone activity of HSPB5 at low pH have been reported for aggregating proteins that are not thought to be physiological clients of HSPB5 (Rajagopal et al., 2015a). Our results indicate that the lower pH conditions in lens give rise to productive binding of aggregation-prone GammaD by HSPB5, resulting in enhanced chaperone activity ("activated").

HSPB5 mutations R120G and D109H are associated with cataract, suggesting they allow for enhanced aggregation in lens. Paradoxically, while their activity is similar to WT at pH 6.5 (Figure 2.2), we observe that unlike HSPB5 WT, both mutant forms are also highly effective chaperones at pH 7.5 (Figure 2.1 C). Thus, the in vitro assays indicate a gain of function, at least under the higher pH condition. Consistent with this notion, both HSPB5 R120G and D109H formed soluble, long-lived complexes with GammaD W130E, but not GammaD WT, when co-incubated at 37 °C in pH 6.5 or 7.5 buffer (Figure 2.3). Both mutated sites are in the structured ACD, which does not itself have chaperone activity towards GammaD W130E (Figure 2.1 B). Introduction of the R120G or D109H mutations into the ACD-only construct does not yield an active species (Figure 2.2). Together with the finding that HSPB5 chaperone activity against GammaD requires the NTR, the results suggest that functional client-interacting regions within the NTR are more available in R120G and D109H oligomers. This in turn implies that mutations in the structured ACD alter the properties and function of the sequence-distant and heterogenous NTR.

2.2.2 *Disease-associated mutations in ACD residues affect NTR structure and dynamics*

To obtain insight into the structure and dynamics of HSPB5 as it exists in oligomers at pH 7.5, we used hydrogen deuterium exchange coupled with mass spectrometry (HDX-MS). HDX reports on the ability of protein backbone amides to exchange hydrogen with deuterium presented

as $^{2}H_2O$. Positions that are in dynamic or unstructured regions exchange rapidly (seconds-minutes), while structured and hydrogen-bonded positions exchange slowly (hours-days) and are described as "protected." Thus, the degree of protection from exchange is indicative of local structure and dynamics. The experimental methodology provides peptide-level resolution and the extent of HDX for a given peptide reports on all backbone amides within that peptide except the two N-terminal residues of each peptide.

The three regions of HSPB5 are distinguishable in terms of their deuterium exchange behaviors (Figure 2.5 A and B). The CTR exchanges fastest, with 100% of sites fully exchanged after 4 seconds at the extreme C-terminal end. This behavior is consistent with a dynamic and unstructured CTR in the context of HSPB5 oligomers. The lowest exchange rates are observed in the ACD, with some ACD-derived peptides incompletely exchanged after 20 hours (Figure 2.6). The slow exchange kinetics reflect the H-bond-rich β-sheet structure of the ACD. The NTR exhibits moderate exchange after 4 seconds, indicating that it is less dynamic than the disordered CTR and that it may be involved in structures and/or interactions that slow amide exchange. By the 30 min timepoint, however, much of the NTR is fully exchanged, indicating that it is not as stably structured as the ACD. The general exchange profiles of the three regions of HSPB5 are similar to what has been reported for two other human sHSPs, HSPB1 and HSPB4 (Clouser et al., 2019; Kaiser et al., 2019), but in contrast to HSPB1 no evidence for bimodal deuterium uptake was observed for any peptide of HSPB5.

High coverage and resolution in the HDX data provide a detailed view of the NTR in the context of HSPB5 oligomers. At the 4 second timepoint, NTR peptides that span residues 1-54 exhibit exchange levels of roughly 35% − 60% and those more proximal to the ACD, whose structured residues begin at around residue 65, exhibit higher exchange levels, up to 68% (Figure

2.5 A). Unlike HSPB1, whose NTR contains a sub-region that is completely exchanged at the 4 second timepoint, there are no fully-exchanged sub-regions within HSPB5's NTR after 4 seconds.

HDX time courses were collected for HSPB5 R120G and D109H (Figure 2.6 A-D). The overall exchange profiles are similar to WT, with the ACD exchanging slowest, the CTR exchanging fastest, and the NTR exhibiting intermediate exchange levels. Notable differences were observed at the peptide level in exchange time course plots (Figures 2.5 C and D, Figure 2.6 A-D). Pairwise comparisons of uptake for each mutant, calculated as the difference in deuterium level between a peptide from the mutant and the corresponding peptide from the WT are shown for all timepoints (Figure 2.7 A-D). These snapshots reveal decreased protection in the NTR at early times (4 seconds, 1 minute) and in the ACD at longer times (30 minutes, 20 hours) for both mutants, with the magnitude of change being generally larger for D109H.

Focusing first on the mutation-harboring ACD, a majority of peptides exhibit higher exchange levels in the mutants at the 30-minute timepoint, consistent with global destabilization of the ACD (Figure 2.5 D, Figure 2.7 C). Peptides that contain residues 79-89 and 97-117 have the largest increase in exchange in both mutants, ranging around 20-30%. These regions are proximal to the two mutation sites (peptides containing the mutation sites were not compared because they have different sequences), so the observation implies that mutation at R120 affects the region near D109, and vice versa. The coupled effect is consistent with the putative salt bridge interaction between the two sidechains observed in some crystal structures (Bagnéris et al., 2009). Increased exchange of a long peptide that includes residues in the β6/7 strand that forms the dimer interface (i.e., residues 117-123) implies that the interface is more dynamic and/or slightly destabilized. In addition, two ACD loops, L3/4 (residues 83-90) and L8/9 (residues 137-143), have increased exchange at all exchange timepoints. These loops are proximal to one another and lead into and

out of one side of the ACD edge groove (formed by β-strands 4 and 8, Figure 2.9). In sum, comparison of the 30-minute exchange profiles reveals that the two mutations affect the same regions within the structured ACD, but the magnitude of increased exchange is larger for D109H. Surprisingly, among the strongest effects are loops that link β-strands and lie on the edges of the β-sandwich ACD structure.

At the 4 second time point, exchange differences are most prevalent in the NTR, where deuterium uptake is increased for virtually every peptide derived from the two mutants (Figure 2.5 C and Figure 2.7 A). The overall patterns are quite similar for the two mutant proteins, although the magnitude of change is larger for peptides from D109H in general. The most distal N-terminal peptides are the least affected and are the most protected NTR peptides in the mutants (Figure 2.5 C and Figure 2.6 A). Peptides spanning residues ~20-55 have larger differences in exchange relative to the WT protein (Figure 2.7). In both mutant oligomers, NTR peptides from the region that is proximal to the ACD display the highest exchange levels (Figure 2.5 C and Figure 2.6 A). Altogether, the HDX data are consistent with a destabilization/increase in dynamics in the ACD and increased accessibility/increased dynamics in the NTR, especially in the central region of the NTR.

2.2.3 *NTR sub-regions interact with ACD grooves*

The observations that mutations in the ACD affect NTR HDX behavior imply an interplay between the NTR and ACD of HSPB5. As both the size and heterogeneity of full-length HSPB5 oligomers defy conventional structural analysis, we turned to the well-behaved, stably structured ACD-only dimer to assess its possible interactions with the NTR by solution NMR. On its own, the highly hydrophobic and heterogenous NTR is ill-behaved and has low solubility. We therefore divided the HSPB5 NTR into four sub-regions informed by the HDX data (and ultimately dictated

by solubility) termed: Distal (residues 1-13), Aromatic (residues 11-22), Conserved (residues 17-34), and Boundary (residues 41-62; Figure 2.10). Synthetic peptides that correspond to each NTR sub-region were titrated into 15N-labeled HSPB5 ACD-only and their effects on the Heteronuclear Single Quantum Coherence (HSQC) NMR spectrum were determined. Because we have previously assigned all features of the HSQC spectrum of the HSPB5 ACD-only dimer, perturbations in that spectrum provide residue-level information (Jehle et al., 2009). Each NTR sub-region exhibited distinct effects on the ACD spectrum. Only the Aromatic peptide produced no detectable perturbations to the HSPB5 ACD spectrum. The Distal and Conserved peptide titrations generated well-defined perturbations, while the Boundary peptide effects were quite weak (Spectra are shown in Figures 2.11, 2.12, and 2.13).

Addition of the Distal peptide to HSPB5 ACD-only is accompanied by chemical shift perturbations (CSPs) and intensity losses in peaks corresponding to ACD edge groove residues (β-strands 4 and 8; Figure 2.8 A and D, Figure 2.9, and Figure 2.11). Smaller perturbations are detected in strands and loops proximal to the dimer interface. The Distal peptide has an Ile3-Ala-Ile5 sequence similar to the "Ile-x-Ile" motif in the CTR of HSPB5 (Ile159-Pro-Ile161) that interacts with the edge groove (Delbecq et al., 2012). Comparison CTR peptide (HSPB5 residues 155-167) reveals that many of the same peaks are affected by both peptides (Figure 2.8 B and E, Figure 2.11). The observed effects are consistent with both peptides binding in a similar manner with similar (low) affinity. There are therefore two edge groove-binding sequences per HSPB5 protomer, one in the NTR and one in the CTR, but only one edge groove. High local concentrations of termini in oligomers and similar apparent affinities for the NTR and CTR Ile-X-Ile motifs suggest there is likely competition between the CTR and Distal NTR for binding to an ACD edge groove.

Titration of the Conserved peptide yielded spectral perturbations consistent with a weak interaction (Figure 2.8 C and F, Figure 2.12). Broadening is observed for peaks corresponding to residues located in the ACD central groove (β-strands 2, 3, and 6/7). Interactions involving the Conserved NTR sub-region and the ACD central groove have been observed in human HSPB1 and HSPB6, suggesting the interaction may be a common feature for all sHSPs (Clouser et al., 2019; Sluchanko et al., 2017). There are two Conserved sub-regions per HSPB5 dimer and only one central groove, leading to another situation in which there are more potential binding partners than there are binding sites.

The NMR results indicate that both the ACD edge and central grooves can harbor or sequester regions within the NTR. The ACD edge groove binds peptides that have an Ile-X-Ile motif and the ACD central groove binds the NTR Conserved sub-region. When observed in trans (i.e., as intermolecular interactions), the apparent affinities/lifetimes are quite modest. However, HSPB5 is present in millimolar concentrations in lens and local concentrations of potential interacting regions are expected to be even higher in HSPB5 oligomers. It is therefore likely that the interactions detected by NMR occur in the context of oligomeric HSPB5.

2.2.4 *NTR sub-regions interact with other NTR sub-regions*

To further identify interactions that occur in the context of HSPB5 oligomers, we adopted a targeted cross-linking/mass spectrometry strategy. Common chemical cross-linking reagents can span many tens of Å and only react with specific reactive amino acids that are solvent accessible. To circumvent these issues, the non-canonical amino acid p-benzoyl-l-phenylalanine (BPA) was installed at single positions in HSPB5 using amber codon suppression (Chin et al., 2002). When excited at ~360 nm, the benzophenone moiety of BPA forms covalent crosslinks to C-H bonds that are within 2.5-3.1 Å, providing a powerful probe for proximity/atomic contacts (Dorman and

Prestwich, 1994). To minimize perturbation, we installed BPA at aromatic sites within the NTR to investigate NTR interactions in HSPB5 oligomers.

As proof-of-principle, we installed BPA within the Distal NTR sub-region, as the NMR results identified its binding site as the ACD edge groove. In sHSPs, Ile-X-Ile interactions occur via a "knob in hole" mechanism, in which a methyl group of each isoleucine "knob" inserts into a hydrophobic "hole" in the ACD edge groove (Delbecq et al., 2012). To minimize possible perturbations due to introduction of the large, aromatic BPA sidechain, Trp9, four residues removed from the putative NTR edge groove-binding motif, was chosen as the site of BPA incorporation. Oligomers composed of W9BPA-HSPB5 were irradiated at 360 nm for 30 minutes at 4 °C. SDS-PAGE analysis of the resulting samples revealed a major product that runs at the expected position of a two HSPB5 protomers with a single intermolecular cross-link (i.e., singly cross-linked species), with similar amounts of higher order species representing >2 crosslinked subunits detected (Figures 2.15 and 2.16). We performed in-gel digests of the singly cross-linked band and subjected the resulting peptides to mass spectrometry (Figure 2.17). Data-dependent fragmentation and bioinformatic analysis of the resulting spectra led to the identification of multiple HSPB5 regions to which BPA at position 9 is cross-linked (Figure 2.14 A). The region with the highest number of peptide spectral matches (PSMs) is the ACD edge groove, at and around residue 138 and around residue 85, confirming the Distal-to-edge groove interaction implied by the solution NMR results. Importantly, the number of PSMs is not a quantitative metric related to the prevalence of a given interaction. In addition, crosslinks to several NTR sub-regions were identified. Notably, the crosslinks are not randomly distributed throughout the NTR but are more localized. The highest density of crosslinks within the NTR is to residues between ~60-70. These include the C-terminal part of the Boundary region and the first structured residues of the

ACD; the latter were perturbed in the NMR distal peptide titration (Figure 2.8 A and D). Cross-links were also detected to Conserved sub-region residues 25-32, the Boundary sub-region residues 38-50, and to the Distal sub-region itself. UV-exposed HSPB5 molecules that migrate as dimers on SDS-PAGE must contain a covalent cross-link between two chains. As all chains contained a BPA, it is also possible that some identified cross-links may be intra-chain. However, MS analysis of material that migrated at the position of monomeric HSPB5 in UV-treated samples (and could in principle contain intra-chain cross-links) did not identify cross-links, indicating that intra-chain crosslinks are rarely formed. Thus, incorporation of BPA at Trp9 both confirmed that the Distal sub-region interacts with ACD edge grooves in a neighboring protomer and revealed novel inter-NTR interactions within HSPB5 oligomers.

To discover additional NTR interactions, BPA was individually installed at NTR positions F24, F47, and F61 (Figure 2.14 B-D). Of these, F24BPA produced the smallest number of identified cross-links and F61BPA produced the highest number. Cross-links were observed to the ACD, specifically to the edge groove, from F47BPA. Although the peptide containing F47 (Boundary) produced NMR perturbations when added to the ACD, they were too weak to assign to specific regions. Thus, the BPA cross-linking results identify a third region of HSPB5 that visits the ACD edge groove. The only other ACD residues that had detectable cross-links in any of the BPA species analyzed are at the N-terminal end of the structured ACD, around residues 65 through 70. BPA installed at positions W9 (see above), F24, and F61 generated such cross-links. In the solution NMR structure of HSPB5 ACD (PDB 2N0K) residues 66-71 form a β2 strand that forms part of the ACD central groove. These residues were distinctly perturbed upon addition of the Conserved peptide (residues 17-34) in NMR titrations, again demonstrating agreement between the in trans NMR data and the in-oligomer cross-linking data. Finally, NTR-to-NTR cross-links

were observed for all BPA species. Cross-links from BPA sites 24 and 61 to the Aromatic sub-region (residues 11-22) are notable, as this peptide showed no evidence of an ACD interaction and is therefore likely to interact primarily with NTR sub-regions. Altogether, the BPA crosslinking data both confirm interactions inferred from NMR experiments and identify numerous novel interactions that involve the NTR in heterogeneous, polydisperse oligomers. The new interactions involving the NTR greatly expand the limited information obtained from past solid-state NMR, cryo-EM, and biochemical studies (Jehle et al., 2011; Peschek et al., 2013; Ghosh and Clark, 2005).

2.3 DISCUSSION

Polydispersity and heterogeneity of human small heat shock proteins have long presented barriers to their structural and mechanistic understanding. Although polydisperse oligomers can in principle be parsed by single-particle cryo-EM, the level of heterogeneity within a given sized sHSP oligomer remains a substantial challenge (Kaiser et al., 2019). What gives rise to such heterogeneity and how does it relate to sHSP function? To address these fundamental questions, we have developed approaches that provide information regarding the heterogeneous oligomer ensembles holistically. Following the notion that sHSPs have evolved to perform their function under physiological conditions towards proteins expressed in the same tissues, we investigated a sHSP that is abundant in eye lens and a bona fide lens client, GammaD. Our efforts were guided by two inherited HSPB5 mutations associated with cataract under the presumption that these were likely loss-of-function or dominant negative mutations that lead to untimely protein aggregation in lens. Our findings reveal new insights into the structure and function of HSPB5. First, HSPB5 distinguishes native GammaD from damaged GammaD even though the mutant/damaged GammaD is folded, consistent with recent reports that HSPB5 WT binds the destabilized GammaS-crystallin G18V mutant but not the function-preserving GammaS G18A mutant

(Sprague-Piercy et al., 2020). Second, the heterogenous NTR is essential for HSPB5 chaperone activity towards GammaD, whereas the structured ACD has no intrinsic activity. A requirement for the NTR has previously been reported for an unfolded model client that forms amorphous aggregates (Mainz et al., 2015). Third, distinct sub-regions within the NTR interact with specific grooves presented on the ACD dimer and/or with other NTR sub-regions. Importantly, the number of binding partners is greater than the number of binding sites, leading to a large, but finite number of potential combinations of interactions within a given oligomer at any given time (Figure 2.18 A). This situation was previously dubbed "quasi-order" and provides a way to describe the heterogeneity in HSPB5 as well as other sHSPs that exist as oligomers (Clouser et al., 2019).

How do changes in client interactions inform our understanding of cataract and myopathy development associated with inherited HSPB5 mutations? Previous work revealed increased interactions between HSPB5 R120G and muscle client desmin that affected client filament network status and mechanical properties in cells and in vitro (Perng et al., 2004; Wang et al., 2001). We observed formation of long-lived, high molecular weight co-complexes of HSPB5 and its lens client, GammaD W130E. Mutant HSPB5 oligomers bind GammaD under conditions where HSPB5 WT does not, resulting in higher apparent chaperone activity under lab conditions where aggregation occurs on a timescale of minutes-to-hours. Furthermore, there is a continual uptake of client over time and this occurs more rapidly and more readily for the mutant HSPB5 species. Extrapolating such behavior to the situation in lens where the lack of protein synthesis means there is a fixed and finite amount of chaperone present over an individual's lifetime, the "more effective" HSPB5 mutants may reach their capacity limit faster than the "less effective" WT chaperone or may interact differently with other lens client proteins. The progressive uptake of GammaD by HSPB5 has parallels to age-dependent changes in wild-type mouse lens that occur over a lifetime

of accumulated damage (Schmid et al., 2021). All lens proteins, including HSPB5, are found in aggregates in cataractous lenses, suggesting similar processes occur in vivo (MacCoss et al., 2002). In lens, HSPB5 is associated with the lens sHSP HSPB4, forming mixed oligomers. Further studies will be needed to address interactions between HSPB4 and GammaD and how mixed oligomer formation affects these interactions. Expression of HSPB4, βA2-crystallin, or GammaD cataract-associated mutants in mice revealed similar changes in the proteome in all cases, which suggested the eye lens requires a delicate balance of interactions to maintain spatial order required for lens transparency (Schmid et al., 2021). Our data indicate HSPB5 R120G and D109H form increased client interactions and support the chaperone capacity model of cataract formation.

2.3.1 *Ideas and Speculation*

Since its discovery in 1998, many studies have been conducted with the goal of understanding how HSPB5 R120G leads to cataract and myopathy. Our results reveal that the R120G and D109H disease-associated mutants are activated chaperones towards the lens client GammaD and can interact productively under conditions where HSPB5 WT cannot (pH 7.5). Consistent with that phenotype, the NTRs are less protected from hydrogen/deuterium exchange and, hence, more available for interaction with client in mutant oligomers. How can sequence changes in the ACD affect the states of the NTR and thus client engagement? Identification of HSPB5 NTR sub-regions that interact with grooves in the ACD provides a plausible direct connection. In particular, a sub-region that contains the only conserved sequence among human sHSP NTRs has now been reported to interact with the central ACD groove in HSPB5 (this work), HSPB1 (Clouser et al., 2019), and HSPB6 (Sluchanko et al., 2017). Solution NMR structures of the HSPB1 and HSPB5 WT ACD-only dimers display a central groove that is electrostatically positive (Figure 2.18 A; PDB 2N3J, 2N0K; Rajagopal et al., 2015a; Rajagopal et al., 2015b). In stark contrast, solution

NMR structures of the HSPB5 R120G ACD-only dimer display a smaller, less pronounced central groove that is electrostatically negative (Figure 2.18 B; P. Rajagopal, PDB 6BP9). The large change is due to a shift in the register of the anti-parallel strands that compose the dimer interface, including the strand that contains R120. Notably, in the only crystal structure of full-length human HSPB6, the conserved NTR sequence, –SRLFDQ–, is inserted with the conserved aspartic acid pointing into the ACD central groove (Sluchanko et al., 2017; PDB 5LTW). Strong conservation of negative charge in the Conserved NTR sub-region suggests this could be a key regulatory interaction among sHSPs (Figure 2.4). We propose that the changes in the central groove due to the R120G mutation provide a structural rationale for the loss of interaction between the Conserved NTR sub-region and the ACD central groove. Although there is currently no structure available for the D109H ACD-only dimer, the concordance of observations between the two mutants suggests that a similar situation occurs for this mutant as well.

Changes in NTR structure/dynamics are not limited to sub-regions that bind the ACD. Based on the network of NTR-NTR interactions observed by BPA crosslinking, we propose that loss of any individual interaction, such as the Conserved/central groove interaction, perturbs the entire network. Indeed, with one exception, all NTR sub-regions are less protected from HDX in mutant oligomers. The Distal NTR interacts via a knob-into-hole interaction with the ACD edge groove and our HDX data suggest that this interaction is maintained in the mutant oligomers. Extensive perturbation of the NTR is an expected consequence of "quasi-order" and was first observed in human HSPB1, where mutations in the Conserved or Boundary NTR sub-regions affected HDX in the opposite sub-region (Clouser et al., 2019). A relationship between these NTR sub-regions was also observed in BS3 cross-linking experiments on HSPB4 (Kaiser et al., 2019) as well as in

our targeted BPA cross-linking experiments, suggesting this interaction may be a common feature of sHSPs.

A model in which loss or change in an NTR interaction alters the entire network of quasi-ordered interactions may provide a means to understand other disease-associated mutations in HSPB5 and other sHSPs. There are numerous mutations of ACD residues that cluster near the central groove. The peculiar sequence of the HSPB5 ACD central groove (which is highly conserved among other human sHSPs) results in a delicate balance of charged, polar, and hydrophobic interactions that span the ACD surface and are highly interdependent. Chemical changes at any single site from mutation, modification, or damage are expected to affect the entire network. Consistent with this idea, phosphorylation of yeast Hsp26 ACD affects availability of its NTR for client interactions (Mühlhofer et al., 2021). Identification of NTR-to-ACD and NTR-to-NTR interactions and experimental approaches that can detect these provide a way to understand the effects of such mutations on sHSP structure and function. The work here, along with previous studies of human HSPB1, establish a framework for describing quasi order of polydisperse and heterogenous small heat shock proteins and investigating their functional consequences.

2.4 Materials and Methods

2.4.1 *Expression and purification of HSPB5 WT and mutants*

E. coli BL21 cells were transformed with HSPB5 WT or mutants in a pET23 vector. Cells were grown to an OD600 of 0.6 at 37 °C while shaking at 200 RPM, then adjusted to 22 °C and induced by addition of 1 mM IPTG. BPA was site-specifically incorporated in HSPB5 amber codon mutants by co-expression with pEVOL-pBpF. pEVOL-pBpF was a gift from Peter Schultz (Addgene plasmid # 31190; http://n2t.net/addgene:31190; RRID:Addgene 31190). HSPB5 BPA mutant cells were cultured identically to HSPB5 WT following induction by 1 mM IPTG and 1

mM Arabinose. After growing overnight, cells were harvested and resuspended in 20 mM Tris, 100 mM NaCl, 10 mM EDTA pH 8. Cells were treated with DNase, RNase, and lysozyme and were subsequently lysed using a french press. PEI (0.1%) was added to the cell lysate and then clarified by centrifugation. The supernatant was retained and was adjusted to 31.5% ammonium sulfate (w/v) and clarified by centrifugation at 17k RPM for 20 minutes. The ammonium sulfate pellet contains HSPB5 and was retained for purification. The ammonium sulfate pellet was solubilized in 20 mM Tris pH 8 and applied to a G25 desalting column equilibrated in 20 mM Tris pH 8. Desalted protein eluted from the G25 column was applied to a DEAE column equilibrated in 20 mM Tris pH 8 and eluted with 20 mM Tris, 100 mM NaCl pH 8. Protein eluted from the DEAE column was diluted at least 2-fold in 20 mM Tris pH 8 and then applied to HiTrap Q columns (Cytiva, 10 mL bed volume) and eluted by a sodium chloride gradient from 0-300 mM over 8 column volumes. Protein eluted from the Q column was concentrated to 2 mL and then applied to a 120 mL SDX200 column equilibrated in 25 mM NaPO4, 150 mM NaCl pH 7.5. The same procedure was used for the HSPB5 ACD-CTR and ACD-only constructs, except a 120 mL SDX75 column was used for the final step.

2.4.2 *Expression and purification of γD-crystallin*

GammaD-crystallin was expressed in *E. coli* BL21 cells as a C-terminal HexaHis-Sumo fusion in pET28a vector. After reaching an OD600 of 0.6 at 37 °C, temperature was adjusted to 20 °C and cells were induced with 0.5 mM IPTG and grown overnight. Cells were harvested and resuspended in 25 mM Tris, 200 mM NaCl, 10 mM imidazole pH 7.6, treated with DNase, RNase, and lysozyme, and lysed using a french press. PEI (0.1%) was added to the cell lysate and then clarified by centrifugation at 20k RPM for 20 minutes. The supernatant was applied to HisTrap columns (Cytiva) equilibrated in 25 mM Tris, 200 mM NaCl, 10 mM imidazole pH 7.6. His-Sumo-

GammaD was eluted from the column using 25 mM Tris, 200 mM NaCl, 500 mM imidazole pH 7.6. GST-SENP1 protease was added to the eluted protein and the mixture was dialyzed in 20 mM Tris, 200 mM NaCl, 10 mM imidazole, 2 mM β-mercaptoethanol pH 7.6 overnight at 4 °C. Cleaved protein was re-applied to a HisTrap column equilibrated in 25 mM Tris, 200 mM NaCl, 10 mM imidazole pH 7.6 and the flowthrough was concentrated and then applied to a 120 mL SDX75 column equilibrated in 20 mM Tris, 50 mM NaCl, 5 mM EDTA, 5 mM BME pH 8. Fractions containing GammaD were concentrated and then stored in 25 mM NaPO4, 150 mM NaCl, 0.1 mM EDTA pH 6.5 or 7.5.

2.4.3 *Chaperone Activity Assay*

Chaperone activity assays were conducted in a 96 well flat-bottom half-area plate with a final volume of 100 µL. GammaD-crystallin was adjusted to a concentration of 1 mM and incubated on ice. Assay wells containing HSPB5 in 25 mM NaPO4, 150 mM NaCl (or buffer only) in 50 µL total volume were pre-heated for 5 minutes at 37 °C. Following pre-heating, 50 µL ice cold GammaD W130E in 25 mM NaPO4, 150 mM NaCl, 0.1 mM EDTA was added. The plate was incubated at 37 °C and A360 measurements were taken once per minute, with 5 seconds of shaking before each measurement.

2.4.4 *Nuclear Magnetic Resonance Spectroscopy*

HSPB5 WT ACD was enriched with ^{15}N by growing in M9 minimal media supplemented with ^{15}N-ammonium chloride and purified as described previously. HSPB5 NTR-derived synthetic peptides were purchased from Genscript. All peptides were produced with N-terminal formylation and C-terminal amidation, except for the Distal NTR peptide (HSPB5 residues 1-13) which had an amidated C-terminus and an unmodified N-terminus. Peptides were dissolved in 16.67-100%

deuterated DMSO, depending on solubility, and titrated into 15N-labelled HSPB5 WT ACD-only in 25 mM MOPS, 100 mM sodium chloride, pH 7.5 buffer containing 10% D2O. The concentration of d-DMSO in the final NMR samples was maintained below 1% to prevent perturbation of HSPB5 ACD-only. HSQC-TROSY NMR spectra were recorded at 295 kelvin on a Bruker 500 MHz Avance III spectrometer or on a 600 MHz Avance II spectrometer equipped with a cryoprobe. Spectra were processed and analyzed using NMRPipe/NMRDraw (Delaglio et al., 1995) and Sparky (Lee et al., 2015) and visualized with NMRView (Johnson, n.d.) in NMRBox (Maciejewski et al., 2017).

2.4.5 *Hydrogen/Deuterium Exchange Mass Spectrometry*

All samples were incubated at 37 °C for 3 hours in water-based buffer and then cooled to room temperature before undergoing deuterium exchange. HSPB5 WT and mutants (0.04 mg/mL) were incubated at room temperature in 85% D2O-based PBS pH 7.5 buffer for 4 seconds, 1 minute, 30 minutes, or 20 hours. Fully deuterated samples were made by incubating protein in 85% D2O buffer at 75 °C for 30 mins. Exchange was quenched by addition of ice-cold quench buffer (1.6% formic acid) and samples were flash frozen in liquid nitrogen. Samples were automatically thawed, digested by immobilized pepsin and AN-PEP (Tsitsiani et al., 2017), and injected on a Waters Synapt G2-Si instrument using a setup built in house around the LEAP PAL system (Watson et al., 2021). HSPB5 peptides were identified by MS/MS on a Thermo Orbitrap Fusion Tribrid instrument and MSE on a Waters Synapt G2-Si followed by data analysis using ProteinProspector (UCSF) or ProteinLynx Global SERVER (Waters). Deuterium uptake was analyzed in HDExaminer 3.0 (Sierra Analytics) and HX-Express (Guttman et al., 2013).

2.4.6 *BPA Cross-linking Mass Spectrometry*

BPA was incorporated in HSPB5 using amber codon suppression technology (Chin et al., 2002). The amber codon was inserted at HSPB5 site 9, 24, 47, or 61 using QuikChange mutagenesis (Agilent). Single-BPA HSPB5 mutants were purified using the standard protocol while taking steps to limit exposure to ambient light. Sample concentrations were determined using BCA. 50 μM HSPB5 BPA mutants were incubated for 3 hours at 37 °C, cooled to 4 °C, placed in a 96-well flat-bottomed half-area plate, and then exposed to UV for 30 minutes at 4 °C. Samples were subjected to SDS-PAGE on a 4-20% acrylamide gradient gel (Bio-Rad). The no-UV monomer and plus-UV dimer bands were excised and were each digested in-gel with MS grade Trypsin (Thermo Scientific) and GluC (New England Biolabs) in ammonium bicarbonate buffer (Thermo Manual - In-Gel Tryptic Digestion Kit). Digests were cleaned up with C18 spin columns (Thermo Scientific) and dried using a speed-vac. Samples were resuspended in 95% water 5% ACN with 0.1% FA with volumes adjusted based on sample weight. Data was collected with an Easy Nano LC coupled to a Thermo Orbitrap Fusion Lumos Tribrid. 0.5 μg of protein was loaded onto an 8-cm trap column. The sample was then then separated on a 25-cm analytical column with a 75 μm inner diameter using an 85-minute gradient from 6% B to 45% B, where A was water and B was 80% acetonitrile, at 300 nL/min. The column was then flushed and regenerated for 35 minutes. Spectra were acquired across the entire LC method using data-dependent acquisition with dynamic exclusion after one time for a duration of 30 seconds and an intensity threshold of 2.0×10^4. Orbitrap detection and Higher-energy C-trap dissociation (HCD) fragmentation (30% normalized collision energy) were used with a target value of 1.00×10^5, maximum injection time of 22 ms, top N of 20, and isolation width of 1.6. MS1 were acquired at a resolution of 120,000 over the range of 400-2000 m/z, and MS2 were acquired with a resolution of 15,000. The mass

spectrometry proteomics data have been deposited to the ProteomeXchange Consortium via the PRIDE partner repository (Perez et al., 2019) with the dataset identifier PXD034114.

2.4.7 *Identification of Crosslinks Using the Trans Proteomic Pipeline (TPP)*

First, Comet (Eng et al., 2013) was used to search for non-crosslinked peptides in the non-UV treated control to construct the protein database. The Comet search database contained the BL21 E. coli database from uniprot (UP000431028), the cRAP database from the Global Proteome Machine with all 5 levels of proteins (cRAP Protein Sequences), the pertinent HSPB5 BPA mutant, and reverse-sequence decoys. The Comet searches were enzyme nonspecific using a peptide mass tolerance of 20.0 ppm. The isotope error offset was 3, and BPA was defined as an additional amino acid, B, that has a mass of 251.09 Da. Methionine oxidation and cysteine iodoacetamide alkylation were variable modifications. Results were validated using Peptide Prophet (Keller et al., 2002). After filtering using a 1% False Discovery Rate (FDR, based on PeptideProphet probabilities) and a minimum of 2 Peptide Spectral Match (PSM), this yields a protein database for the sample.

Second, crosslinks in the UV-treated samples were identified using Kojak (Hoopmann et al., 2015) and the protein database for the sample. The Kojak search settings matched those described for the Comet searches expect the precursor tolerance was 15 ppm and enzyme selection rules were used. For the trypsin digested samples, the preexisting trypsin setting was used. For the trypsin-GluC digested samples, the cleavage sites of D and E were added to the trypsin settings. Crosslinks were defined as from BPA to any residue with no mass change. Crosslink results were validated using PeptideProphet. For ions of each charge state, probabilities were determined using PeptideProphet and were used to define the thresholds used to filter results to a 1% FDR. For histograms, each PSM was associated with the residue that was assigned the highest probability of

participating in a crosslink with BPA. When more than one residue was assigned the same probability, an equal fraction of that PSM was assigned to each of those residues.

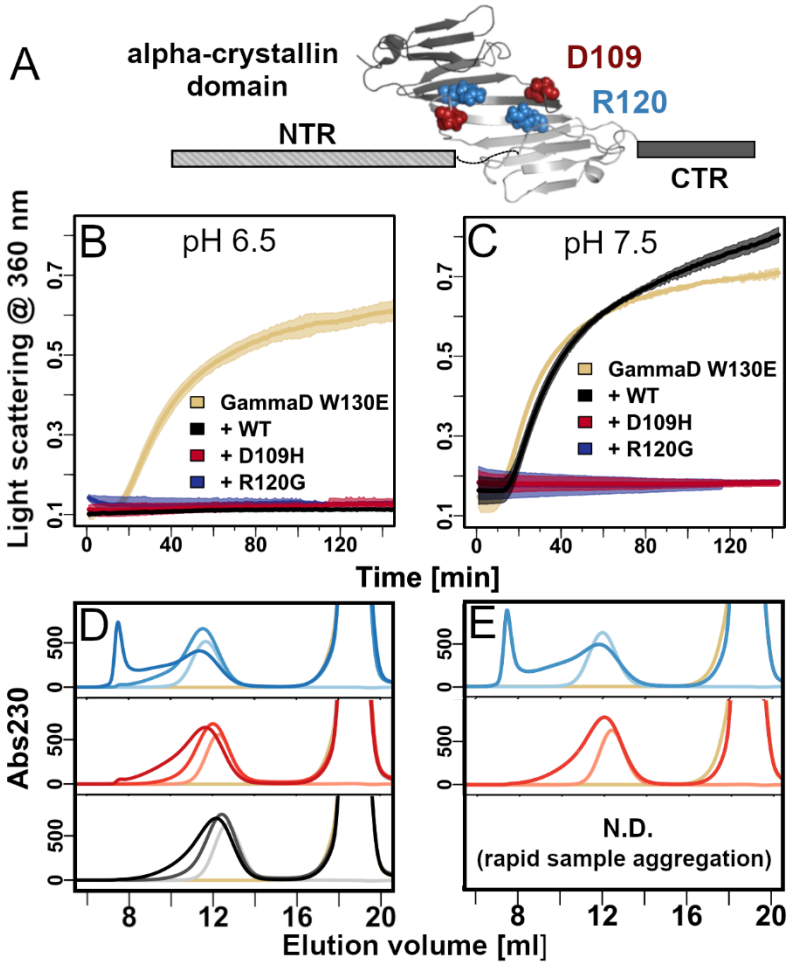

Figure 2.1. HSPB5 disease-associated mutants are activated chaperones against GammaD-crystallin W130E. A) Domain architecture of human HSPB5 N-terminal region (NTR), a-crystallin domain (ACD, PDB: 2N0K), and C-terminal region (CTR). The NTR and CTR were omitted from one ACD protomer for clarity. Side chains of disease-associated mutation sites R120 (blue) and D109 (red) are shown as spheres. B) GammaD aggregation assay conducted at pH 6.5. 500 µM GammaD W130E (yellow) was incubated alone or in the presence of 100 µM HSPB5 WT (full length; black), HSPB5 ACD (gray), or HSPB5 ACD-CTR (cyan) at 37 °C. Aggregation was monitored by absorbance at 360 nm. C) GammaD aggregation assay conducted at pH 7.5. 500 µM GammaD W130E (yellow) was incubated alone or in the presence of 100 µM HSPB5 WT (black), HSPB5 D109H (red), or HSPB5 R120G (blue) at 37 °C. D) Size exclusion chromatography of co-incubated samples containing GammaD W130E and HSPB5. In each panel the lightest color trace is for 100 µM HSPB5 WT (grey), R120G (light blue), or D109H (light red) incubated at 37 °C for one hour at pH 6.5. Darker shades show samples co-incubated with 500 µM GammaD W130E for 1 hour (medium shade) or 3 hours (darkest shade). 500 µM GammaD W130E injected without pre-incubation is shown in yellow in all panels. E) Same as D but co-incubations were performed at pH 7.5 for 1 hour.

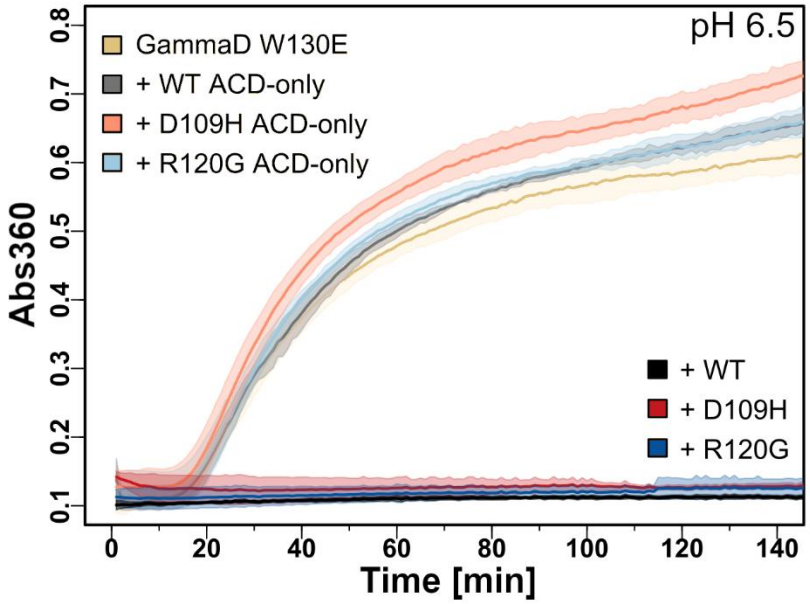

Figure 2.2. HSPB5 disease-associated mutations do not impart chaperone activity to the isolated ACD-only dimer. GammaD aggregation assay conducted in pH 6.5 buffer at 37 °C. All curves are replotted from figure 2.1 panel B except D109H ACD (peach) and R120G ACD (sky blue).

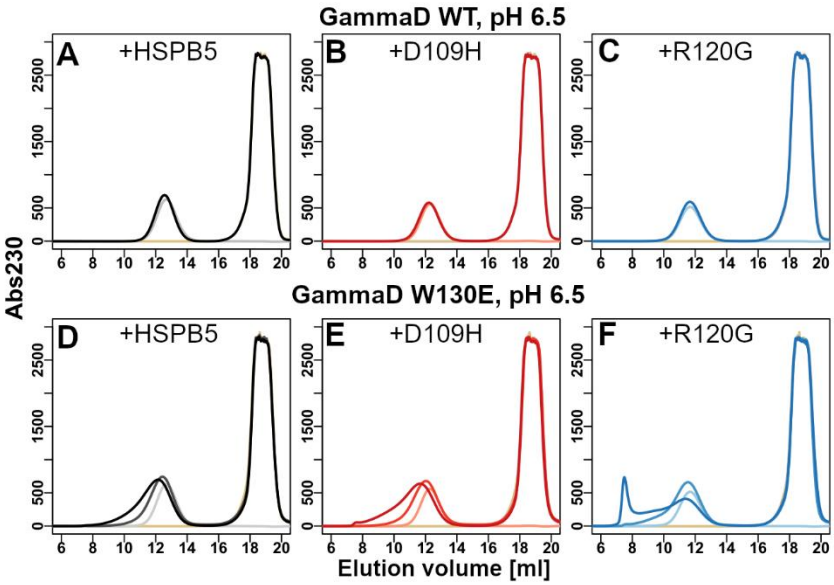

Figure 2.3. HSPB5 WT and disease-associated mutants bind destabilized but not WT GammaD. HSPB5 WT (A, black), D109H (B, red), or R120G (C, blue) were incubated alone or with GammaD WT for 3 hours at 37 °C in pH 6.5 buffer and then injected on a Superose6 column. Comparable data from co-elution experiments with GammaD W130E are plotted again below (same as Figure 2.1 panel D).

Figure 2.4. Alignment of human sHSP sequences. Alignment of human HSPB5, HSPB1, HSPB2, HSPB3, HSPB4, HSPB6, and HSPB8 amino acid sequences. The full sequence of each was used for alignment. HSPB5 residue numbers are shown above. Top, amino terminus through the N-terminal region Conserved sub-region, with the conserved sequence underlined in black and the aspartate that interacts with the ACD central groove highlighted in red. Bottom, region corresponding to HSPB5 ACD β-strands 5 and 6/7 with the positions of D109 (red) and R120 (blue) indicated.

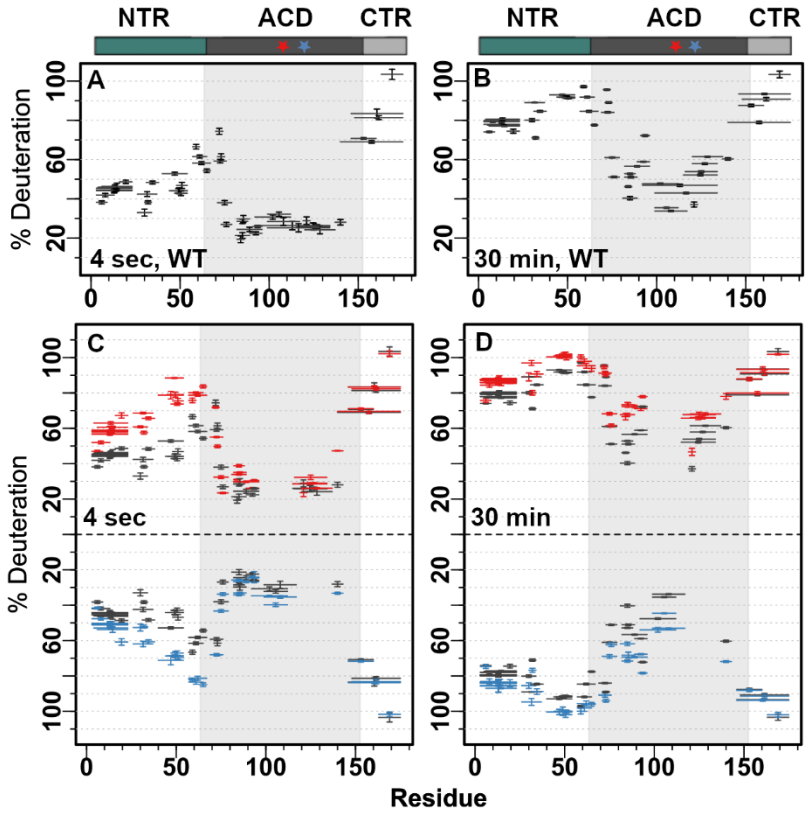

Figure 2.5. Hydrogen/Deuterium exchange reveals long-range effects of HSPB5 ACD mutations on oligomer structure and dynamics. A) Percent deuteration of HSPB5 WT at the 4 sec timepoint or B) 30 min timepoint relative to a fully deuterated control sample. Horizontal bars indicate exchangeable residues for each peptide, with the peptide center shown as a square. Y-axis error bars show standard deviation of all technical replicates. C) Percent deuteration of HSPB5 D109H (red, upper panel) or R120G (blue, lower panel) at the four second or D) 30 min timepoint. Data for HSPB5 WT are replotted in panels C and D (black). Domain boundaries are shown above the plots with ACD mutation sites marked with red (D109H) or blue (R120G) stars. The ACD boundaries are indicated in each plot by the gray inset.

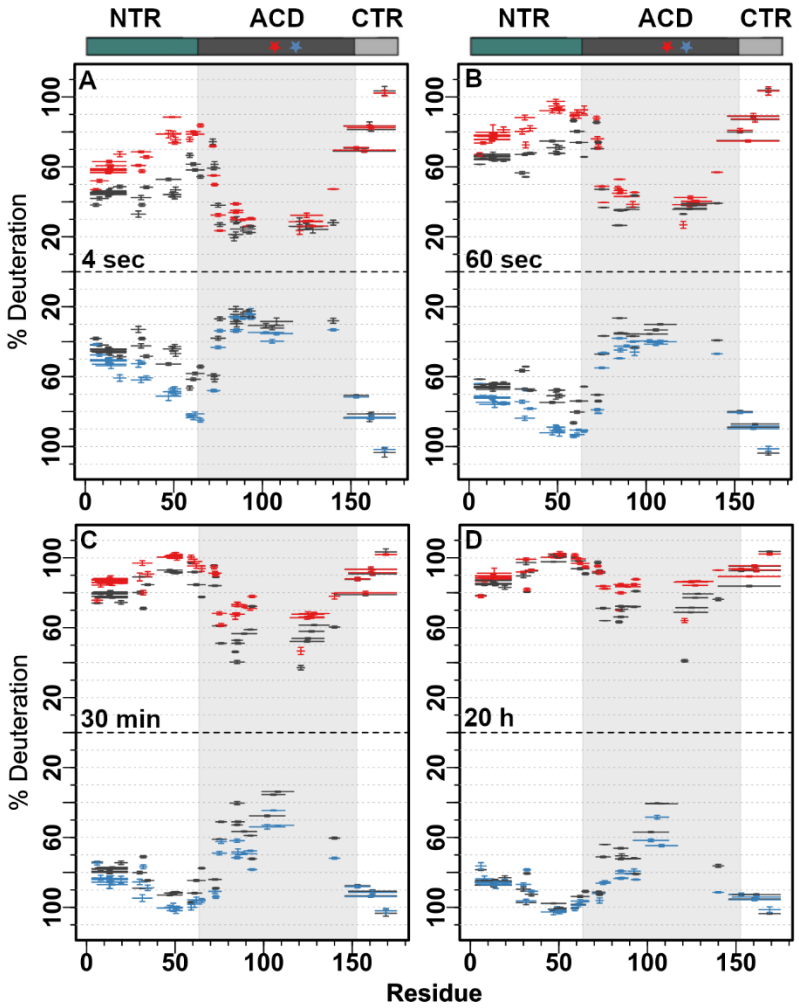

Figure 2.6. All Hydrogen/Deuterium exchange data for HSPB5 WT and mutants. Percent deuteration of HSPB5 WT (black), D109H (red), or R120G (blue) at the A) 4 second, B) 1 minute, C) 30 minute, or D) 20 hour time point. X-axis error bars indicate exchangeable residues for each peptide and the square denotes the peptide center. Y-axis error bars show standard deviation of all technical replicates.

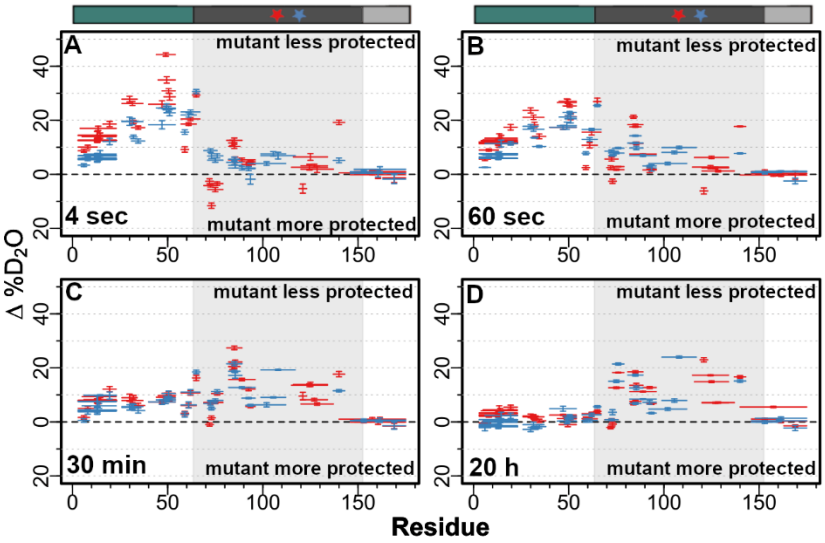

Figure 2.7. Change in ACD mutant percent deuteration relative to HSPB5 WT. Change in percent deuteration (calculated as mutant % Deuteration minus WT % Deuteration) versus HSPB5 residue number for the A) 4 second, B) 1 minute, C) 30 minutes and D) 20 hour time points. HSPB5 D109H is plotted in red, HSPB5 R120G is plotted in blue.

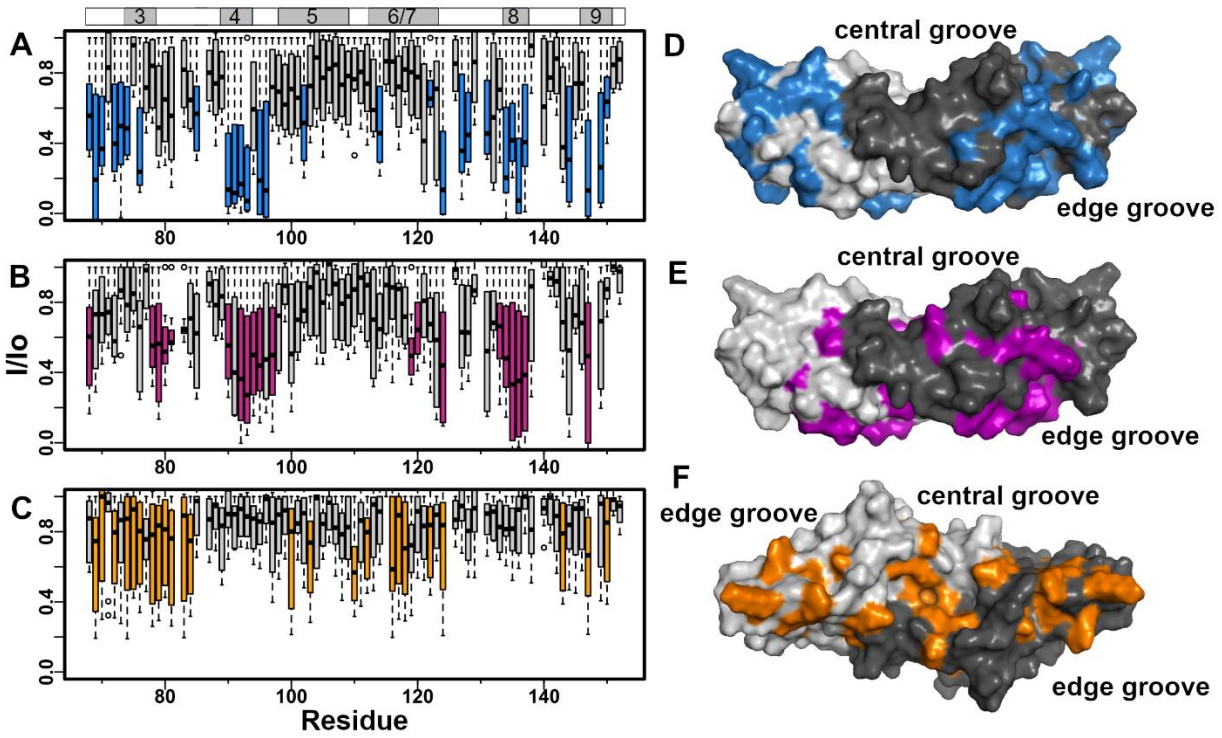

Figure 2.8. HSPB5 NTR- and CTR-derived synthetic peptides interact with ACD grooves. Solution NMR was used to determine the effects of NTR-derived peptides titrated into samples containing ^{15}N-ACD-only dimer. NMR peak intensity of HSPB5 WT ACD-only in the presence of peptides relative to ACD-only alone (I/Io) versus HSPB5 ACD residue number is presented as box plots. The Distal (panel A, blue, residues 1-13), CTR (panel B, pink, residues 155-167), and Conserved (panel C, orange, residues 17-34) peptides generated perturbations that could be mapped to distinct surfaces on the ACD. Significant effects are plotted on the HSPB5 ACD-only structure (PDB 2N0K). Note that the ACD structure in panel C is rotated 90 degrees downward relative to the views in panels A and B.

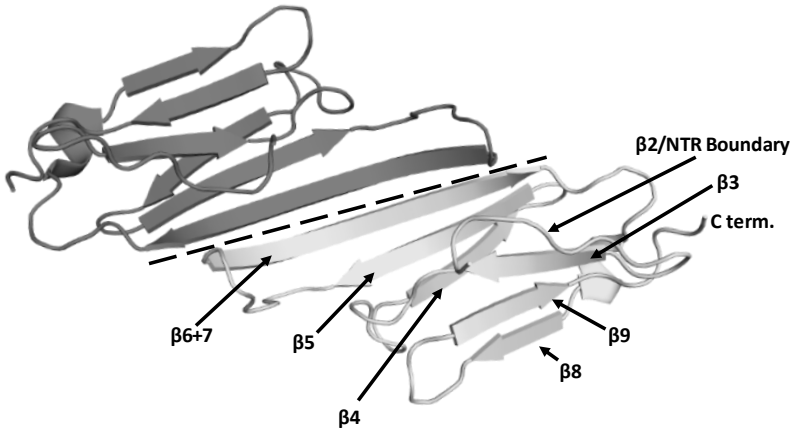

Figure 2.9. Structure of HSPB5 WT ACD-only dimer calculated from solution NMR restraints (PDB 2N0K, Rajagopal et al., 2015a). The dimer interface is marked with a dashed black line. Beta strands 2 through 9, which comprise the entirety of the ACD, are labeled. The N-terminal boundary and C-terminus are indicated.

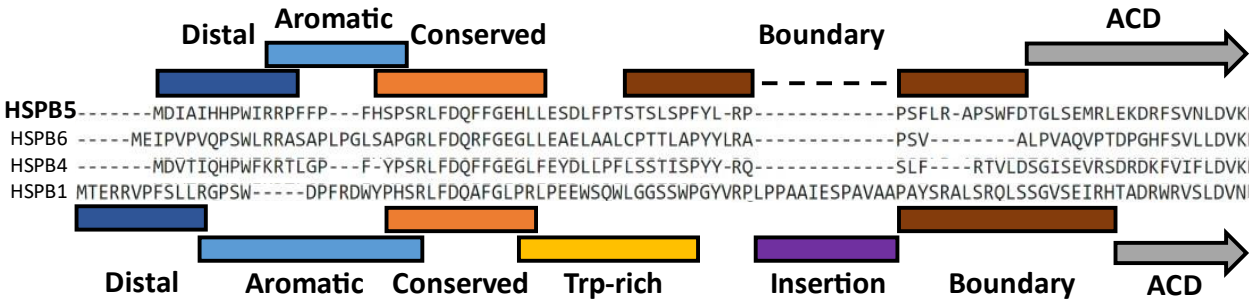

Figure 2.10. Alignment of human HSPB5, HSPB1, HSPB4, and HSPB6 N-terminal Region amino acid sequences created using Clustal Omega. HSPB5 NTR-derived synthetic peptides used in this study are shown above the sequence and HSPB1 NTR-derived synthetic peptides used in (Clouser et al., 2019) are shown below. The start of the ACD for HSPB5 and HSPB1 is indicated by a gray arrow.

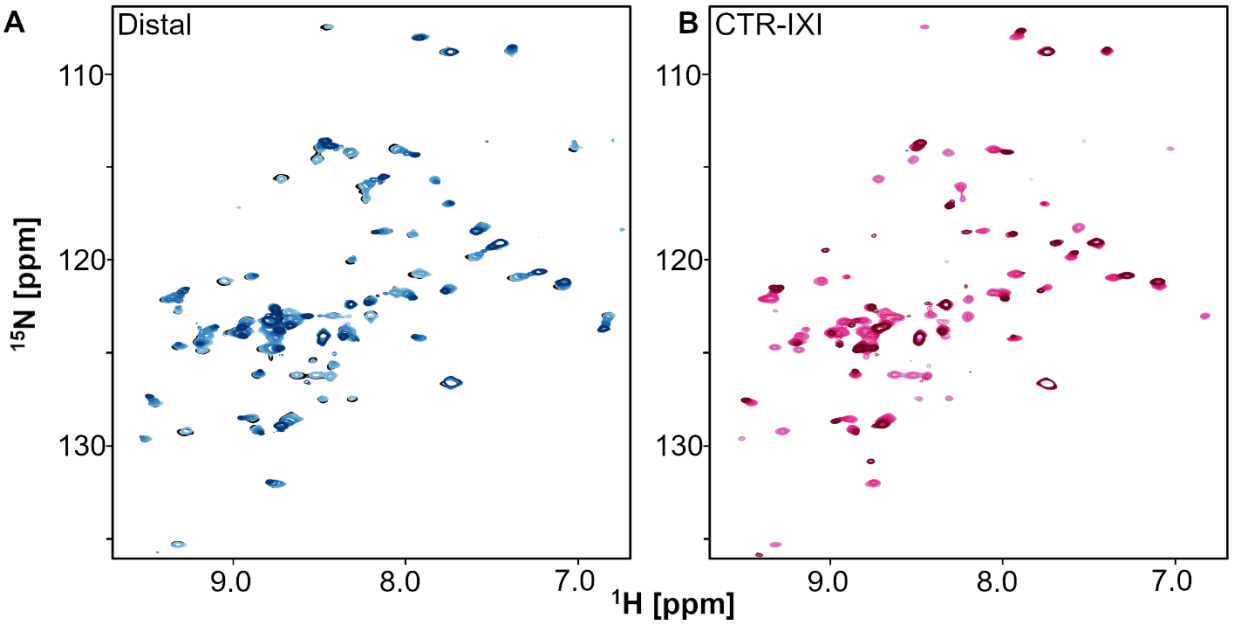

Figure 2.11. Titration series of 200 mM HSPB5 ACD-only WT in 25mM MOPS, 100mM NaCl, pH 7.5. A) Titration with 0.085, 0.1, 0.25, 0.5, 1, 2, and 3 molar equivalents of Distal peptide (HSPB5 residues 1-13). B) Titration with 0.05, 0.1, 0.25, 0.5, 1, 2, and 3 molar equivalents of CTR-IXI peptide (HSPB5 residues 155-167). ACD-only with no peptide added is shown in black, then increasing amounts of peptide are shown in a gradient from light color to dark. All titration points contain less than 1% DMSO (v/v).

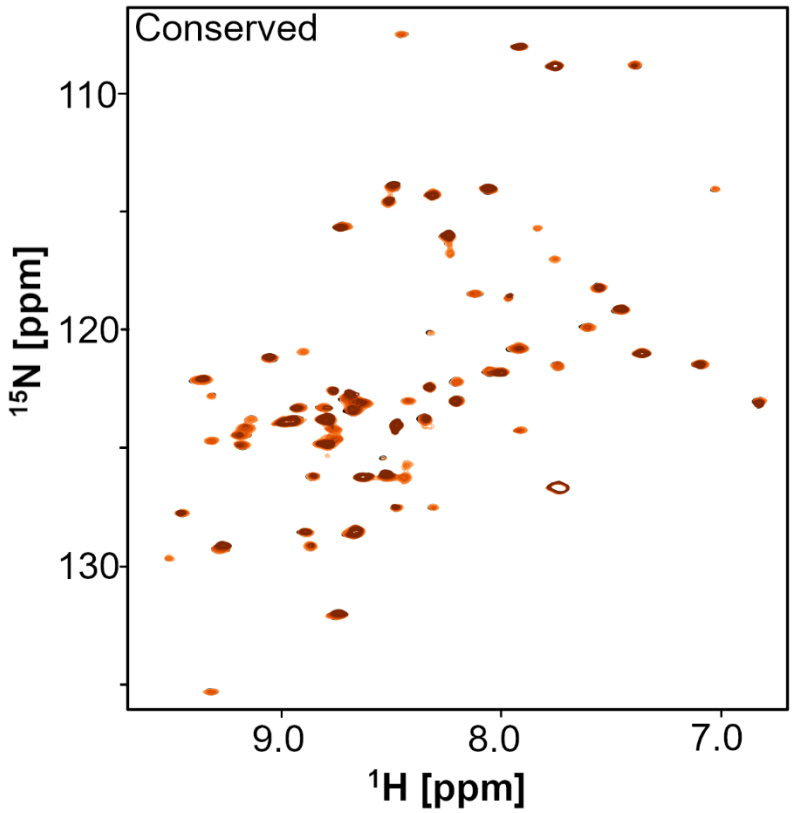

Figure 2.12. Titration series of 200mM HSPB5 ACD-only WT in 25mM MOPS, 100mM NaCl, pH 7.5. Titration with 0.05, 0.1, 0.25, 0.5, 1, 2, 3, and 4 molar equivalents of Conserved peptide (HSPB5 residues 17-34). ACD-only with no peptide added is shown in black, then increasing amounts of peptide are shown in a gradient from light color to dark. All titration points contain less than 1% DMSO (v/v).

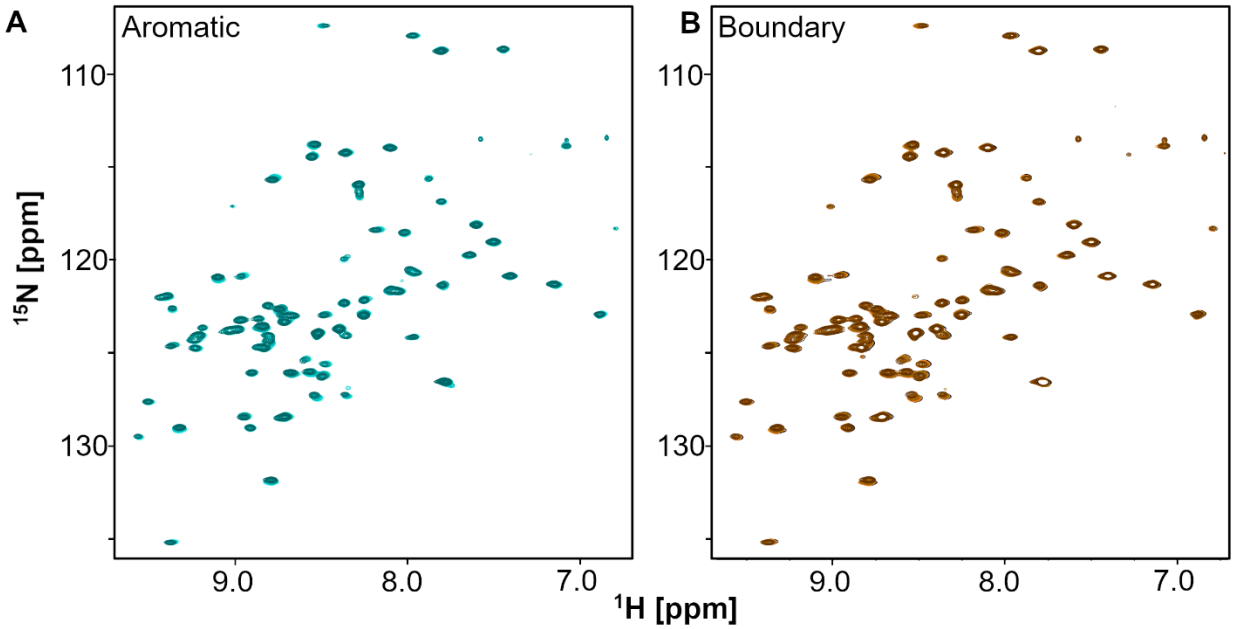

Figure 2.13. Titration series of 200uM HSPB5 ACD-only WT in 25mM MOPS, 100mM NaCl, pH 7.5. A) Titration with 0.25, 0.5, 1, 2.5, and 5 molar equivalents of Aromatic peptide (HSPB5 residues 11-22). B) Titration with 0.25, 0.5, 1, and 2.5 molar equivalents of Boundary peptide (HSPB5 residues 41-62). ACD-only with no peptide added is shown in black, then increasing amounts of peptide are shown in a gradient from light color to dark. All titration points contain less than 1% DMSO (v/v).

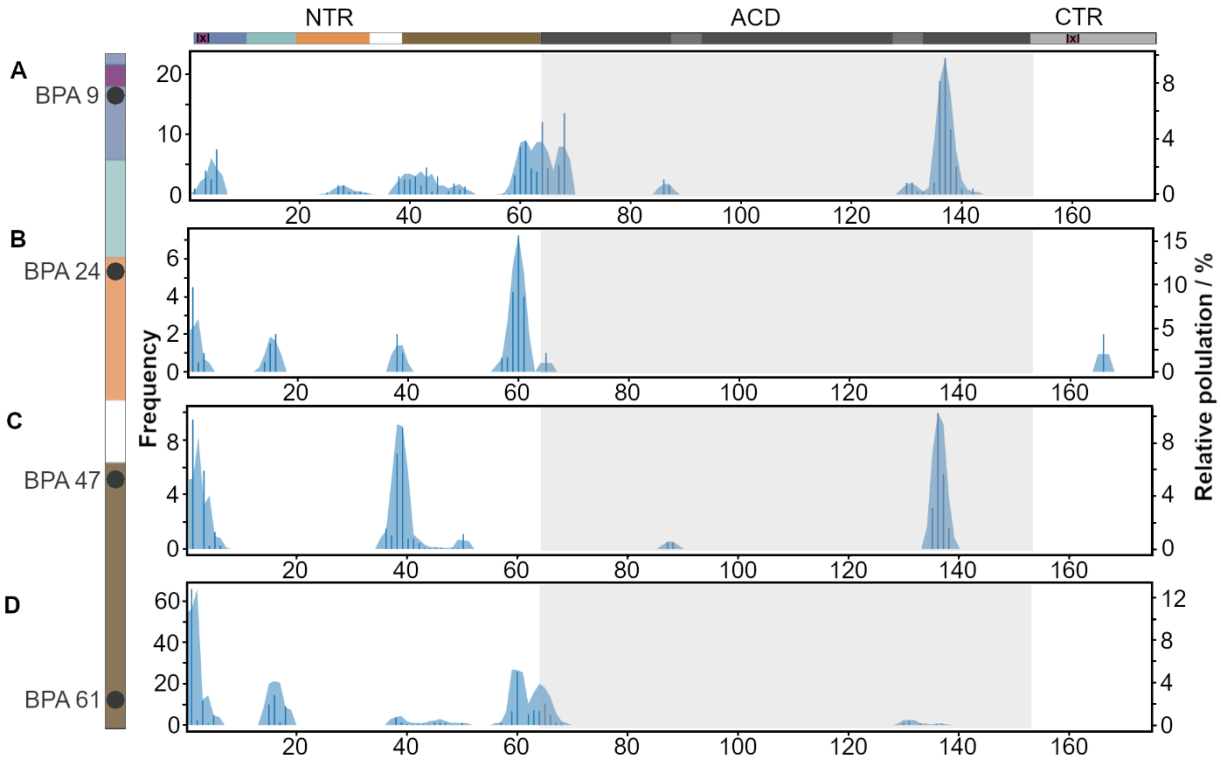

Figure 2.14. BPA cross-linking reveals HSPB5 NTR interactions. Amber codon suppression was used to install the photo-activatable cross-linker p-benzoyl-l-phenylalanine (BPA) in full length HSPB5 at residues A) 9, B) 24, C) 47, or D) 61. Cross-links formed between BPA and other sites in HSPB5 are shown in blue. Bars indicate the total number of peptide spectral matches for each crosslink identified and blue shading shows the relative number of crosslinks in a 3-residue sliding window. HSPB5 domain boundaries are shown and NTR sub-regions are colored for the Distal (dark blue), Aromatic (light blue), Conserved (orange), and Boundary (brown). The ACD boundaries are indicated by a light gray inset and the ACD edge groove is colored in dark gray. Ile-X-Ile motifs in the NTR Distal sub-region and CTR are indicated in purple.

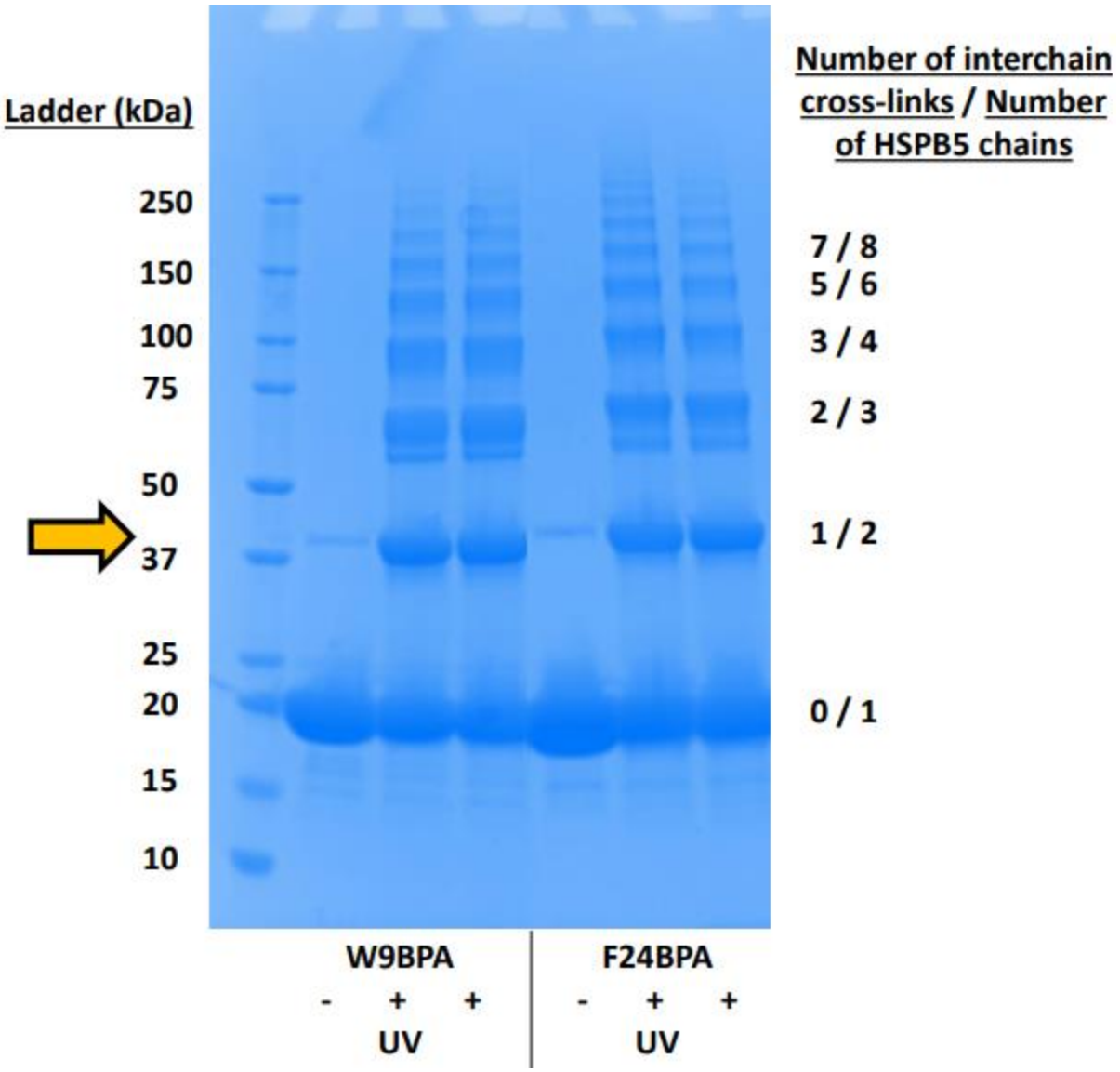

Figure 2.15. UV cross-linking reactions for HSPB5 BPA mutants W9BPA and F24BPA. HSPB5 BPA mutants were incubated at 4 °C with (+) or without (-) exposure to 360 nm UV light. The band with one intermolecular cross-link (identified by gold arrow) was selected for in-gel digestion.

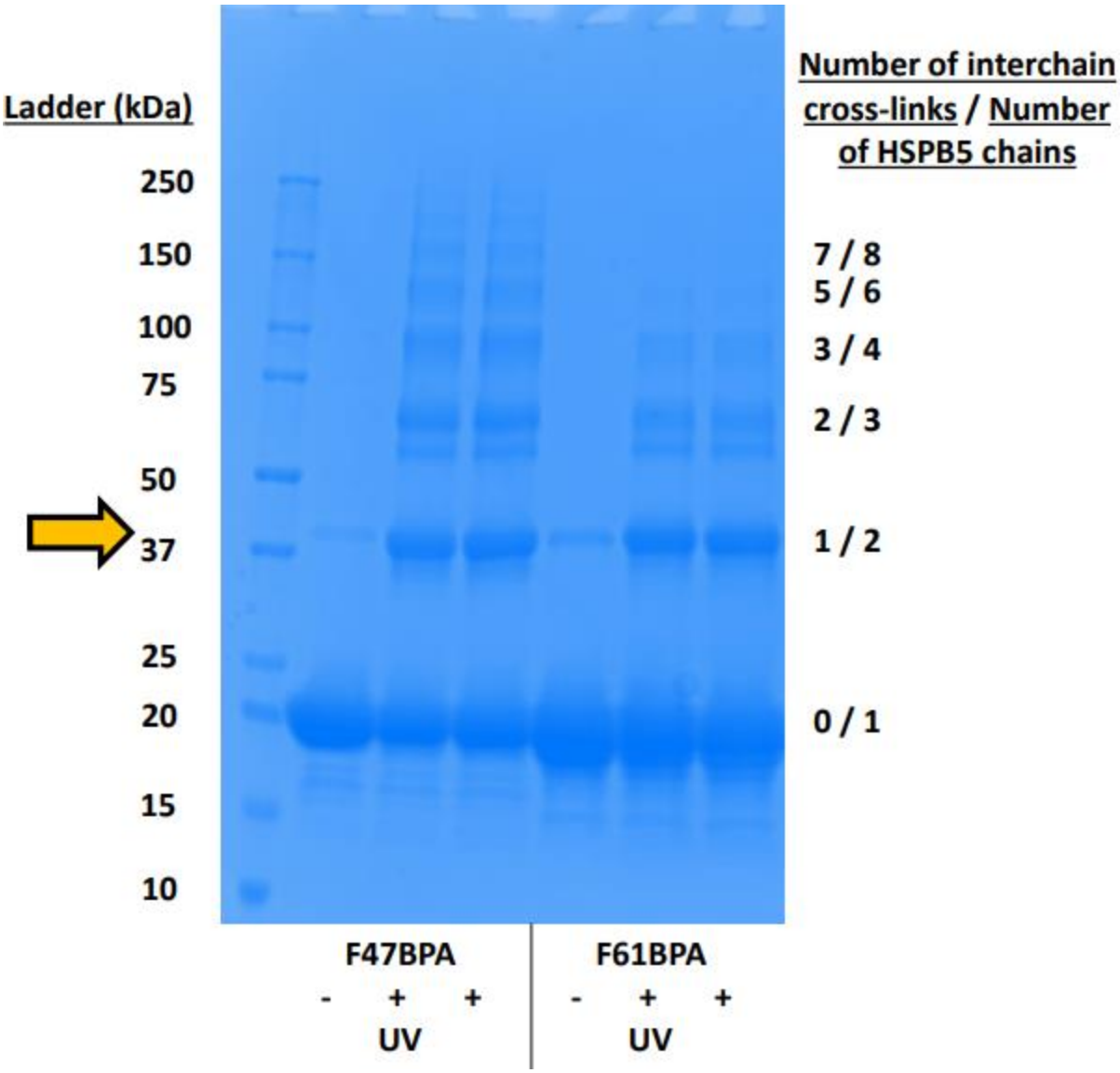

Figure 2.16. UV cross-linking reactions for HSPB5 BPA mutants F47BPA and F61BPA. HSPB5 BPA mutants were incubated at 4 °C with (+) or without (-) exposure to 360 nm UV light. The band with one intermolecular cross-link (identified by gold arrow) was selected for in-gel digestion.

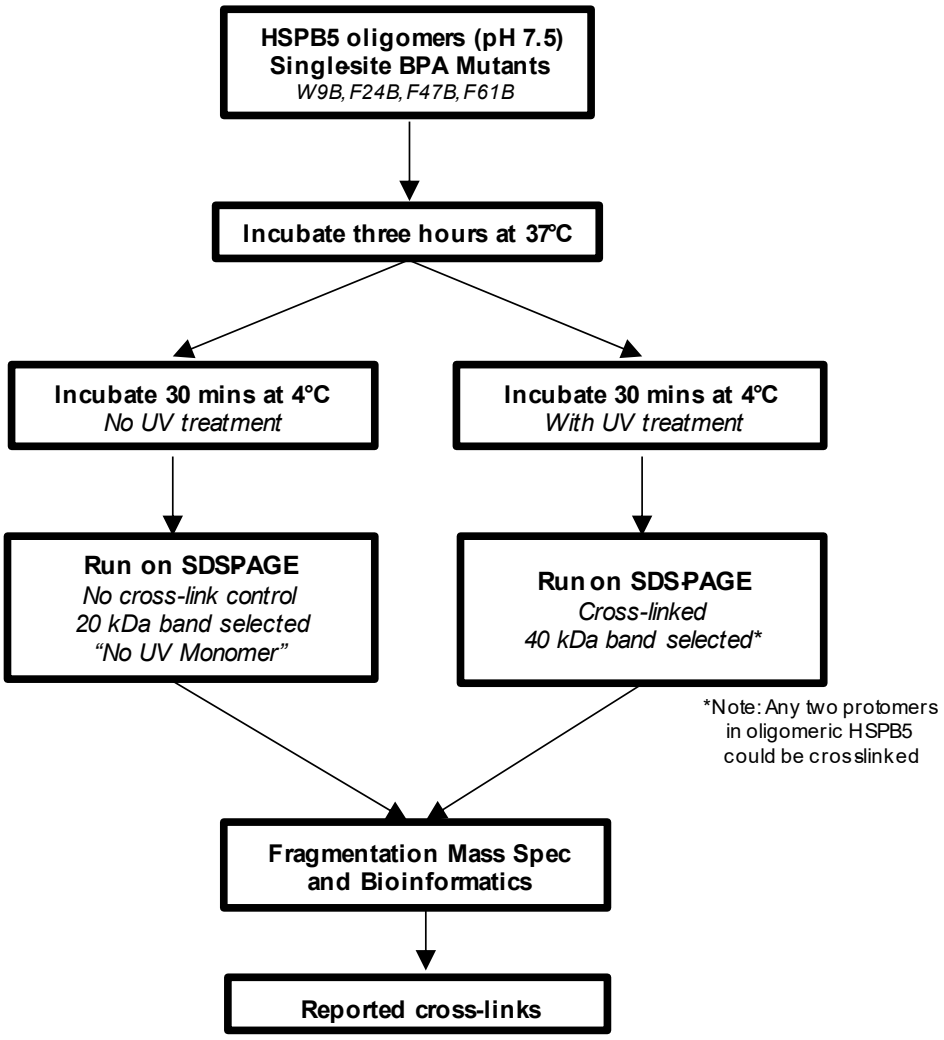

Figure 2.17. Workflow for BPA cross-linking experiments.

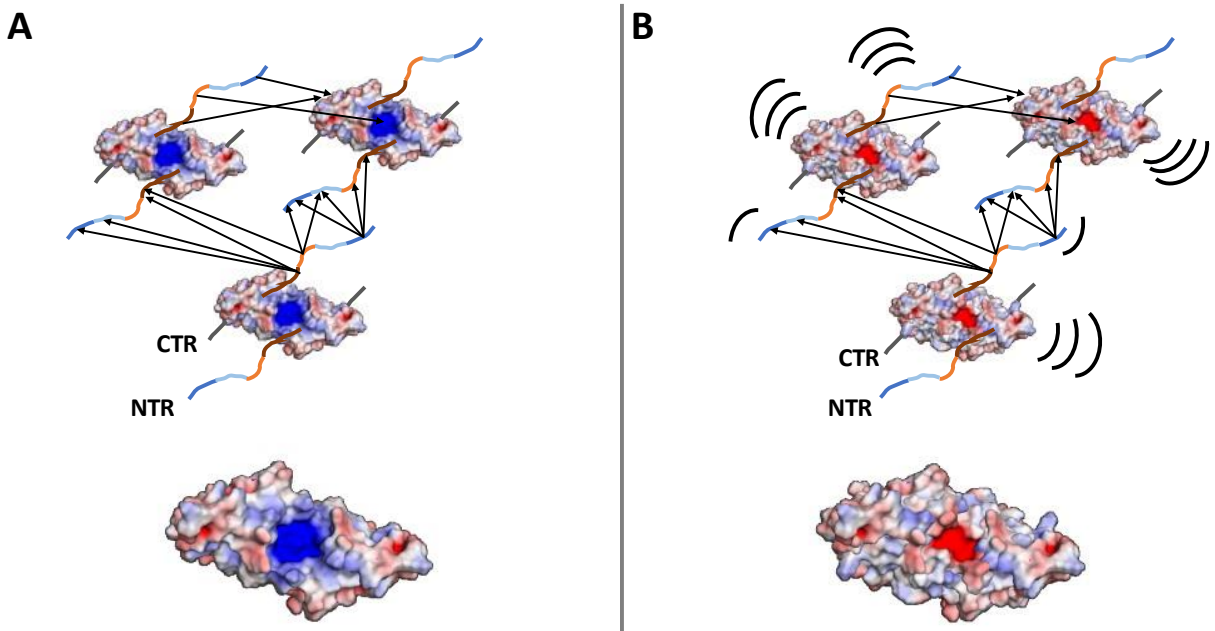

Figure 2.18. Summary of HSPB5 interactions and changes imparted by the R120G and D109H mutations. Specific NTR to NTR and NTR to ACD interactions (black arrows) determined for HSPB5 WT (A) and inferred for HSPB5 R120G (B). APBS electrostatics images are shown below for HSPB5 WT ACD-only (PDB: 2N0K) and R120G ACD-only (PDB: 6BP9) solution NMR ensembles, revealing a change in the central groove charge from positive to negative. The R120G and D109H mutations decrease structure and/or increase dynamics of the NTR and ACD (curved black lines).

Chapter 3. DISORDERED REGION ENCODES ALPHA-CRYSTALLIN CHAPERONE ACTIVITY TOWARDS LENS CLIENT GAMMAD-CRYSTALLIN

[Adapted from Woods, Ulmer, Bush, Guttman, and Klevit (2022) "Disordered Region Encodes α-crystallin Chaperone Activity Towards Lens Client γD-crystallin" (submitted)]

Abstract:

Small heat shock proteins (sHSPs) are a widely expressed family of ATP-independent molecular chaperones that are among the first responders to cellular stress. Mechanisms by which sHSPs delay aggregation of client proteins remain undefined. sHSPs have high intrinsic disorder content of up to ~60% and assemble into large, polydisperse homo- and hetero-oligomers, making them challenging structural and biochemical targets. Two sHSPs, HSPB4 and HSPB5, are present at millimolar concentrations in eye lens, where they are responsible for maintaining lens transparency over the lifetime of an organism. Together, HSPB4 and HSPB5 compose the hetero-oligomeric chaperone known as α-crystallin. To identify determinants of sHSP function, we compared the effectiveness of HSPB4 and HSPB5 homo-oligomers and HSPB4/HSPB5 hetero-oligomers in delaying the aggregation of the lens client protein γD-crystallin. In chimeric versions of HSPB4 and HSPB5, chaperone activity tracked with the identity of the 60-residue disordered N-terminal regions (NTR). A short 10-residue stretch in the middle of the NTR ("Critical sequence") contains three residues that are responsible for high HSPB5 chaperone activity towards γD-crystallin. These residues affect structure and dynamics throughout the NTR. Abundant interactions involving the NTR Critical sequence reveal it to be a hub for a network of interactions within oligomers. We

propose a model whereby the NTR Critical sequence influences local structure and NTR dynamics that modulate accessibility of the NTR, which in turn modulates chaperone activity.

3.1 INTRODUCTION

The ATP-independent small heat shock protein (sHSP) chaperone family plays important roles in protein homeostasis in all tissues in humans (Carra et al., 2017). Interactions with client proteins are generally believed to be transient, and detailed understanding of sHSPs is limited by their tendency to form large, heterogenous, and structurally polydisperse oligomers (Janowska et al., 2019). Two highly-related sHSPs which have such properties, called HSPB4 and HSPB5, are present at millimolar levels in eye lens and form mixed oligomers in a 3:1 molar ratio (α-crystallin; Horwitz et al., 1999). Together, HSPB4 and HSPB5 promote proper vision by preventing formation of insoluble protein aggregates, or cataract, a leading cause of blindness worldwide (Hashemi et al., 2020). Therefore, it is of great interest to understand how these sHSPs interact with their lens clients and how these interactions are modulated.

All sHSPs consist of a central α-crystallin domain (ACD) that is structurally conserved and N- and C-terminal Regions (NTR and CTR) that differ in sequence and length and are presumed to be disordered (Delbecq and Klevit, 2013; Clark et al., 2011; Bagnéris et al., 2009). The ACD forms an antiparallel dimer that is considered the building block of sHSP oligomers. Interactions involving the NTR and CTR drive oligomer formation, and the NTR has been reported to be required for productive interactions with some client proteins (Peschek et al., 2013; Baughman et al., 2020; Mainz et al., 2015). Involvement of the NTR in chaperone activity is supported by its sequence characteristics: rich in hydrophobic and aromatic segments interspersed by proline residues. We showed that the NTR of HSPB5 is required for productive interactions with lens

client protein γD-crystallin (Chapter 2). Among human sHSPs, the NTRs of HSPB4 and HSPB5 are most similar (67.6% similarity vs 49.3% for next most similar sHSP pair; Figure 3.1). As HSPB4 and HSPB5 are both expressed in lens, we hypothesized that comparing their ability to chaperone lens clients could offer insight into their mechanism of action.

High stability of lens proteins prevents their use in sHSP activity assays at physiological temperature, but the development of a γD-crystallin mutant that mimics a photodamaged, aggregation-prone state enables such assessments (γD-W130E; Serebryany et al., 2016). Although γD-W130E remains folded at 37 °C, it can undergo rare conformational excursions that lead to aggregation in a time and concentration-dependent manner. We used γD-W130E to compare the chaperone activity of HSPB4 and HSPB5 under mildly acidic conditions as found in lens (Bassnett and Duncan, 1985; Mathias et al., 1991). We find that HSPB4 and HSPB5 have markedly different abilities to prevent the aggregation of γD-W130E and that mixed HSPB4/HSPB5 oligomers have activity most closely resembling that of HSPB4. Through use of chimeric constructs, we have identified three NTR residues that account for most of the observed difference in chaperone activity. The identity of these residues influences structure and dynamics of the entire NTR in a manner that trends with chaperone activity. Our results reveal that NTR structure, dynamics, and interactions can be modulated by a remarkably small number of amino acid identities within a long, disordered region and these in turn affect the accessibility of binding sites for client.

3.2 RESULTS

3.2.1 *HSPB4 and HSPB5 have different chaperone activity towards lens client γD-crystallin*

The major eye lens chaperone is α-crystallin, a hetero-oligomer composed of two sHSPs, HSPB4 and HSPB5 in a 3:1 ratio (Horwitz et al., 1999). We compared the ability of HSPB4 and

HSPB5, both individually and as mixed oligomers, to delay and/or inhibit aggregation of a γD-crystallin mutant (γD-W130E) that is aggregation prone at 37 °C (Serebryany et al., 2016).

In all experiments, we used HSPB4 with its two native cysteine residues mutated to serine (hereto referred to as HSPB4) to prevent possible disulfide exchange with client, as was observed for clients p53 and MDH during in vitro chaperone activity assessments (Kaiser et al., 2019). At pH 6.5 and 37 °C, γD-W130E aggregates spontaneously as evidenced by time-dependent increase of A360 (Figure 3.2 A). The presence of 15 μM HSPB4 or HSPB5 had markedly different effects on the aggregation time course (Figure 3.2 A). Whereas HSPB5 delayed aggregation for over 2 hours, HSPB4 had little effect and led to increased A360 at later stages of the assay, indicating that only HSPB5 has high chaperone activity against γD-W130E under the experimental conditions. As HSPB4 appeared inactive, we also assessed HSPB4 at a 4-fold higher concentration (60 μM) and found that it displays activity, albeit much lower than that of HSPB5 (Figure 3.3). To test the chaperone activity of HSPB4/HSPB5 hetero-oligomers, 15 μM HSPB5 was equilibrated with 45 μM HSPB4 for 1 hour at 37 °C prior to its addition to γD-W130E to allow hetero-oligomers to form. Surprisingly, the HSPB4/5 mixture exhibited chaperone activity more like HSPB4, despite containing a concentration of HSPB5 that is highly effective on its own (Figure 3.2 B). The results demonstrate that HSPB4 and HSPB5 have substantially different chaperone activity towards γD-W130E and that HSPB4-like ("B4-like") chaperone activity dominates in a physiologically relevant mixture of HSPB4 and HSPB5.

The above results raise the question of what region(s) and/or properties of HSPB5 contribute to the observed enhancement in chaperone activity. HSPB4 and HSPB5 are the two most highly related of the ten human sHSPs, with highest sequence similarity within the structurally-conserved α-crystallin domain (ACD). Among all sHSPs, sequence divergence is highest within the

disordered N- and C-terminal regions (NTR, CTR). Based on previous studies that revealed that the NTR of HSPB5 is required for its chaperone activity against γD-W130E (Woods et al., 2022), chimeric constructs were created in which the NTRs of HSPB4 and HSPB5 were swapped, taking care to design the boundary between the NTR and ACD to retain the entire structured ACD intact ("N4-B5" has the NTR of HSPB4 swapped onto HSPB5, "N5-B4" is the alternate chimera; Figure 3.4). A similar approach was previously taken, but that work used a restriction endonuclease site within the HSPB4 and HSPB5 genes to facilitate cloning, resulting in the first ~15 ACD residues also being swapped (Kumar and Rao, 2000). Under identical experimental conditions as above, N4-B5 has B4-like activity and N5-B4 has B5-like activity (Figure 3.2 A). Thus, the observed chaperone activity follows the NTR identity. Furthermore, the results suggest that the activity afforded by the HSPB5 NTR is modulated in the context of mixed HSPB4/HSPB5 oligomers.

3.2.2 *Sequence identity of the Middle NTR sub-region has a dominant effect on chaperone activity*

To further parse the NTRs of HSPB4 and HSPB5, the ~60-residue region was sub-divided into three essentially equal parts, named based on their position relative to the structured ACD: the Distal sub-region (residues 1-19), the Middle sub-region (residues 20-42), and the Proximal sub-region (residues 43-62) (Figure 3.1). New chimeric proteins were generated in which a single sub-region from one sHSP was inserted into the other sHSP, creating, for example, "455-B5" which contains the Distal residues of HSPB4 and the Middle and Proximal residues of HSPB5 in the context of HSPB5 ACD/CTR and so forth. Relative to HSPB5, 455-B5 has 10 amino acid substitutions (all within the first 19 residues), 545-B5 has six (all within residues 20-42), and 554-B5 has 14 (all within residues 43-62).

The chaperone activity of each chimera towards γD-W130E was compared to those of HSPB4 and HSPB5. Swapping the Distal sub-region has no discernable effect, as 455-B5 has B5-like activity (Figure 3.2 B). In contrast, swapping either the Middle or Proximal sub-regions of HSPB4 into HSPB5 (545-B5 and 554-B5, respectively) resulted in B4-like activity (Figure 3.2 A and B), suggesting that these NTR sub-regions could be responsible for the observed difference in activity. Importantly, the C-terminal portion of the HSPB5 Proximal NTR is a transiently-ordered continuation of the ACD β-sandwich structure, raising the possibility that installing the Proximal sub-region of one sHSP onto the ACD of a different sHSP could result in a "mismatch" at the edge of the β-sheet (Jehle et al., 2011). To test this possibility explicitly, a 554-B4 chimera was generated. The 554-B4 chimera exhibited high chaperone activity (i.e., was B5-like; Figure 3.2 B), providing strong support for the notion that the low activity observed for 554-B5 likely results from a mismatch between the ACD and Proximal NTR rather than the Proximal sub-region being directly responsible for chaperone activity. Taken together, we conclude that the Middle sub-region is predominantly responsible for the lower activity that results from installing the NTR of HSPB4 into HSPB5.

To test if the converse is true, i.e., whether swapping the Middle sub-region of HSPB5 into HSPB4 enhances chaperone activity, we installed the HSPB5 Middle sub-region into HSPB4 (454-B4). Although this alteration does not completely restore chaperone activity, the construct is substantially more active than HSPB4 and is therefore more B5-like (Figure 3.2 A). The first half of the Middle sub-region contains the only conserved sequence among sHSP NTRs (Conserved sequence), whereas the second half contains sequence that is only partly conserved in HSPB4 and HSPB5 (Figure 3.1). Thus, the enhancement of activity afforded by installation of HSPB5's NTR

Middle sub-region is brought about by a small number of amino acid differences in the second half of this sub-region.

Comparing the two sHSPs, the 10-residue sequence of the C-terminal half of the Middle sub-region contains six differences, at positions H31G/L33F/S35Y/F38L/T40L and an inserted Phenylalanine between residue 39 and 40. A triple mutant that substitutes three residues of HSPB4 into HSPB5 (H31G/L33F/S35Y; "B5-GFY") had a similar effect to swapping the entire Middle sub-region (i.e. 545-B5; Figure 3.2 B). We tested all combinations of double mutants at these positions; all exhibited lower activity than HSPB5 WT, but all were more active than B5-GFY and HSPB4 WT (Figure 3.2 B). Thus, the B5-GFY triple mutant contains a minimal set of sequence substitutions necessary for the observed difference in chaperone activity between HSPB4 and HSPB5 WT. The results clearly reveal a dominant role for the C-terminal half of the Middle NTR, which we will refer to from here on as the Critical sequence. Putting this new insight into the context of mixed HSPB4/HSPB5 (wild-type) oligomers, we hypothesize that the observed modulation of HSPB5 chaperone activity is due to the action of the HSPB4 Critical sequence on HSPB5 subunits.

To test the generality of the effect of the Critical sequence on chaperone activity, we installed the Critical sequence swaps H31G/L33F/S35Y into the HSPB5 cataract- and myopathy-associated mutant R120G ("R120G-GFY"; Vicart et al., 1998). This mutant is an enhanced chaperone of γD-W130E and has strongly decreased protection from HDX in the NTR and ACD (Woods et al., 2022). The Critical sequence substitutions strongly decrease R120G chaperone activity (Figure 3.2 B). Therefore, the identity of these three Critical sequence residues can affect the activity of an activated sHSP mutant that has a more dynamic and/or less structured NTR.

3.2.3 *NTR Critical sequence affects structure and dynamics of the entire NTR*

Potential changes in local secondary structure resulting from substitutions in the NTR were assessed by circular dichroism (CD) (Figure 3.5). Spectra of all species are consistent with primarily β-structure, with negative ellipticity that spans from roughly 200 to 250 nm and a minimum near 215 nm. Spectra of N4-B5 and N5-B4 look most similar to HSPB4 and HSPB5, respectively. N5-B4 has roughly 20% less negative ellipticity relative to HSPB4 and N4-B5 has roughly 40% greater negative ellipticity relative to HSPB5, suggesting both chimeras differ in β-structure. Spectra of Middle sub-region swaps and Critical sequence substitutions were compared to assess how identity of the Middle NTR affects secondary structure in HSPB4 and HSPB5. The spectra of 545-B5 and B5-GFY have larger negative ellipticity (by roughly 9%) relative to HSPB5 WT, consistent with a small increase in β-structure content. Conversely, swapping the Middle sub-region of HSPB5 into HSPB4 yields roughly 10% less CD signal than HSPB4, consistent with decreased β-structure content. Finally, structural changes resulting from mixed oligomer formation were assessed by comparison of the CD spectrum of a 3:1 ratio of HSPB4:HSPB5 with a theoretical spectrum calculated from the experimental HSPB4- or HSPB5-only spectra (3x HSPB4 + 1x HSPB5 = B4/B5 mixture). The spectrum of the mixed oligomers has roughly 17% more CD signal at the minimum relative to the theoretical spectrum, consistent with increased β-structure content (Figure 3.6). Taken together, the results indicate that identity of the Critical sequence is a major determinant of chaperone activity and influences secondary structure content, presumably of the NTR, in oligomers.

The large differences in chaperone activity associated with sequence changes in the Middle NTR suggests that the sub-region may modulate availability of client-binding sites. Hydrogen/deuterium exchange coupled with mass spectrometry (HDX-MS) was used to probe

how the sequence changes affect structure and/or dynamics of the entire molecule. HDX measures exchange of backbone amide hydrogens with deuterium when incubated in D_2O-based buffer. The extent of exchange in a region is reflective of its local structure and dynamics. Less structured and/or more dynamic regions exchange rapidly, whereas regions with stable structure and/or low dynamics exchange slowly and are described as protected. Differences in the extent of deuteration for a given region indicate changes in structure and dynamics (Masson et al., 2019).

A range of deuterium uptake was observed for homo-oligomeric assemblies of HSPB4 and HSPB5, with similar patterns of exchange to other reports (Figures 3.7 and 3.8; HSPB1, Clouser et al., 2019; HSPB4, Kaiser et al., 2019; and this work, HSPB5 at pH 7.5, Woods et al., 2022). Peptides derived from the CTR exchange very rapidly, ACD-derived peptides exchange slowly reflecting the stable β-sandwich structure, and peptides from the NTR have intermediate exchange rates. Many more peptides could be followed in the HDX data for HSPB4 and no peptides had identical sequence between HSPB4 and HSPB5, but the exchange patterns of the two sHSPs can be compared qualitatively. A notable difference is for peptides from the Middle NTR, which had deuterium uptake values of ~32-42% in HSPB5 and ~26% in HSPB4 at the 4-second timepoint. Thus, in its native context, the HSPB4 Middle sub-region appears more sequestered or structured than the analogous sub-region in HSPB5, though differences in Middle NTR peptide lengths (and sequence) prevent detailed interpretation. In addition, the Proximal NTR and peptides at the beginning of the ACD are more protected in HSPB4.

To assess the effect of substituting the entire HSPB4 Middle sub-region or three HSPB4 Middle residues into HSPB5, HDX profiles of 545-B5 and B5-GFY were compared to HSPB5. The overall exchange profiles are similar (Figure 3.8). For each peptide of identical sequence observed in the HSPB5 and 545-B5 or B5-GFY datasets, the difference in percent deuteration of

each mutant relative to wild-type was calculated (ΔHDX = Mutant %D – WT %D; Figures 3.9, 3.10, 3.11, and 3.12 lower panels). In all cases where the difference plot shows a significant difference (we consider |ΔHDX| values of ≥ 5% to be significant), ΔHDX values are below zero, meaning that the peptide is more protected in the mutant than in the wild-type context. The entire NTR is affected in both constructs, with the 545-B5 Middle sub-region swap mutant having larger effects than the B5-GFY triple mutant. Higher protection of the Distal and Proximal NTR sub-regions was observed at 4-seconds, 1-minute, and 30-minute exchange time points (Figures 3.9, 3.10, and 3.11 lower panels). In addition, most of the ACD-derived peptides had lower deuterium uptake after 20-hours exchange, though none of the differences were greater than 5% (Figure 3.12 lower panel). Increased protection at long exchange timepoints is suggestive of increased stability of existing structure. Overall, the HDX results reveal that the identity of as few as three residues in the NTR Critical sequence dictate the degree to which the entire NTR is sequestered, structured, and/or dynamic.

The observation that the HSPB4 Middle sub-region can alter the properties of the entire NTR when installed into HSPB5 raises the question of whether the Middle sub-region of HSPB5 can similarly affect the properties of HSPB4 when installed into that context. An analogous analysis was performed on HDX data collected for HSPB4 and the Middle sub-region swap chimera, 454-B4. The ΔHDX plot for the 4-second exchange timepoint is shown in the top panel of Figure 3.9. Substitution of the Middle sub-region of HSPB5 into HSPB4 results in lower protection of all peptides derived from the NTR at 4-second, 1-minute, and 30-minute time points (i.e., ΔHDX > 0; Figure 3.9, 3.10, and 3.11 top panels). Differences are largest near the mutation sites and lowest at the extreme ends of the NTR. Peptic digestion of HSPB4 yielded higher resolution and redundancy than for HSPB5 and revealed extensive changes in the ACD at 30-minute and 20-hour

exchange times. Two clusters of peptides with ΔHDX ≥ 5% were evident around residues ~60-90 and ~128-155, corresponding to the first 30 ACD residues and the last two ACD β-strands (Figures 3.11 and 3.12 top panels). We note that these residues are nearby each other in the ACD structure and constitute the entire "top" sheet of the ACD β-sandwich and the ACD edge groove (strands 2, 3, 4, 8, and 9; Figure 3.13). Low coverage at the ACD dimer interface in fully-deuterated control samples prevented quantitation of changes in percent deuteration there, but direct comparison of deuteration values indicates that swapping of the HSPB5 Middle sub-region into HSPB4 causes increased HDX at the ACD dimer interface at long exchange times (20-hours; Figure 3.14). Altogether, the results demonstrate that sequence changes in the Middle NTR sub-region affect structure and dynamics throughout the entire NTR and in regions of the ACD, with the extent of exchange trending with chaperone activity against γD-W130E.

3.2.4 *HSPB5 NTR Critical sequence interacts directly with other NTR sub-regions*

The observation that mutations in the Middle NTR sub-region affect HDX throughout the NTR implies that the sub-region is involved in interactions with other sub-regions within an oligomer. Polydispersity and high heterogeneity of HSPB5 oligomers are refractory to standard structural investigation, so we adopted a targeted cross-linking mass spectrometry approach to identify interactions involving the Middle NTR. We opted to install p-benzoyl-l-phenylalanine, a non-natural amino acid, at single sites in HSPB5 NTR using amber-codon suppression (BPA; Chin et al., 2002). When excited by UV light, BPA forms covalent bonds to CH- groups in direct contact (within 3 Å), overcoming the relatively long spacer arms of commonly used chemical cross-linkers. The BPA excited state quickly decays to the ground state if no cross-link is generated, allowing for repeated excitation and multiple opportunities for cross-links to form (Dorman and Prestwich, 1994).

To probe inter-subunit interactions within HSPB5 oligomers that involve the Critical sequence, BPA was installed at amino acid positions 33 or 38 (L33BPA and F38BPA, respectively). Oligomers composed of each variant were equilibrated for 1 hour at 37 °C prior to UV irradiation at 4 °C for 30 minutes. The resulting samples were resolved by SDS-PAGE, revealing a band containing two HSPB5 protomers with one intermolecular cross-link as the major product, with similar amounts of higher-order species representing three or more covalently-linked HSPB5 chains (Figures 3.21, 3.22, 3.23, and 3.24). Qualitatively, L33BPA produced lower amounts of cross-linked material than F38BPA. In-gel digest was performed on the singly cross-linked band and the resulting peptides were analyzed by mass spectrometry. Bioinformatic analysis of the fragmentation data identified positions of cross-links formed by BPA (Figure 3.25).

Cross-linked positions identified in L33BPA and F38BPA samples are shown as histograms across the HSPB5 sequence in Figure 3.19. Although similar numbers of cross-linked peptides could be identified in the two species, the crosslinking patterns are remarkably distinct. Cross-links from BPA at position 33 cluster mainly in the Distal NTR while links from position 38 are mainly to the Critical sequence and to a region on the structured ACD known as the edge groove. To further expand the view provided by the above results, BPA crosslinking was performed under identical conditions on HSPB5 variants with BPA individually placed at positions in the Distal, Middle, and Proximal NTR (specifically, residues 9, 17, 24, or 61). Each BPA position results in a distinct and discrete pattern of cross-links, consistent with the notion that NTRs are not completely disordered within oligomers (Figure 3.20). Notably, every BPA variant generated crosslinks to the Critical sequence, suggesting that the Critical sequence serves as a hub for a network of NTR-to-NTR interactions in HSPB5 (Figure 3.26 B). The results provide a rationale

for how the Critical sequence, located in the middle of the ~60-residue NTR, can influence the structure and dynamics of the entire NTR.

3.3 DISCUSSION

Human sHSPs remain among the most enigmatic of protein chaperones, largely due to intrinsic properties that confound detailed structural and functional studies under physiologically relevant experimental conditions (Halsbeck et al., 2019). A mimic of a UV-damaged version of the major eye lens client protein γD-crystallin (i.e., γD-W130E) that spontaneously aggregates at 37 °C has enabled direct comparison of the chaperone activity of the two most abundant sHSPs in lens, HSPB4 and HSPB5 (Serebryany et al., 2016). We found that HSPB4 and HSPB5 have markedly different chaperone activity and that the high intrinsic activity of HSPB5 is suppressed when present with HSPB4 in the ratio that exists in lens. Using a series of chimeric constructs, we identified the source of activity difference to be a short sequence in the middle of the NTR. We dub this the Critical sequence (residues ~31-42), as substitution of the HSPB5 sequence into HSPB4 changes the chaperone activity from B4-like (i.e., very low) to B5-like (i.e., very high), and vice versa.

Targeted UV crosslinking of HSPB5 oligomers revealed that the Critical sequence is close to all NTR sub-regions, at least transiently. The identity of the Critical sequence alters CD spectra, consistent with it inducing changes in secondary structure content, and alters HDX protection patterns throughout the NTR. Taking all observations together, a B4-like Critical sequence is associated with increased β-structure content, higher protection of the NTR from HDX, and lower chaperone activity towards γD-W130E. A B5-like Critical sequence is associated with lower β-structure content, lower protection of the NTR, and higher chaperone activity. Finally, observation

of interactions between the Critical sequence and the ACD edge groove in addition to small but significant effects of Critical sequence identity on the HDX protection in regions of the ACD nearby the edge groove indicate that the Critical sequence serves as the interaction network hub of the NTR. Thus, even small changes in the structure or dynamics of the Critical sequence can affect properties and activity of the entire NTR. The associations observed in this study lead us to conclude that a small section of the disordered NTR (~10 residues out of 60) is largely responsible for the dynamics, local structure(s), and activity of the sHSPs HSPB4 and HSPB5 (Figure 3.26 A and B).

Although HSPB5 is highly expressed in eye lens, muscle, and neurons, HSPB4 is only expressed in high abundance in lens (Bartelt-Kirbach et al., 2017; Dimauro et al., 2018; Wistow, 2012). Despite its high level of similarity to HSPB5, evolutionary analysis suggests that HSPB4 may be specialized for a role in lens (Wistow, 2012). Studies have found that the ratio of HSPB4 to HSPB5 that exists in lens (3:1) is optimal for stabilization of structure against temperature-induced changes (Selivanova and Galzitskaya, 2020; Horwitz et al., 1999). Our CD data on HSPB4/HSPB5 hetero-oligomers indicate that they have increased β-structure content, which may contribute to the reported stabilization. The B4-like chaperone activity of mixed oligomers suggests that such stabilization may limit or alter the interaction between HSPB5 and γD-W130E, thereby dampening productive chaperone activity as observed under laboratory conditions. We cannot rule out the alternative possibility that HSPB4 out-competes HSPB5 interactions with γD-W130E. While the observation of low HSPB4 chaperone activity against γD-W130E may seem counter-intuitive, interactions between highly activated HSPB5 and γD-W130E result in long-lived co-complexes that eventually co-aggregate (Woods et al., 2022), so there may be pressure to modulate client binding in lens.

Relatively few structural details are known for the NTR of sHSPs. Sparse structural data exists for HSPB1, HSPB2/HSPB3, HSPB4, HSPB5, and HSPB6 (Clouser et al., 2019; Clark et al., 2018; Kaiser et al., 2019; Woods et al., 2022; Sluchanko et al., 2017). In all cases, portions of NTRs are observed or inferred to contact the structurally-conserved ACD. In particular, Distal regions are inserted into ACD edge grooves in structures of HSPB2/3 and HSPB6 and the Conserved sequence of the Middle NTR is inserted into the central ACD groove in HSPB6 (Clark et al., 2018, PDB 6F2R; Sluchanko et al., 2017, PDB 5LTW). A similar interaction appears in the tetramer of HSPB2/HSPB3, though the resolution was insufficient to unambiguously identify the exact NTR residues involved (Clark et al., 2018; PDB 6F2R). The HSPB4 NTR was not well resolved in cryo-EM studies, suggesting it is either highly heterogenous or highly dynamic, but NTR to ACD interactions are implied by BS3 crosslinking experiments that link the Distal, Middle, and Proximal NTR to the ACD (Kaiser et al., 2019). Our studies reveal that all three HSPB5 NTR sub-regions interact with the ACD edge groove, and we also detect an interaction between the Middle NTR Conserved sequence and the central groove (Fig. 3.4B; Woods et al., 2022). Finally, multiple NTR-to-ACD edge groove and Conserved sequence-to-ACD central groove interactions have been reported for HPSB1 (Clouser et al., 2019). Thus, evidence from a growing number of human sHSPs appears to converge on a model in which there are multiple possible interactors within NTRs onto ACDs, and the number of interactors outnumbers the number of available grooves. Each such interaction is likely weak and transient, giving rise to the known high heterogeneity of sHSPs.

Compared to other sHSPs, more is known about local structure that exists in the HSPB5 NTR (Jehle et al., 2011). Solid-state NMR (ssNMR) provided evidence for two short β-strands, "β1" and "β2" in the Proximal sub-region that associate with each other and with the first stably

structured portion of the ACD, strand β3. Additionally, ssNMR revealed evidence of α-helical structure for HSPB5 residues 23-32, spanning the Conserved sequence and ending at the start of the Critical sequence (Jehle et al., 2011). It is noteworthy that a helical conformation will not fit into an ACD central groove, so the Conserved sequence must be non-helical when bound to the groove. Importantly, the ssNMR data revealed high heterogeneity within the NTR, indicating that the local structures implied by the data represent examples of what is likely a multitude of local structures that co-exist.

As pointed out previously, there are far more NTR sub-regions capable of interacting with an ACD than there are available ACD sites in an oligomer (Clouser et al. 2019; Woods et al., 2022). This situation suggests that NTRs also take part in interactions with other NTRs. Previous evidence for such interactions includes HDX and NMR experiments performed on HSPB1 (Clouser et al., 2019) and single cysteine disulfide formation for Cys residues installed in the Distal and Proximal sub-regions of HSPB5 (residues 19, 45, 57, 59, and 63; Jehle et al., 2011; Peschek et al., 2013). Our targeted BPA cross-linking experiments build on the prior data and reveal numerous novel NTR cross-links. Altogether, current available data are consistent with a highly interactive and interconnected NTR.

Surprisingly, we find that a short 10-residue stretch in the middle of the NTR (Critical sequence) dictates the chaperone activity, HDX protection, and local secondary structure of HSPB4 and HSPB5. Remarkably, as few as three amino acid swaps are required to change the behavior of HSPB5 into that of HSPB4. What is special about the Critical sequence and the three amino acids in question? We offer two speculations. First, the HSPB4 Critical sequence has alternating hydrophobic residues (F32, Y34, L36) suggestive of a short β-strand with a hydrophobic face; the corresponding residues in HSPB5 are L33, S35, L37. The triple residue-

swap mutant yields F33, Y35, L37 in HSPB5, creating a more hydrophobic strand should it exist. Second, the first residue of the HSPB4 Critical sequence is a glycine; it is histidine in HSPB5. Gly30 at the boundary between the Conserved and Critical sequences may serve to disfavor helical structure, whereas the His in HSPB5 would not. The swap of this residue could therefore disfavor helical structure (observed in ssNMR) and favor adoption of extended β-structure, consistent with the observed change in CD. Drawing from the observation that Conserved sequences (with virtually identical sequences) of sHSPs have been captured in at least three different conformations (extended, loop, and helical; Kaiser et al., 2019; Jehle et al., 2011; Sluchanko et al., 2017), we propose that which conformers are favored depends on both the surrounding sequence (i.e., the Critical sequence) and on possible interactions. In this way, substitution of the Critical sequence alters the local structure and consequently the interactions involved. Thus, changes in one region are expected to be transmitted to all other regions directly (via interaction) or indirectly (via changes in relative structure/dynamics). The functional consequences of such changes may depend on the identity of the client. In the case of lens client γD-W130E, changes that yield increased NTR accessibility are associated with enhanced ability to delay aggregation, and vice versa. Future studies with additional bona fide cellular clients will be required to see if this property is generalizable.

Finally, we note that the ability of the HSPB4 Critical sequence to transform HSPB5 into a lower activity γD-W130E chaperone does not require that the sequence be installed directly into HSPB5 in the form of a chimera or mutant. Mixed hetero-oligomers of HSPB4/HSPB5, as they exist in lens, display the same ability, leading to the conclusion that the modulation can work in trans. This new insight could have broad implications, as many cell types express more than one of the ten sHSPs and numerous examples of heteromeric sHSP species have been reported

(Zantema et al., 1992; Kato et al., 1992; Mymrikov et al., 2012). It seems reasonable to expect that different combinations and cellular levels of sHSPs will have differing levels of activity and sensitivity to changes in cellular conditions and client needs, as has been shown for various mixed oligomers *in vitro* (Mymrikov et al., 2020; Preis et al., 2017). A fuller understanding of how sHSP activity can be modulated endogenously may ultimately lead to ways to modulate activity exogenously.

3.4 Materials and Methods

3.4.1 *Expression and purification of HSPB4 or HSPB5 WT and mutants*

HSPB4 or HSPB5 WT and mutants were cloned into pET23 vector and expressed in E. coli BL21 DE3 cells (NEB). HSPB5 BPA mutants were created by installing the amber codon (TAG) at target sites and were co-expressed with pEVOL-pBpF. pEVOL-pBpF was a gift from Peter Schultz (Addgene plasmid # 31190; http://n2t.net/addgene:31190; RRID:Addgene_31190). Cells were grown at 37 °C until reaching an OD600 nm of 0.4 – 0.8, then temperature was adjusted to 22 °C and expression was induced with 1 mM IPTG or 1 mM IPTG and 1 mM arabinose in the case of BPA mutants. Cells were grown overnight, harvested by centrifugation, and resuspended in lysis buffer (20 mM Tris, 100 mM NaCl, 10 mM EDTA pH 8). Cells were lysed using a french press after adding DNase, RNase, and lysozyme. PEI (0.1% v/v) was added to the lysate and then the lysate was clarified by centrifugation. Ammonium sulfate (30% w/v) was added to the clarified lysate, then the ammonium sulfate pellet was isolated by centrifugation and the supernatant was discarded. The ammonium sulfate pellet was resuspended in 20 mM Tris pH 8 (buffer A) and applied to a G25 column equilibrated with buffer A. Desalted protein was pooled and applied to a DEAE column equilibrated with buffer A and eluted by a sodium chloride gradient. Protein eluted

from the DEAE column was diluted in buffer A and then applied to a HiTrap Q column (Cytiva) equilibrated in buffer A. Protein was eluted from the Q column using a sodium chloride gradient and then was pooled, concentrated, and applied to a SDX200 column equilibrated with 25 mM $NaPO_4$, 150 mM NaCl pH 6.5. Pure protein was flash-frozen in liquid nitrogen and stored at -80 °C.

3.4.2 *Expression and purification of γD-W130E*

γD-W130E was cloned into pET28a vector and expressed in E. coli BL21 DE3 cells (NEB) as a fusion on the C-terminus of 6xHis-SUMO. Cells were grown at 37 °C until reaching an OD600 nm of 0.4 – 0.8, then temperature was adjusted to 20 °C and expression was induced with 0.5 mM IPTG. Cells were grown overnight, harvested by centrifugation, and resuspended in 20 mM Tris, 200 mM NaCl, 10 mM imidazole pH 7.6 (lysis buffer). Cells were lysed using a french press after adding DNAse, RNAse, and lysozyme. PEI (0.1% v/v) was added to the lysate and then the lysate was clarified by centrifugation. Clarified lysate was filtered (0.45 μm) and then applied to a HisTrap column (Cytiva) equilibrated with lysis buffer. Bound protein was eluted with imidazole. GST-SENP3 (SUMO protease) was added to the eluted protein and then the mixture was dialyzed overnight in lysis buffer + 2 mM β-Mercaptoethanol. Dialyzed protein was re-applied to a HisTrap column equilibrated with lysis buffer. The flow through was concentrated and then injected on an SDX75 column equilibrated with 20 mM Tris, 50 mM NaCl, 10 mM EDTA, 5 mM β-mercaptoethanol pH 8. Fractions containing purified protein were pooled and stored in this buffer until the day before it was used for chaperone activity assays, at which point it was buffer exchanged to 25 mM $NaPO_4$, 150 mM NaCl, 2 mM EDTA pH 6.5.

3.4.3 *Chaperone Activity Assay*

Chaperone activity of HSPB4 or HSPB5 WT and mutants was assessed using γD-W130E as client. Aggregation of γD-W130E was measured at 37 °C in a 96-well plate reader (BioTek) by monitoring absorbance at 360 nm. All small heat shock protein samples were incubated for 1 hour at 37 °C before adding to assay wells. Wells containing small heat shock proteins (or buffer only) were assembled and then incubated at 37 °C for 5 minutes, then ice-cold γD-W130E was added (γD-W130E final concentration 500 μM; small heat shock protein final concentration 15 μM for homo-oligomers, 60 μM for mixed HSPB4/HSPB5 oligomers; final buffer conditions 25 mM NaPO4, 150 mM NaCl, 1 mM EDTA pH 6.5).

3.4.4 *Circular Dichroism Spectroscopy*

Circular dichroism spectra were collected using a Jasco J-1500 instrument. Samples (10 μM) were equilibrated at 37 °C for 1 hour in 5 mM $NaPO_4$, 30 mM NaCl, 0.2 mM EDTA pH 6.5. 10 wavelength scans from 300 nm to 200 nm were accumulated at 37 °C and averaged automatically. The 3:1 HSPB4:HSPB5 mixture contained 40 μM protein in total and the plot is truncated because the high tension limit was reached at 206 nm.

3.4.5 *Hydrogen/Deuterium Exchange Mass Spectrometry*

Samples (20 μM) were equilibrated in water-based buffer (25 mM NaPO4, 150 mM NaCl, 1 mM EDTA pH 6.5) for 1 hour at 37 °C and then cooled to room temperature. Internal exchange standards Tyr-Pro-Ile “YPI” and Tyr-Gly-Gly-Phe-Leu “Leucine-enkephalin” were added to samples. Samples were diluted 10-fold into 25 mM NaPO4, 150 mM NaCl, 1 mM EDTA pH 6.5 buffer made in 95% D2O (85% D2O final, 2 μM protein) and incubated for 4 seconds, 1 minute, 30 minutes, or 20 hours at room temperature. Fully-deuterated samples were created by incubating

in 85% D2O at 75 °C for 30 minutes. Exchange was quenched by addition of ice-cold quench buffer (1.4% v/v formic acid, final concentration 0.7%) and flash frozen in liquid nitrogen. Samples were automatically thawed, digested by immobilized pepsin, and injected on a Waters Synapt G2-Si mass spectrometer using a home-built system based around the LEAP PAL (Watson et al., 2022). Peptides from pepsin digests were identified by MS/MS on a Thermo Orbitrap Fusion Tribrid mass spectrometer followed by analysis using ProteinProspector (UCSF). Deuterium uptake was analyzed in HDExaminer 3.0 (Sierra Analytics) and HX-Express (Guttman et al., 2013). Percent deuteration at each time point was calculated relative to the fully-deuterated control and compared for each peptide with identical sequence.

3.4.6 *BPA Crosslinking Mass Spectrometry*

BPA was incorporated in HSPB5 using amber codon suppression technology (Chin et al., 2002). The amber codon was inserted at HSPB5 residue 9, 17, 24, 33, 38, or 61 using QuikChange mutagenesis (Agilent). Single-BPA HSPB5 mutants were purified using the standard protocol while taking steps to limit exposure to ambient light. Sample concentrations were determined using BCA. 50 μM HSPB5 BPA mutants were incubated for 1 hour at 37 °C, cooled to 4 °C, placed in a 96-well flat-bottomed half-area plate, and then exposed to UV for 30 minutes at 4 °C. Samples were subjected to SDS-PAGE on a 4-20% acrylamide gradient gel (Bio-Rad). The no-UV monomer and plus-UV dimer bands were excised and were each digested in-gel with MS grade Trypsin (Thermo Scientific) and GluC (New England Biolabs) in ammonium bicarbonate buffer (Thermo Manual - In-Gel Tryptic Digestion Kit). Digests were cleaned up with C18 spin columns (Thermo Scientific) and dried using a speed-vac. Samples were resuspended in 95% water 5% ACN with 0.1% FA with volumes adjusted based on sample weight. Data was collected with an Easy Nano LC coupled to a Thermo Orbitrap Fusion Lumos Tribrid. 0.5 μg of protein was loaded

onto an 8-cm trap column. The sample was then then separated on a 25-cm analytical column with a 75 µm inner diameter using an 85-minute gradient from 6% B to 45% B, where A was water and B was 80% acetonitrile, at 300 nL min−1. The column was then flushed and regenerated for 35 minutes. Spectra were acquired across the entire LC method using data-dependent acquisition with dynamic exclusion after one time for a duration of 30 seconds and an intensity threshold of 2.0×104. Orbitrap detection and Higher-energy C-trap dissociation (HCD) fragmentation (30% normalized collision energy) were used with a target value of 1.00×105, maximum injection time of 22 ms, top N of 20, and isolation width of 1.6. MS1 were acquired at a resolution of 120,000 over the range of 400-2000 m/z, and MS2 were acquired with a resolution of 15,000. The mass spectrometry proteomics data have been deposited to the ProteomeXchange Consortium via the PRIDE partner repository (Perez-Riverol et al., 2019) with the dataset identifier PXD034114.

3.4.7 *Identification of Crosslinks Using the Trans Proteomic Pipeline (TPP)*

First, Comet (Eng et al., 2013) was used to search for non-crosslinked peptides in the non-UV treated control to construct the protein database. The Comet search database contained the BL21 E. coli database from uniprot (UP000431028), the cRAP database from the Global Proteome Machine with all 5 levels of proteins (cRAP Protein Sequences), the pertinent HSPB5 BPA mutant, and reverse-sequence decoys. In addition, the wild-type HSPB5 was included in the database for samples that were analyzed on the same date as other samples containing that protein. The Comet searches were enzyme nonspecific using a peptide mass tolerance of 20.0 ppm. The isotope error offset was 3, and BPA was defined as an additional amino acid, B, that has a mass of 251.09462859 Da. Methionine oxidation and cysteine iodoacetamide alkylation were variable modifications. Results were validated using Peptide Prophet (Keller et al., 2002). After filtering using a 1% False

Discovery Rate (FDR, based on PeptideProphet probabilities) and a minimum of 2 Peptide Spectral Match (PSM), this yields a protein database for the sample.

Second, crosslinks in the UV-treated samples were identified using Kojak (Hoopmann et al., 2015) and the protein database for the sample. The Kojak search settings matched those described for the Comet searches expect the precursor tolerance was 15 ppm and enzyme selection rules were used. For the trypsin digested samples, the preexisting trypsin setting was used. For the trypsin-GluC digested samples, the cleavage sites of D and E were added to the trypsin settings. Crosslinks were defined as from BPA to any residue with no mass change. Crosslink results were validated using PeptideProphet. For ions of each charge state, probabilities were determined using PeptideProphet and were used to define the thresholds used to filter results to a 1% FDR. For histograms, each PSM was associated with the residue that was assigned the highest probability of participating in a crosslink with BPA. When more than one residue was assigned the same probability, an equal fraction of that PSM was assigned to each of those residues.

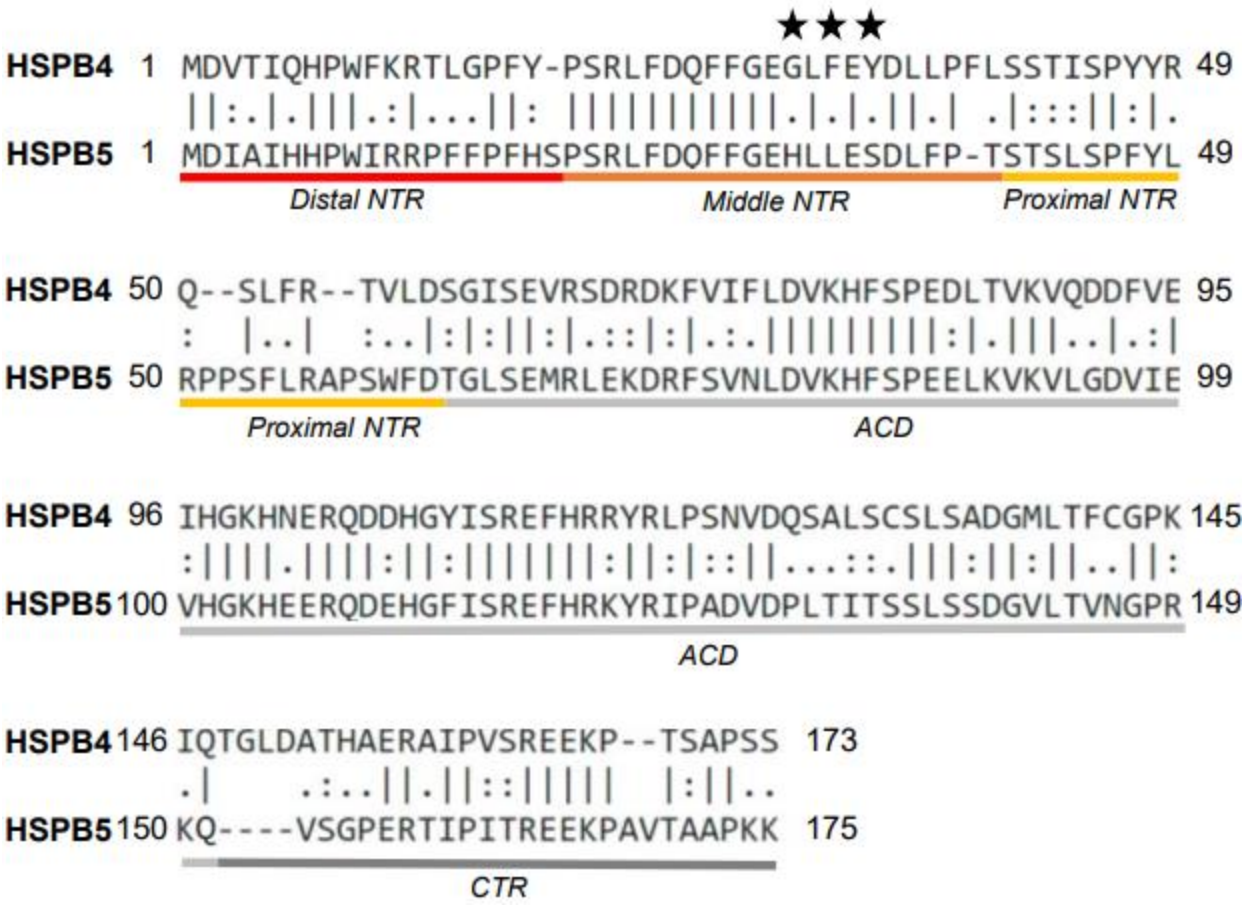

Figure 3.1. Alignment of human HSPB4 and HSPB5. The full sequences of human HSPB4 and HSPB5 were aligned using the EMBOSS Needle server (EMBL-EBI). Locations of the Distal NTR, Middle NTR, Proximal NTR, ACD, and CTR are shown by colored lines. The three Critical sequence residues that have a dominant effect on chaperone activity are marked with black stars.

A

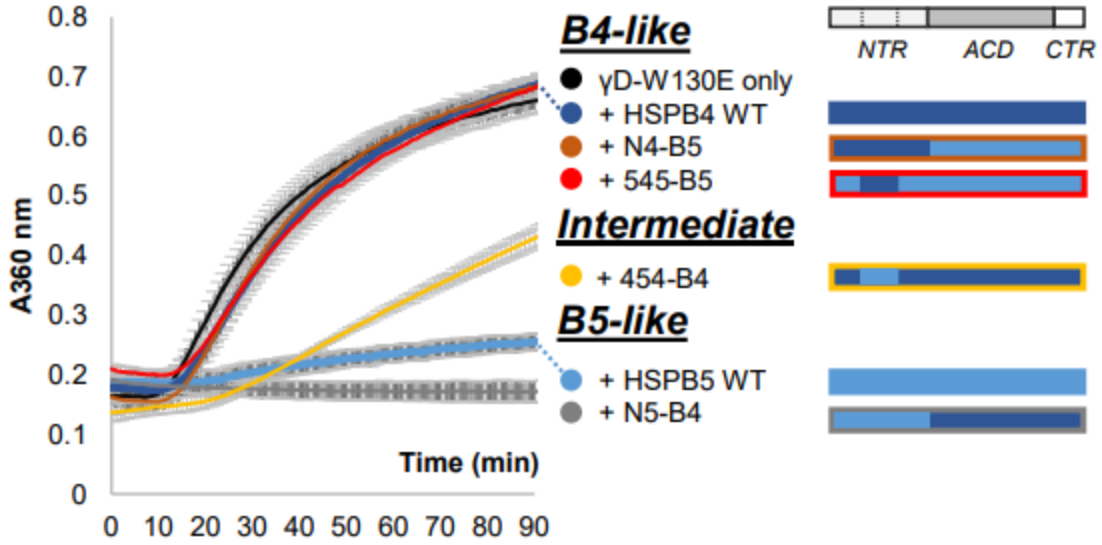

B

sHSP species	Activity	Graphic
3:1 B4:B5 Mixture	B4-like	
455-B5	B5-like	
554-B5	B4-like	
554-B4	B5-like	
B5 H31G/L33F/S35Y	B4-like	
B5 H31G/L33F	Intermediate	
B5 H31G/S35Y	Intermediate	
B5 L33F/S35Y	Intermediate	
B5 R120G	B5-like	
R120G H31G/L33F/S35Y	Intermediate	

Figure 3.2. Sequence identity of the Middle NTR sub-region has a dominant effect on chaperone activity. A) Left: chaperone activity assay of HSPB5 and HSPB4 WT and N-terminal Region (NTR) sequence swap chimeras using γD-W130E as client. The plot shows absorbance at 360 nm versus time and is indicative of client aggregation. Samples are classified by activity: high – "B5-like", "Intermediate", or low – "B4-like". Right: key showing the identities of the NTR sub-regions, α-crystallin domain (ACD), and C-terminal Region (CTR) for each sample, with light blue bars representing HSPB5 regions and dark blue bars representing HSPB4 regions. B) Summary of chaperone activity of all constructs tested. The white line for B5 R120G and R120G H31G/L33F/S35Y shows the approximate location of the R120G mutation in the ACD. N = 3 for all samples, average A360 value ± 1 standard deviation is shown.

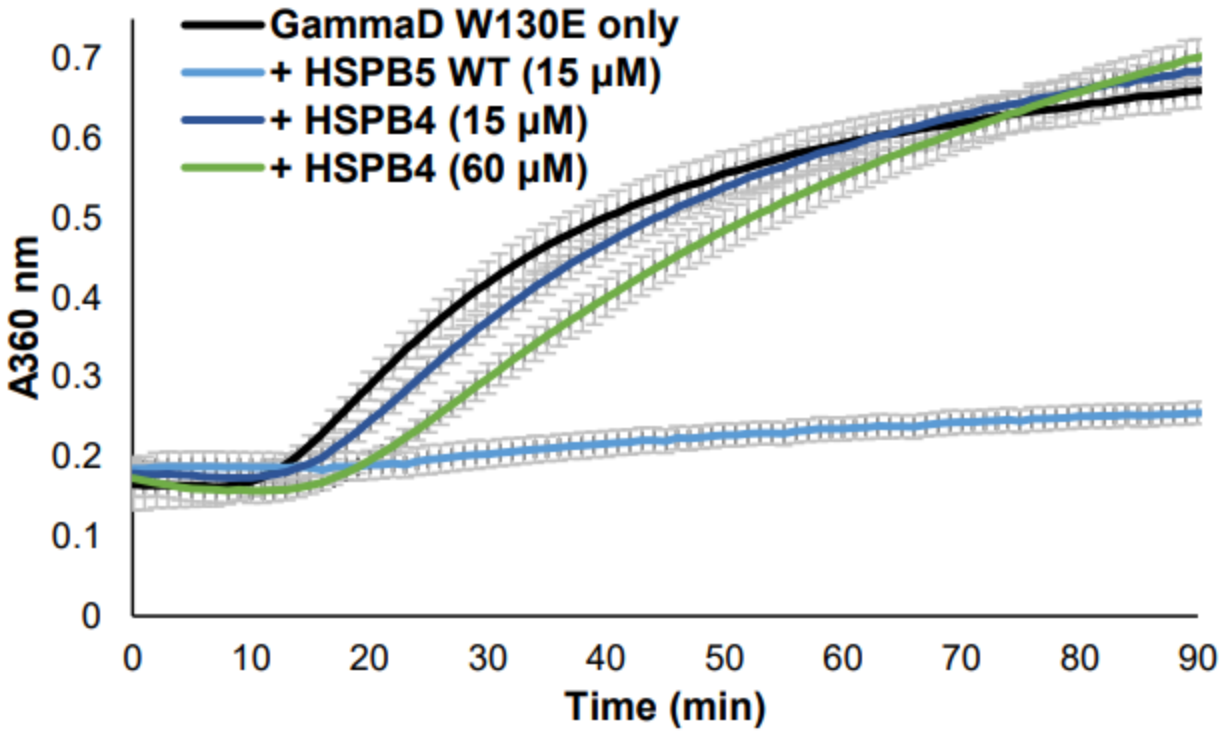

Figure 3.3. Chaperone activity assessment of HSPB4 and HSPB5 using γD-W130E as client.

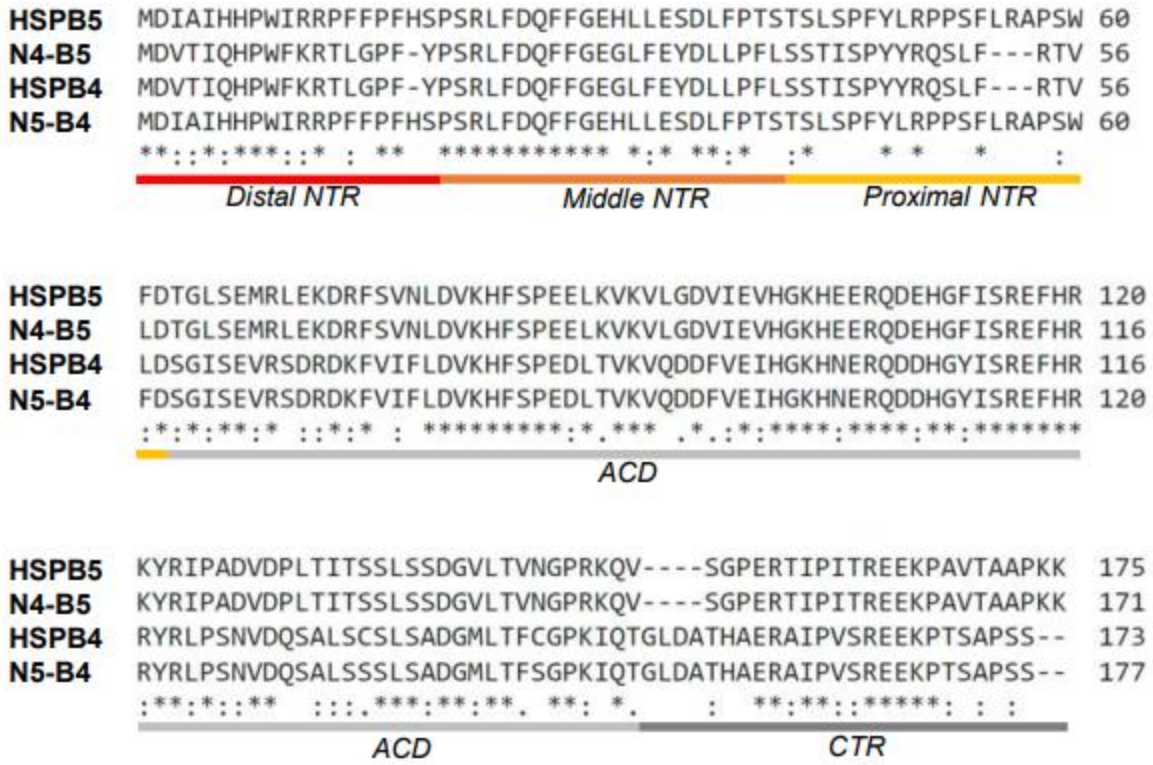

Figure 3.4. Alignment of human HSPB4 and HSPB5 with the N5-B4 and N4-B5 chimeras. Full length sequences of human HSPB4 and HSPB5 and the N4-B5 and N5-B4 chimeras aligned using Clustal Omega (EMBL-EBI). Locations of the Distal NTR, Middle NTR, Proximal NTR, ACD, and CTR are shown by colored lines.

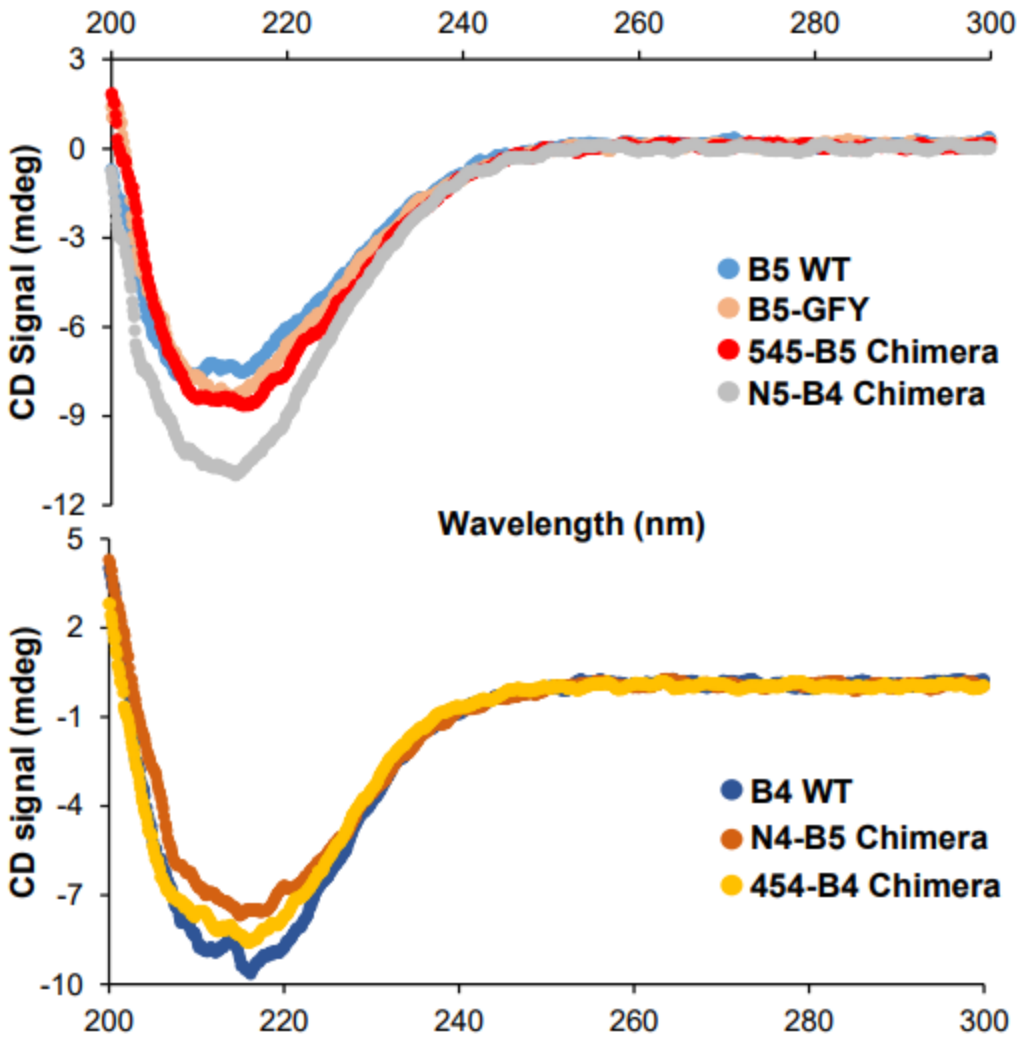

Figure 3.5. Circular dichroism spectra of HSPB4 and HSPB5 and sequence-swap chimeras. Circular dichroism spectra sHSP samples collected at 37 °C. Top panel: CD spectra of HSPB5 WT (light blue), B5-GFY (peach), 545-B5 chimera (red), and N5-B4 chimera (gray). Lower panel: CD spectra of HSPB4 WT (dark blue), N4-B5 chimera (orange), and 454-B4 chimera (gold).

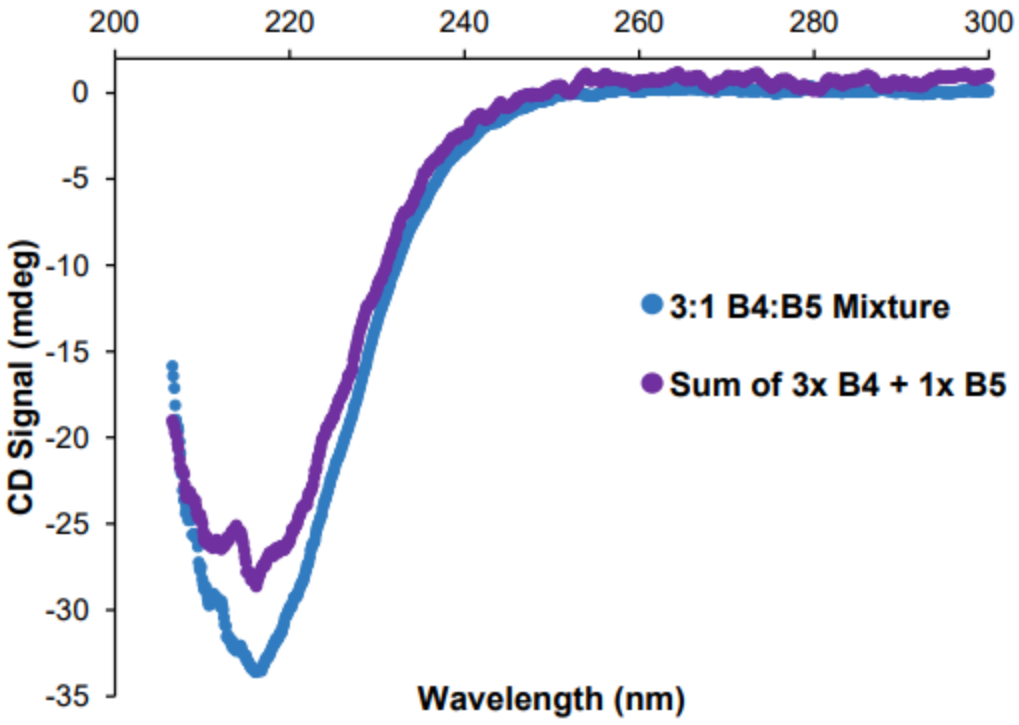

Figure 3.6. Circular dichroism spectrum of HSPB4/HSPB5 mixture (blue) compared to a theoretical curve resulting from addition of HSPB4- and HSPB5-only spectra (purple).

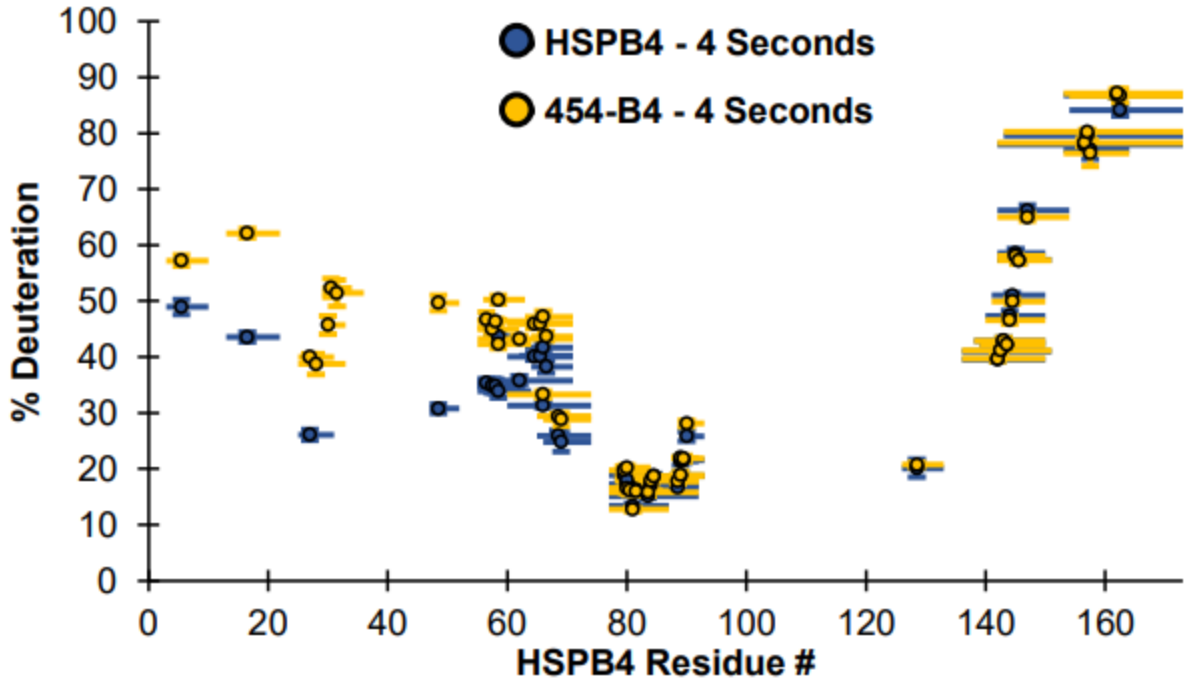

Figure 3.7. Percent deuteration of HSPB4 and 454-B4 at the four second HDX time point. Mean percent deuteration (relative to a fully-deuterated control) is shown for each unique peptide found in the HSPB4 and 454-B4 data sets. Peptide centers are represented by a circle (HSPB4 – black outline with dark blue fill; 454-B4 – black outline with gold fill). Peptide length is shown using horizontal bars (with the first two residues of each peptide omitted). Error is shown with vertical bars (± 1 standard deviation). N = 3-7

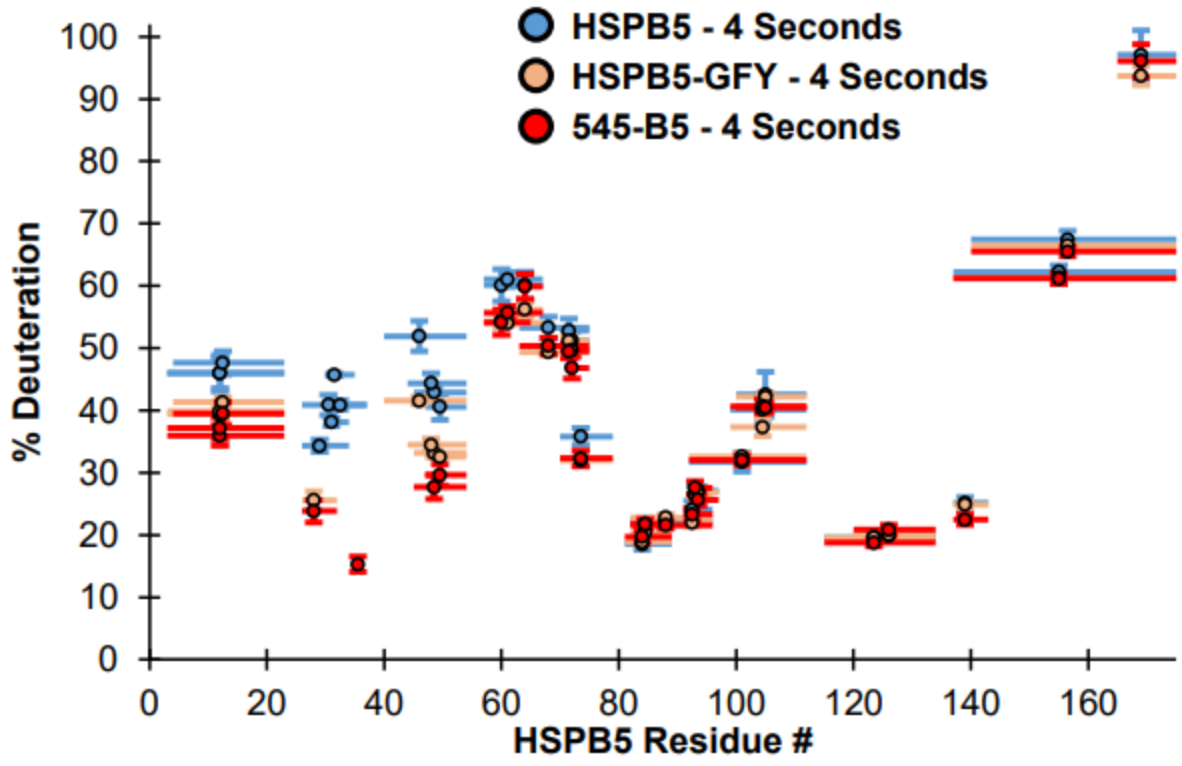

Figure 3.8. Percent deuteration of HSPB5, B5-GFY, and 545-B5 at the four second HDX time point. Mean percent deuteration (relative to a fully-deuterated control) is shown for each unique peptide found in the HSPB5, B5-GFY, and 545-B5 data sets. Peptide centers are represented by a circle (HSPB5 – black outline with light blue fill; B5-GFY – black outline with peach fill; 545-B5 – black outline with red fill). Peptide length is shown using horizontal bars (with the first two residues of each peptide omitted). Error is shown with vertical bars (± 1 standard deviation). N = 3-7

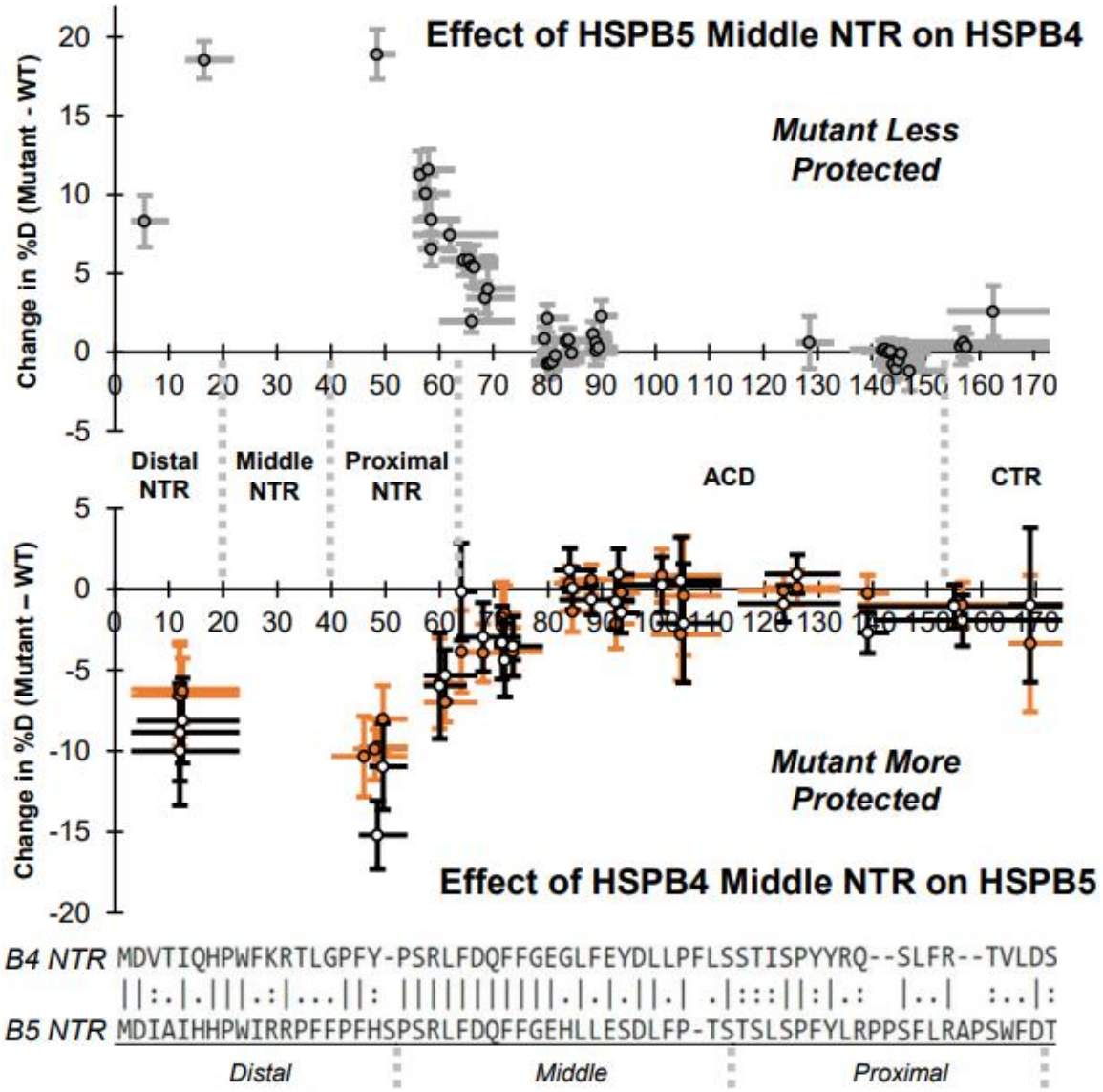

Figure 3.9. Identity of the NTR Middle sub-region influences HDX throughout the NTR at the 4 second exchange time point. Top panel: The effect of installing HSPB5's Middle NTR sub-region in otherwise HSPB4 (454-B4) is shown in gray as the change in percent deuteration (mean 454-B4 %D – mean HSPB4 %D; N = 3-7). Values above 0 indicate 454-B4 is less protected from HDX than HSPB4. Gray circles outlined in black represent the peptide center, horizontal bars represent peptide length (minus the first two residues), and vertical error bars show error (± 1 standard deviation). Lower panel: The effect of installing HSPB4's Middle NTR sub-region (545-B5) or the residue swaps H31G/L33F/S35Y (B5-GFY) in HSPB5 are shown in black and orange as the change in percent deuteration (mutant mean %D – HSPB5 mean %D). Values below 0 indicate the mutants are more protected from HDX. N = 3-7, change in mean %D value ± 1 standard deviation is shown. Boundaries of the Distal NTR, Middle NTR, Proximal NTR, ACD, and CTR are shown between the panels. Bottom: Alignment of HSPB4 and HSPB5 NTR with the Distal, Middle, and Proximal NTR sub-regions shown.

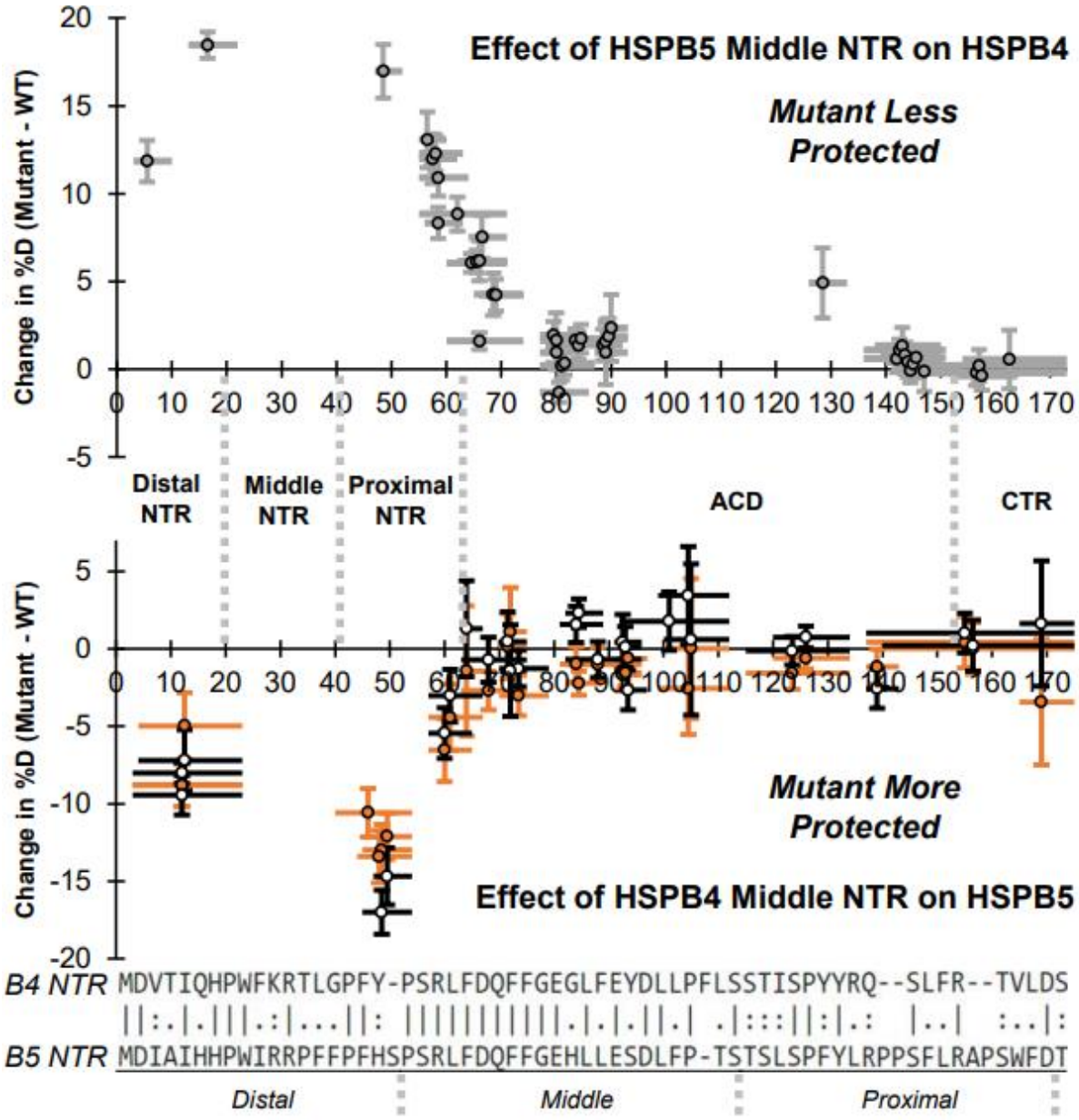

Figure 3.10. Identity of the NTR Middle sub-region influences HDX throughout the NTR at the 1 minute exchange time point. Top panel: The effect of installing HSPB5's Middle NTR sub-region in otherwise HSPB4 (454-B4) is shown in gray as the change in percent deuteration (mean 454-B4 %D – mean HSPB4 %D; N = 3-7). Values above 0 indicate 454-B4 is less protected from HDX than HSPB4. Gray circles outlined in black represent the peptide center, horizontal bars represent peptide length (minus the first two residues), and vertical error bars show error (± 1 standard deviation). Lower panel: The effect of installing HSPB4's Middle NTR sub-region (545-B5) or the residue swaps H31G/L33F/S35Y (B5-GFY) in HSPB5 are shown in black and orange as the change in percent deuteration (mutant mean %D – HSPB5 mean %D). Values below 0 indicate the mutants are more protected from HDX. N = 3-7, change in mean %D value ± 1 standard deviation is shown. Boundaries of the Distal NTR, Middle NTR, Proximal NTR, ACD, and CTR are shown between the panels. Bottom: Alignment of HSPB4 and HSPB5 NTR with the Distal, Middle, and Proximal NTR sub-regions shown.

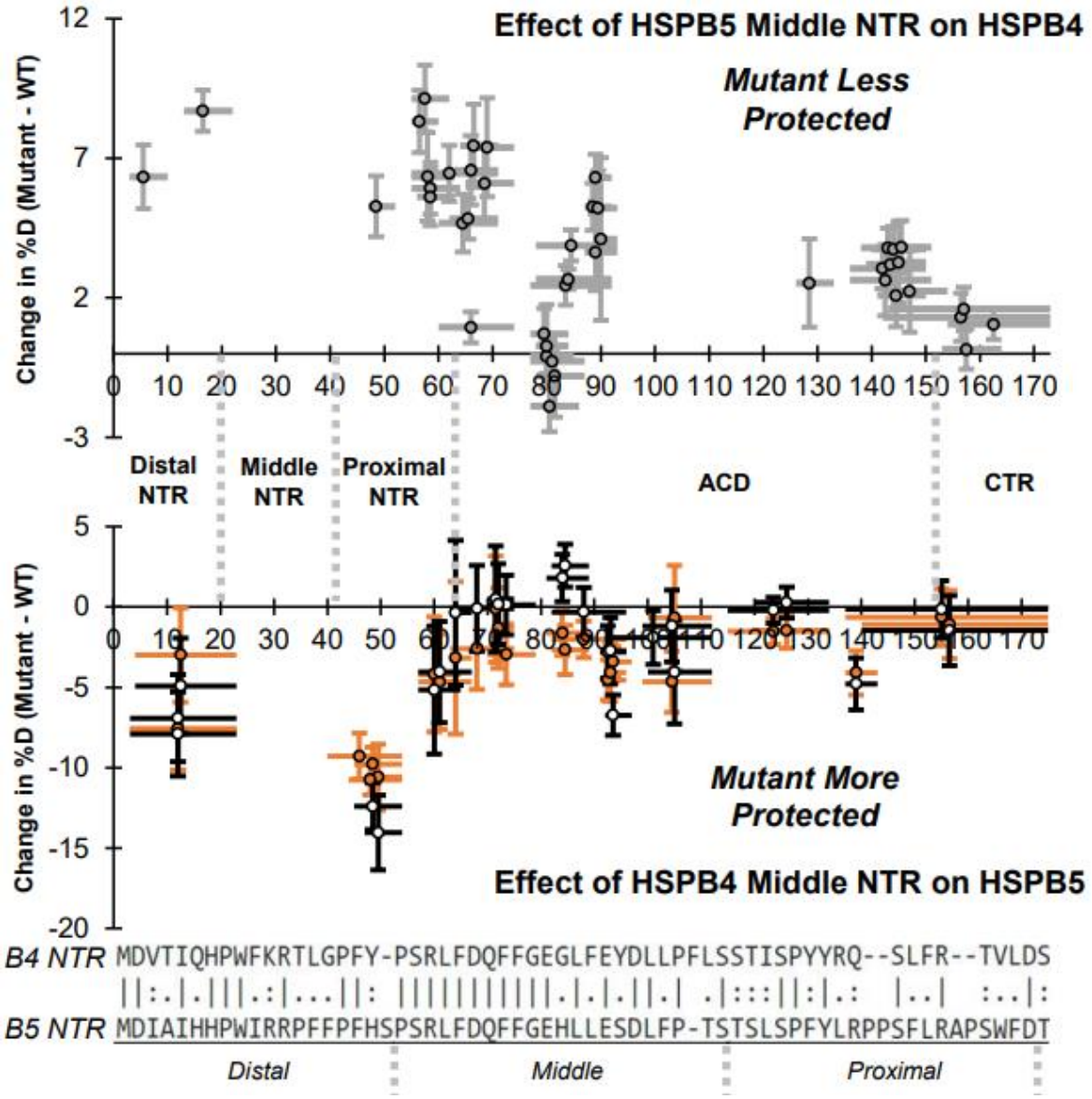

Figure 3.11. Identity of the NTR Middle sub-region influences HDX throughout the NTR at the 30 minute exchange time point. Top panel: The effect of installing HSPB5's Middle NTR sub-region in otherwise HSPB4 (454-B4) is shown in gray as the change in percent deuteration (mean 454-B4 %D – mean HSPB4 %D; N = 3-7). Values above 0 indicate 454-B4 is less protected from HDX than HSPB4. Gray circles outlined in black represent the peptide center, horizontal bars represent peptide length (minus the first two residues), and vertical error bars show error (± 1 standard deviation). Lower panel: The effect of installing HSPB4's Middle NTR sub-region (545-B5) or the residue swaps H31G/L33F/S35Y (B5-GFY) in HSPB5 are shown in black and orange as the change in percent deuteration (mutant mean %D – HSPB5 mean %D). Values below 0 indicate the mutants are more protected from HDX. N = 3-7, change in mean %D value ± 1 standard deviation is shown. Boundaries of the Distal NTR, Middle NTR, Proximal NTR, ACD, and CTR are shown between the panels. Bottom: Alignment of HSPB4 and HSPB5 NTR with the Distal, Middle, and Proximal NTR sub-regions shown.

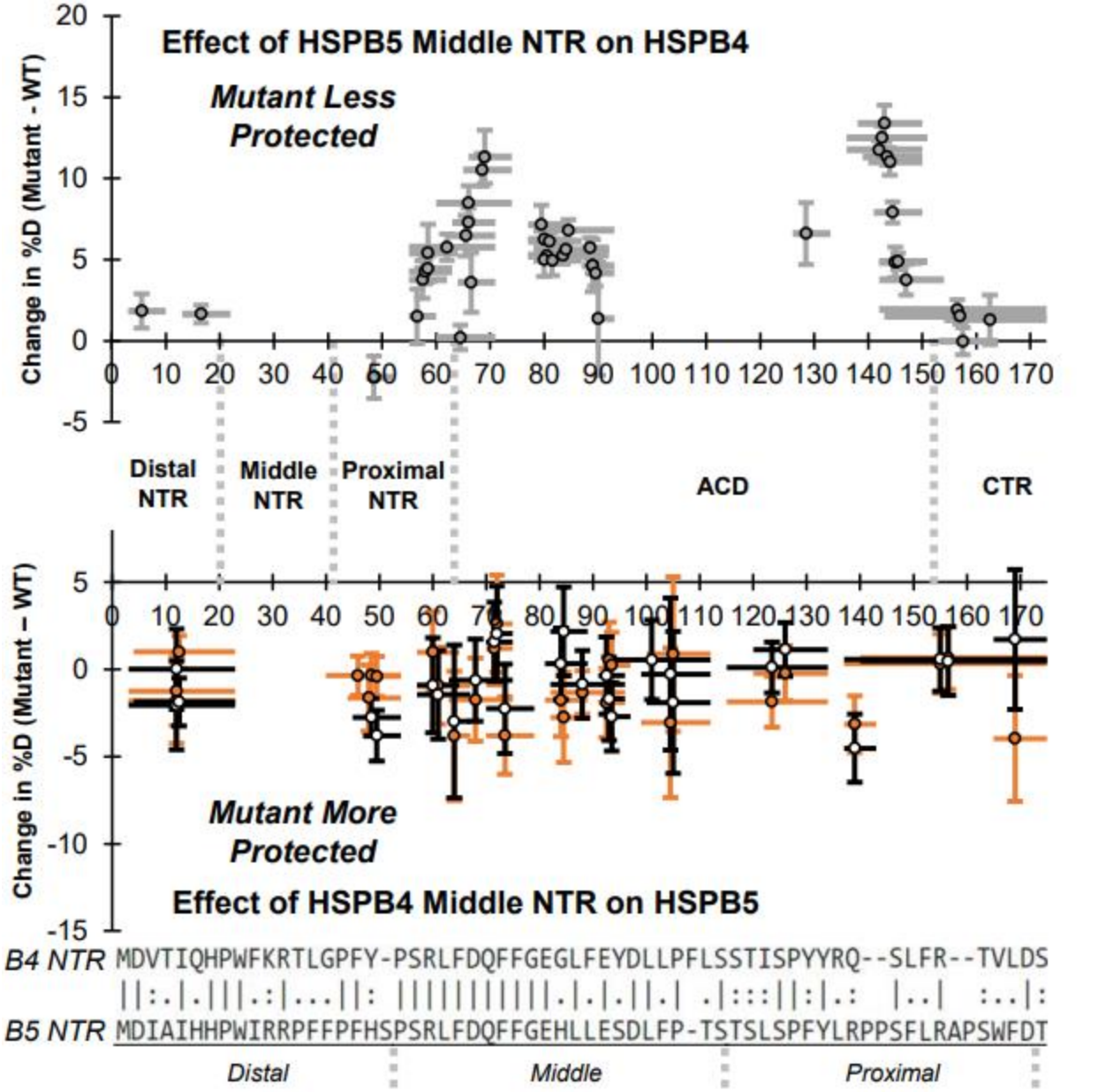

Figure 3.12. Identity of the NTR Middle sub-region influences HDX throughout the ACD at the 20 hour exchange time point. Top panel: The effect of installing HSPB5's Middle NTR sub-region in otherwise HSPB4 (454-B4) is shown in gray as the change in percent deuteration (mean 454-B4 %D – mean HSPB4 %D; N = 3-7). Values above 0 indicate 454-B4 is less protected from HDX than HSPB4. Gray circles outlined in black represent the peptide center, horizontal bars represent peptide length (minus the first two residues), and vertical error bars show error (± 1 standard deviation). Lower panel: The effect of installing HSPB4's Middle NTR sub-region (545-B5) or the residue swaps H31G/L33F/S35Y (B5-GFY) in HSPB5 are shown in black and orange as the change in percent deuteration (mutant mean %D – HSPB5 mean %D). Values below 0 indicate the mutants are more protected from HDX. N = 3-7, change in mean %D value ± 1 standard deviation is shown. Boundaries of the Distal NTR, Middle NTR, Proximal NTR, ACD, and CTR are shown between the panels. Bottom: Alignment of HSPB4 and HSPB5 NTR with the Distal, Middle, and Proximal NTR sub-regions shown.

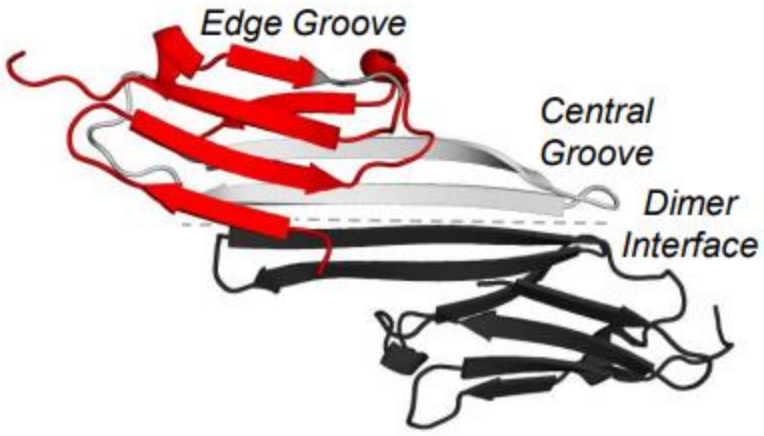

Figure 3.13. Significant changes in 454-B4 chimera ACD HDX relative to HSPB4 after 20 hours exchange. Changes in percent deuteration greater than 5% for Middle NTR swap chimera 454-B4 vs. HSPB4 WT at the 20 hour exchange time point are plotted in red on the HSPB4 ACD structure (PDB 3N3E). The two protomers within the ACD dimer are colored dark gray and light gray and the dimer interface is shown by the dashed gray line. Locations of the ACD edge groove and central groove are marked. Residues that did not have a high-quality fully-deuterated control (and thus cannot be analyzed by percent deuteration) are colored light gray. Comparison of absolute deuterium uptake for these residues suggest they are also affected by installing HSPB5 Middle NTR into HSPB4 (Figure 3.14).

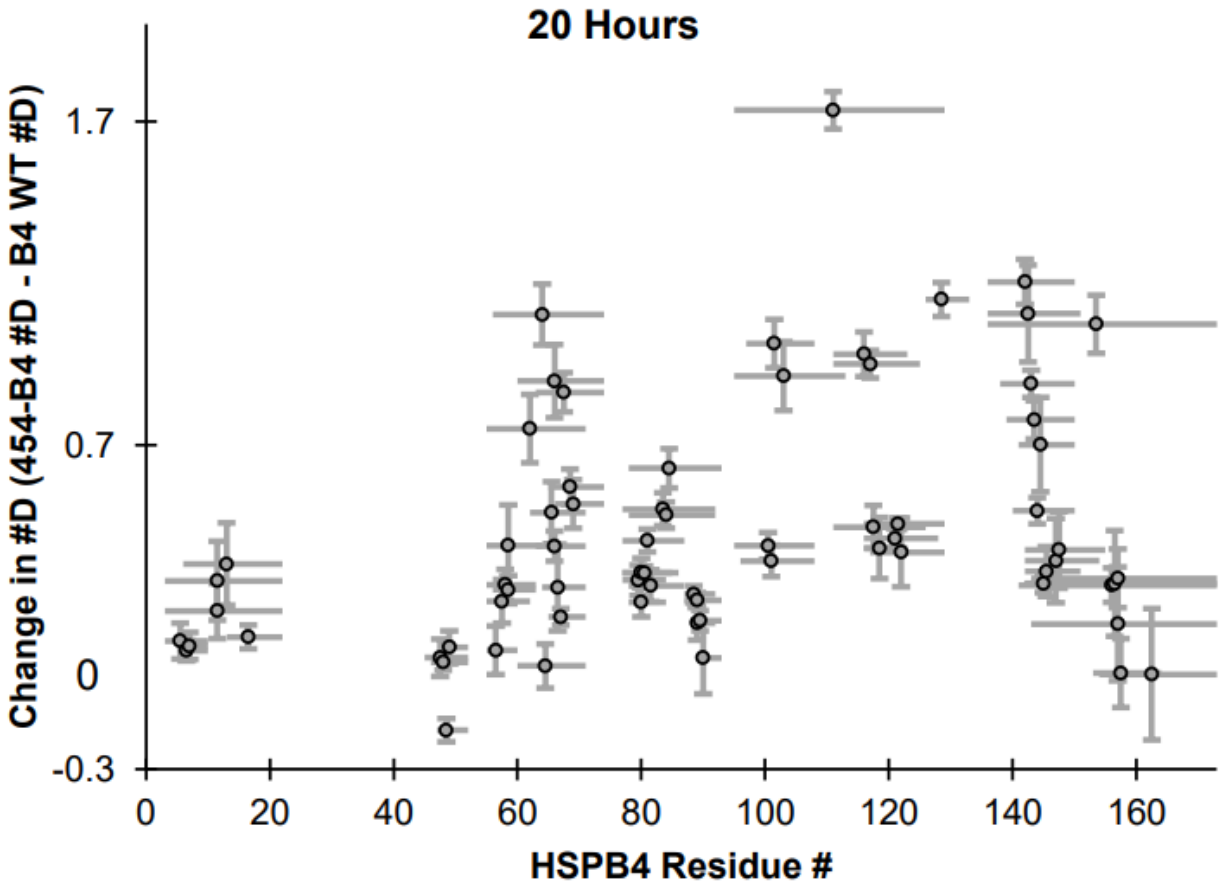

Figure 3.14. Change in absolute deuteration at the 20 hour HDX time point when HSPB5 Middle NTR is installed in HSPB4. The change in deuteration (#D) at the 20 hour time point for each peptide of identical sequence found in both the HSPB4 and 454-B4 data sets (calculated as 454-B4 #D – HSPB4 #D). Peptide centers are represented by a gray filled circle with black outline. Peptide length is shown using horizontal bars (with the first two residues of each peptide omitted). Error is shown with vertical bars (± 1 standard deviation). N = 3-7

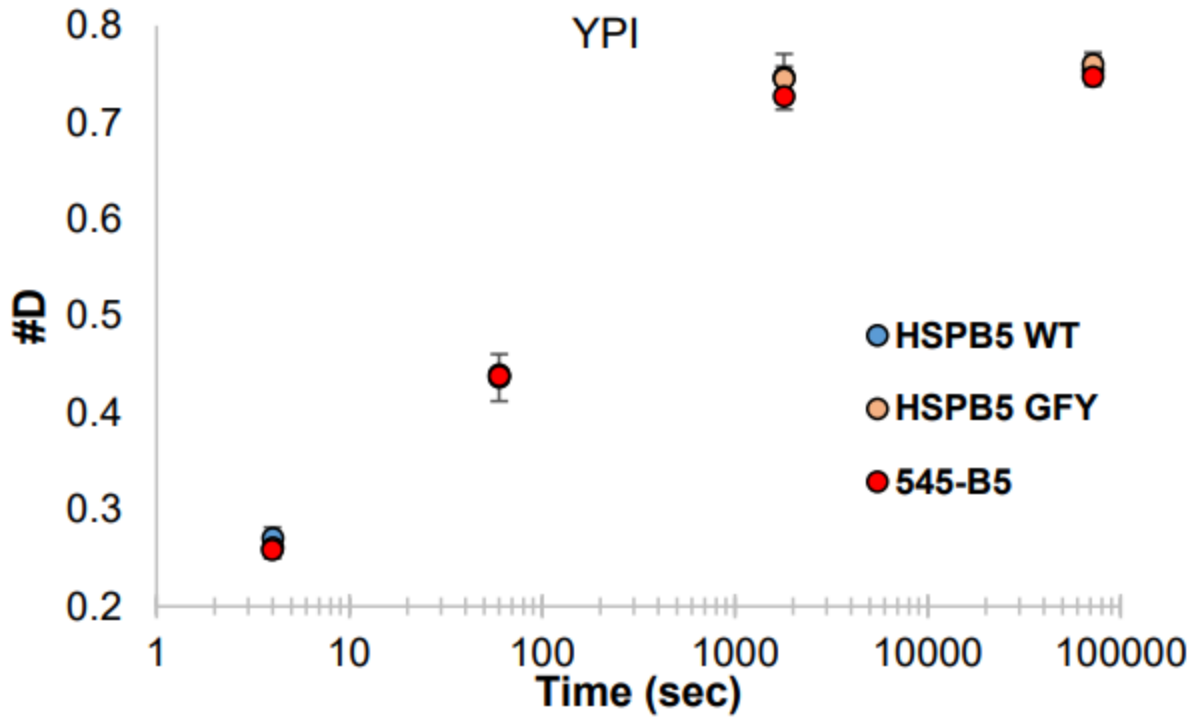

Figure 3.15. Deuteration of the 'YPI' tripeptide internal exchange standard for HSPB5, B5-GFY, and 545-B5. The mean deuteration level (#D) and error (vertical bars; ± 1 standard deviation) are shown. N = 3-7

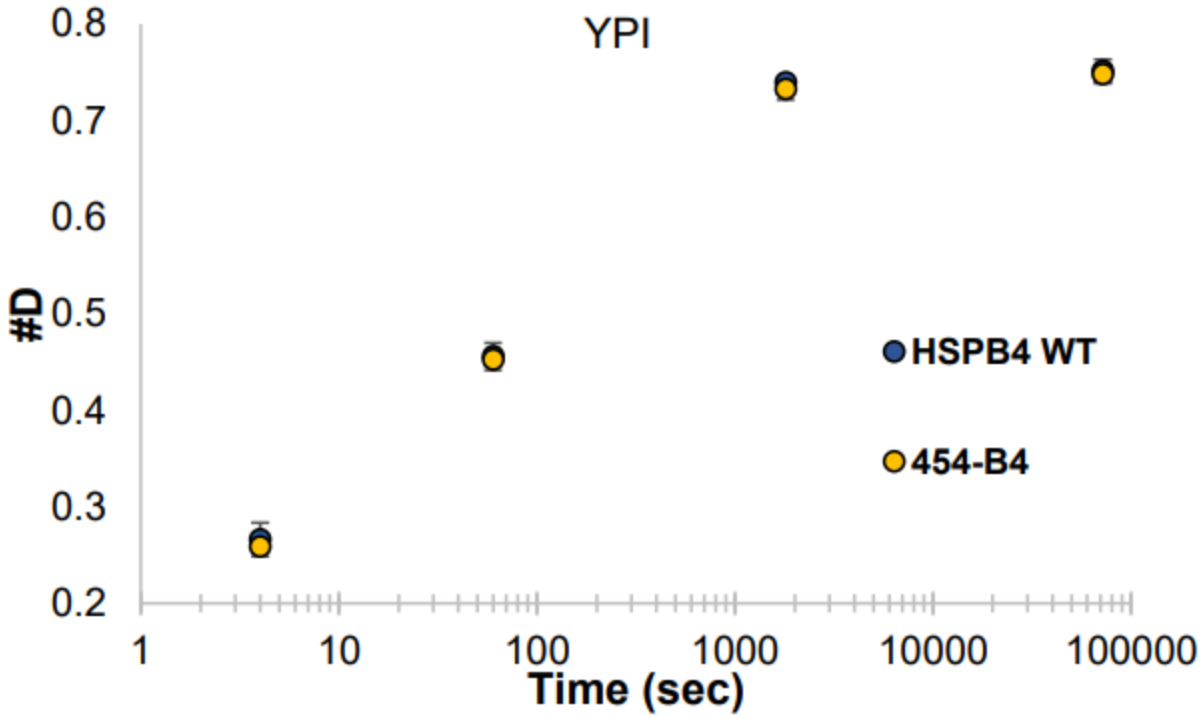

Figure 3.16. Deuteration of the 'YPI' tripeptide internal exchange standard for HSPB4 and 454-B4. The mean deuteration level (#D) and error (vertical bars; ± 1 standard deviation) are shown. N = 3-7

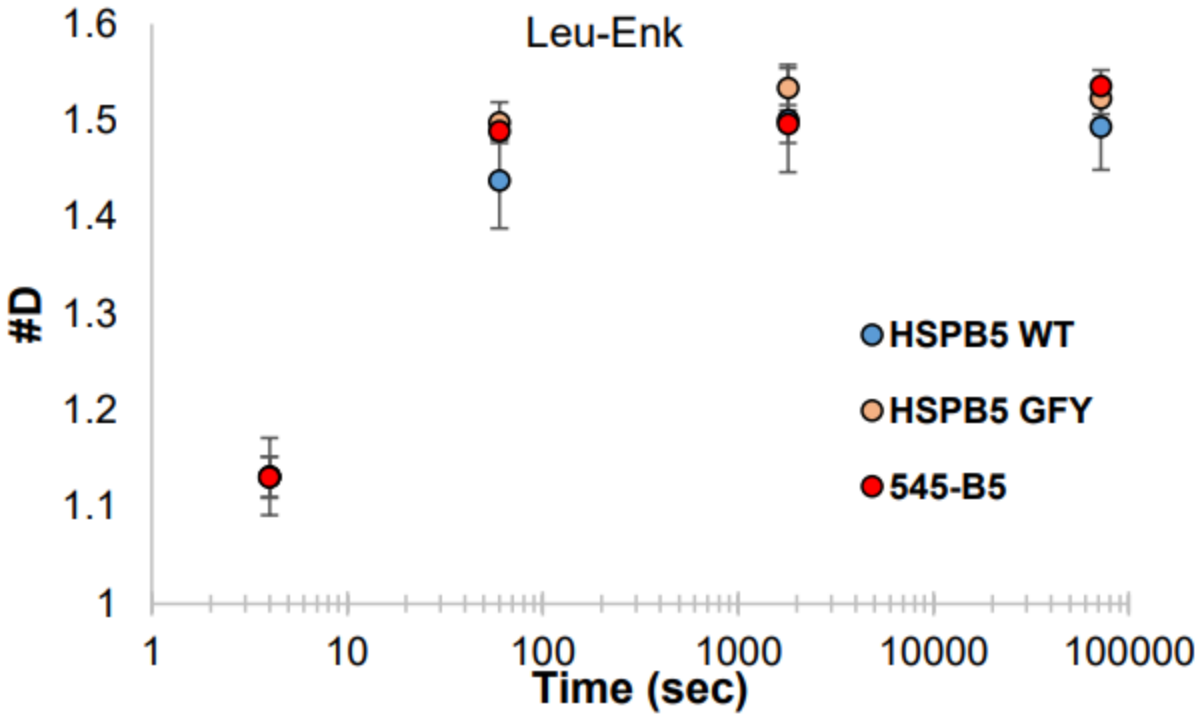

Figure 3.17. Deuteration of the Leucine-enkephalin pentapeptide internal exchange standard (YGGFL) for HSPB5, B5-GFY, and 545-B5. The average deuteration level (#D) and error (vertical bars; ± 1 standard deviation) are shown. N = 3-7

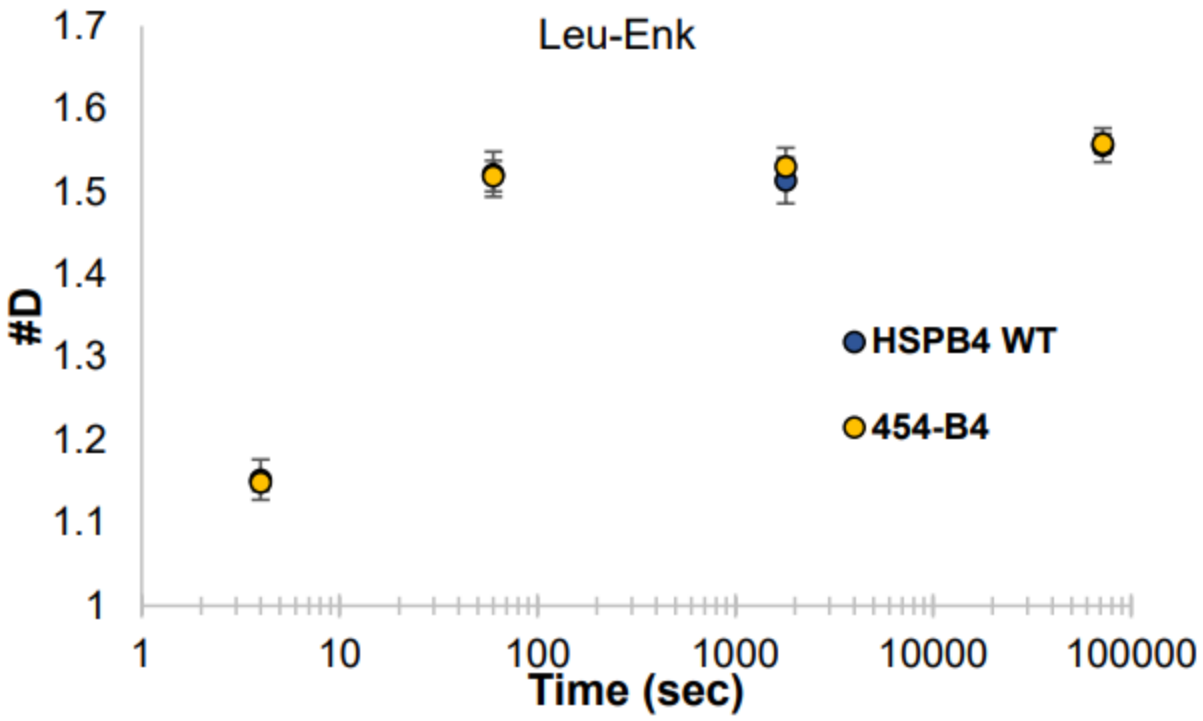

Figure 3.18. Deuteration of the Leucine-enkephalin pentapeptide internal exchange standard (YGGFL) for HSPB4 and 454-B4. The mean deuteration level (#D) and error (vertical bars; ± 1 standard deviation) are shown. N = 3-7

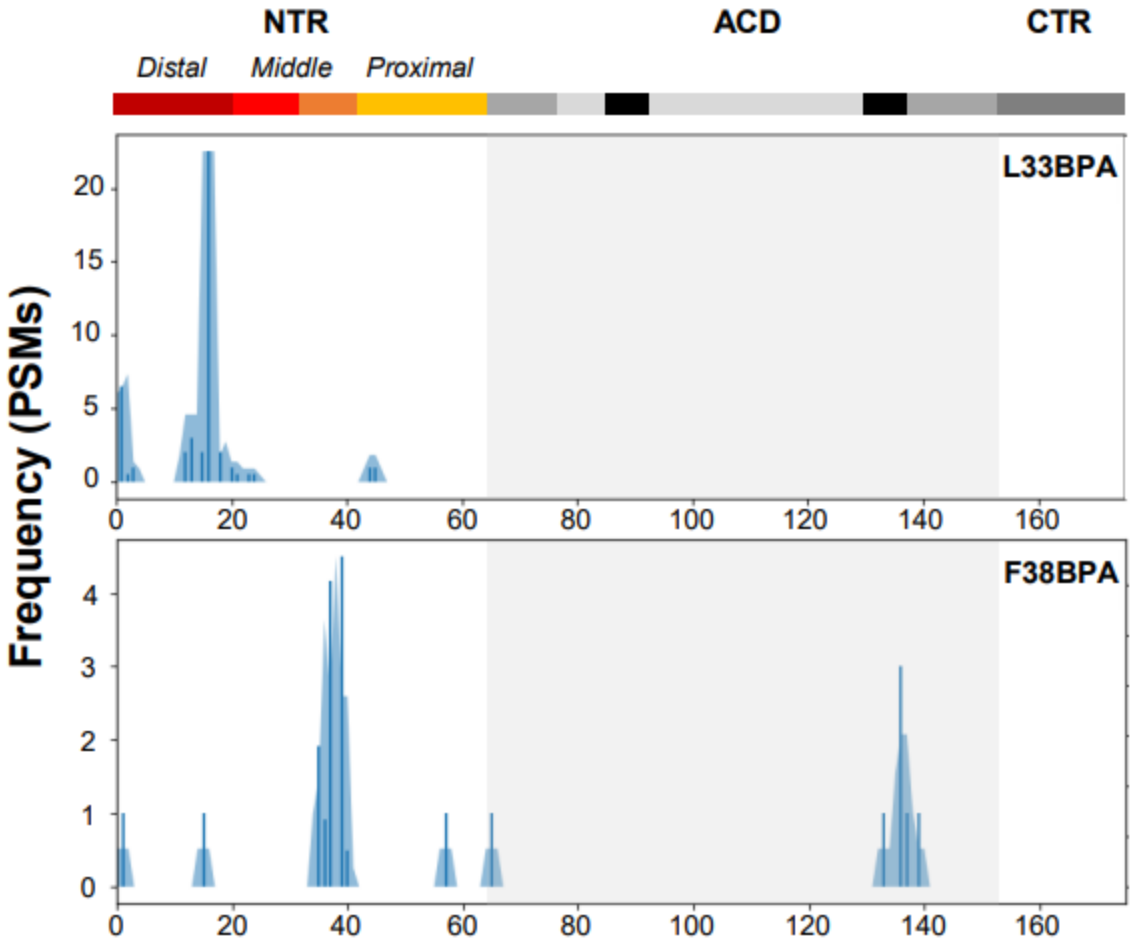

Figure 3.19. HSPB5 NTR Critical sequence interacts directly with other NTR sub-regions. BPA was individually installed at position 33 or 38 in the HSPB5 NTR Critical sequence using amber codon suppression. Positions cross-linked to by BPA (X-axis) installed at site 33 or 38 are shown as blue bars representing the number of peptide spectral matches (PSMs) identified in fragmentation mass spectrometry data, and blue shading shows the number of cross-links in a 3-residue sliding window. Domain boundaries are shown above the plots for the NTR (Distal sub-region: maroon, Middle NTR Conserved sequence: red, Middle NTR Critical sequence: orange, Proximal sub-region: gold), ACD (gray, with locations of the ACD edge groove in black and ACD central groove in light gray), and CTR (dark gray). Boundaries of the ACD are shown by the light gray inset. All plots are the result of MS identification in one cross-linking reaction.

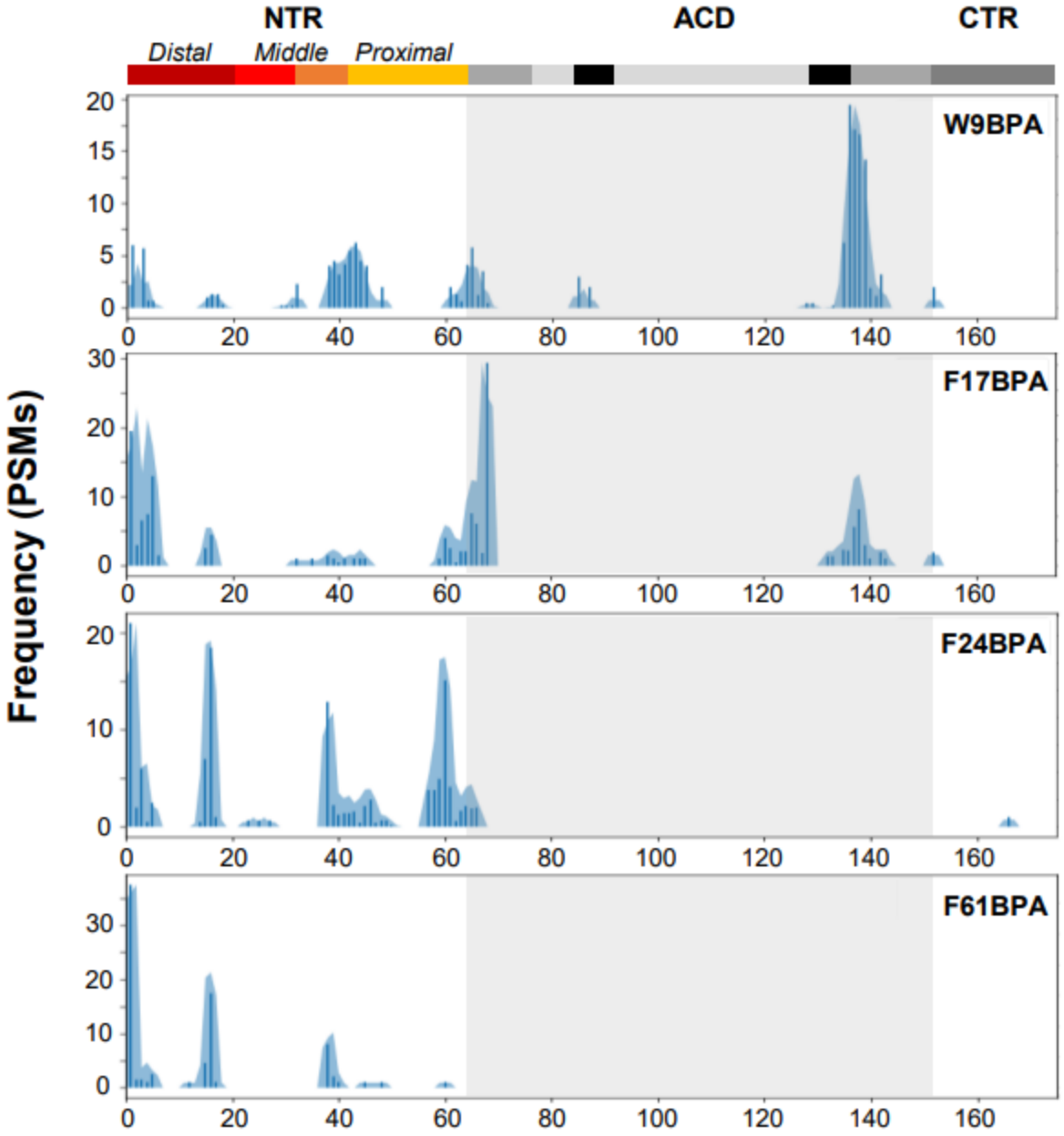

Figure 3.20. HSPB5 NTR interactions identified in BPA cross-linking experiments. BPA was individually installed at positions 9, 17, 24, or 61 in HSPB5 NTR using amber codon suppression. Positions cross-linked to by BPA (X-axis) are shown as blue bars representing the number of peptide spectral matches (PSMs) identified in fragmentation mass spectrometry data, and blue shading shows the number of cross-links in a 3-residue sliding window. Domain boundaries are shown above the plots for the NTR (Distal sub-region: maroon, Middle NTR Conserved sequence: red, Middle NTR Critical sequence: orange, Proximal sub-region: gold), ACD (gray, with locations of the ACD edge groove in black and ACD central groove in light gray), and CTR (dark gray). Boundaries of the ACD are shown by the light gray inset. All plots are the result of MS identification in one cross-linking reaction.

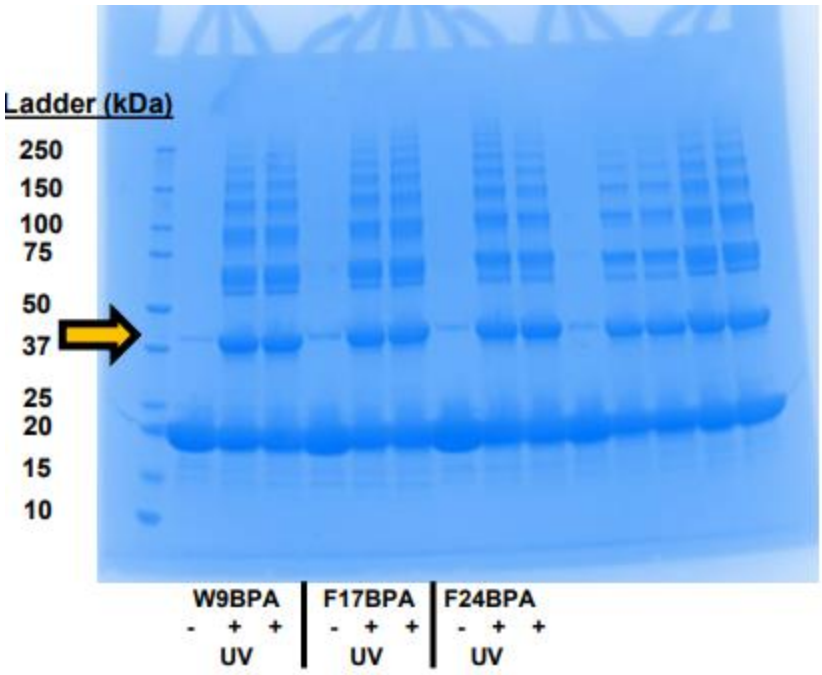

Figure 3.21. SDS-PAGE analysis of HSPB5 W9BPA, F17BPA, and F24BPA cross-linking reactions. Sample were run on a gradient 4-20% polyacrylamide gel (Bio-Rad). Samples exposed to UV light are marked with a + and unexposed samples are marked with a –. The band containing two HSPB5 protomers with a single intermolecular cross-link (identified by a gold arrow) was selected for in-gel digestion.

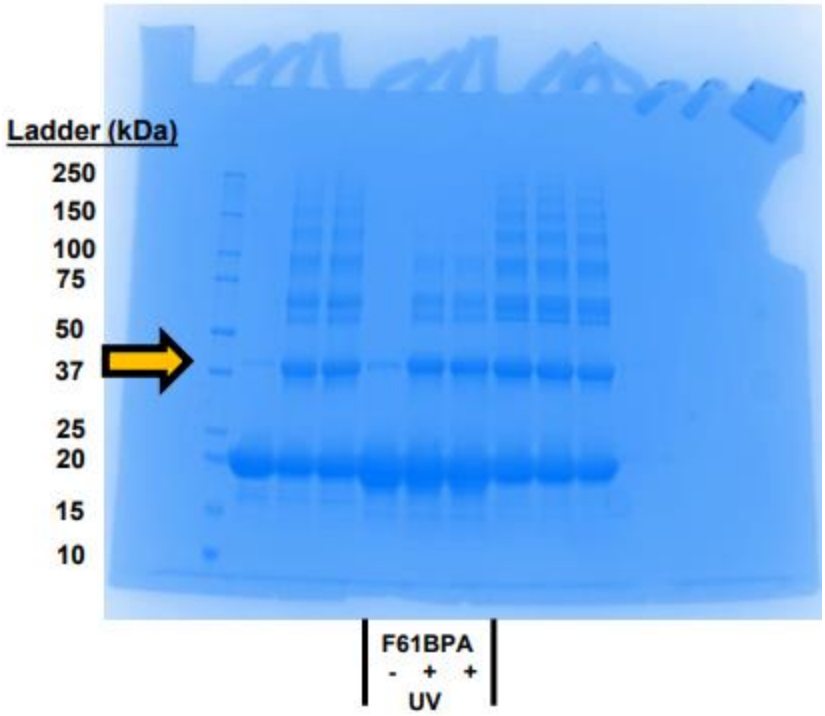

Figure 3.22. SDS-PAGE analysis of HSPB5 F61BPA cross-linking reactions. UV treated (+) and untreated (-) samples were run on a gradient 4-20% polyacrylamide gel (Bio-Rad). The band containing two HSPB5 protomers with a single intermolecular cross-link (identified by a gold arrow) was selected for in-gel digestion.

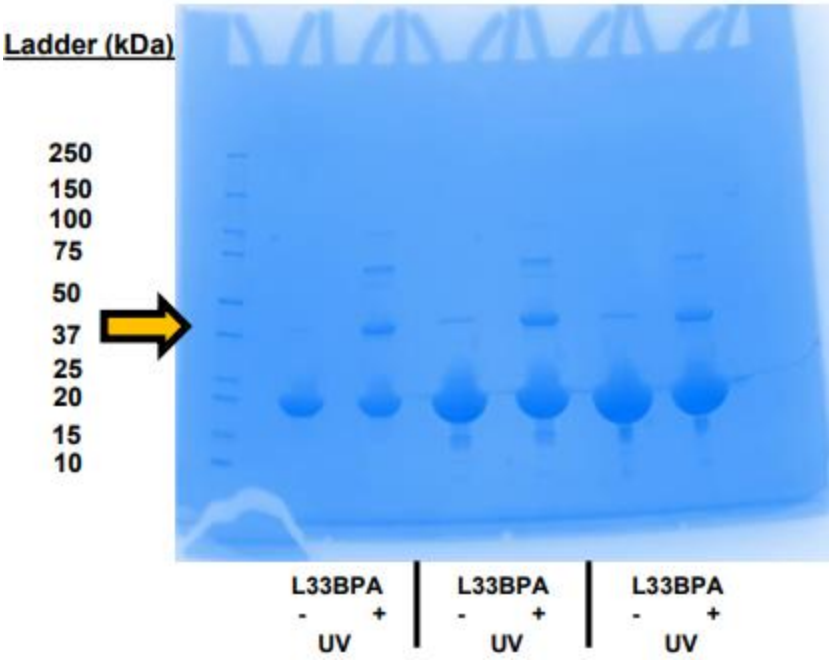

Figure 3.23. SDS-PAGE analysis of HSPB5 L33BPA cross-linking reactions. UV treated (+) and untreated (-) samples were run on a gradient 4-20% polyacrylamide gel (Bio-Rad). The band containing two HSPB5 protomers with a single intermolecular cross-link (identified by a gold arrow) was selected for in-gel digestion.

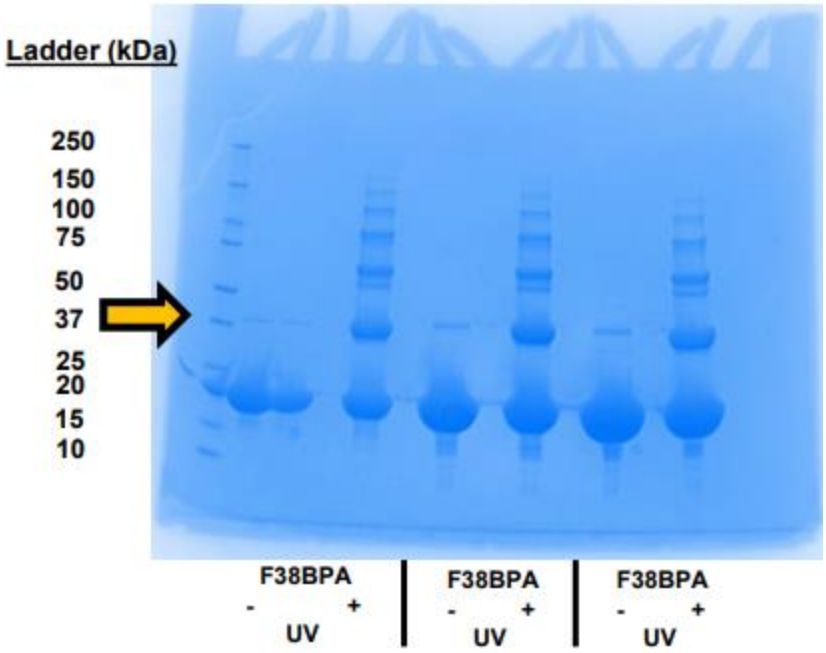

Figure 3.24. SDS-PAGE analysis of HSPB5 F38BPA cross-linking reactions. UV treated (+) and untreated (-) samples were run on a gradient 4-20% polyacrylamide gel (Bio-Rad). There was a loading error for the first untreated sample. The band containing two HSPB5 protomers with a single intermolecular cross-link (identified by a gold arrow) was selected for in-gel digestion.

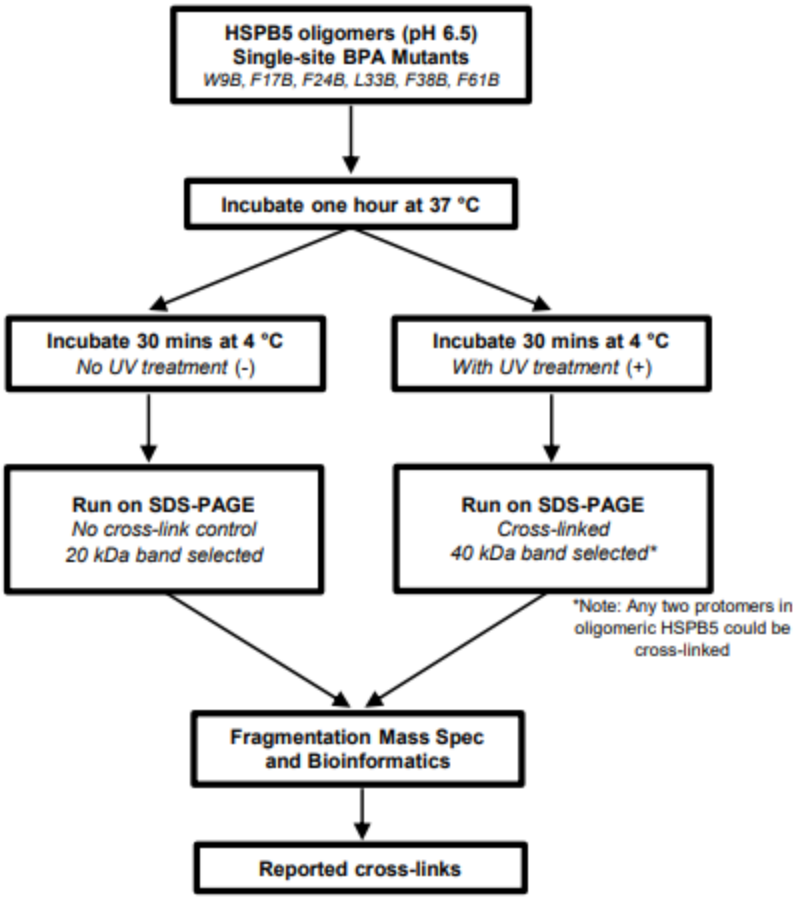

Figure 3.25. Workflow for HSPB5 BPA mutant cross-linking experiments and identification of cross-links.

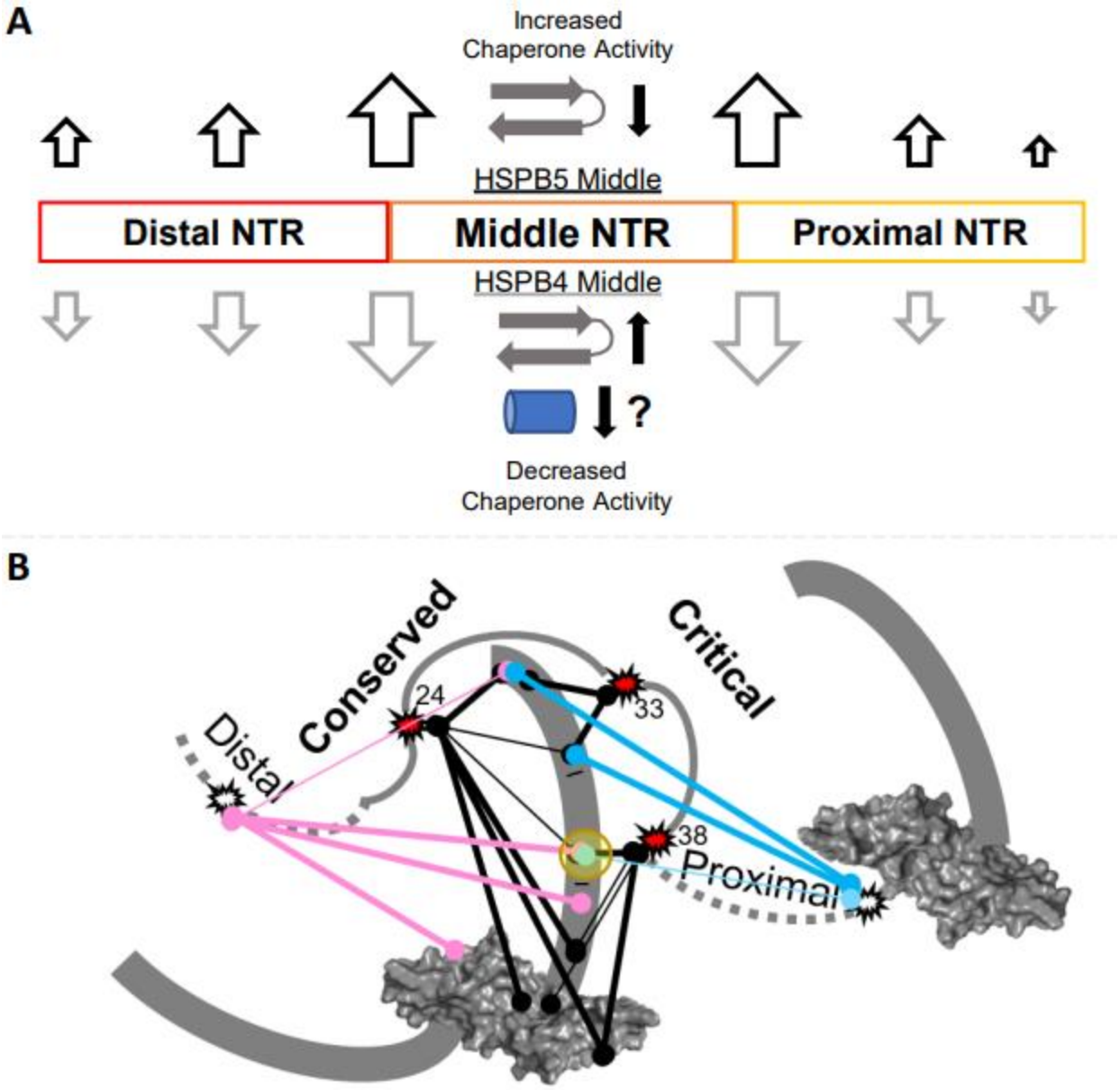

Figure 3.26. Summary of the effects of Middle NTR swaps in HSPB4 or HSPB5. A) Installation of HSPB5 Middle NTR in HSPB4 increases HDX throughout the NTR at short exchange time points (4 seconds, 1 minute, 30 minutes) and is associated with decreased β structure and increased chaperone activity (454-B4 vs. HSPB4). Installation of HSPB4 Middle NTR in HSPB5 decreases HDX throughout the NTR at short exchange time points (4 seconds, 1 minute, 30 minutes) and is associated with increased β structure and decreased chaperone activity (B5-GFY or 545-B5 vs. HSPB5). Experimental evidence for Middle NTR Conserved sequence α-helix formation in HSPB5 (Jehle et al., 2011) raises the possibility that the residue swaps affect helical propensity. B) Summary of BPA cross-links identified from sites 9, 17, 24, 33, 38, and 61 indicate the Critical sequence is a hub of NTR interactions.

BIBLIOGRAPHY

Andley UP, Hamilton PD, Ravi N, Weihl CC. 2011. A knock-in mouse model for the R120G mutation of αB-crystallin recapitulates human hereditary myopathy and cataracts. *PLoS ONE* **6**:e17671. doi:10.1371/journal.pone.0017671

Andley UP, Malone JP, Townsend RR. 2014. In vivo substrates of the lens molecular chaperones αA-crystallin and αB-crystallin. *PLoS ONE* **9**:e95507. doi:10.1371/journal.pone.0095507

Augusteyn RC. 2004. Dissociation is not required for a-crystallin's chaperone function. *Experimental Eye Research* doi:10.1016/j.exer.2004.08.010

Bagnéris C, Bateman OA, Naylor CE, Cronin N, Boelens WC, Keep NH, Slingsby C. 2009. Crystal structures of α-crystallin domain dimers of αB-crystallin and Hsp20. *The Journal of Molecular Biology* **392**:1242-1252. doi:10.1016/j.jmb.2009.07.069

Baldwin AJ, Lioe H, Hilton GR, Baker LA, Rubinstein JL, Kay LE, Benesch JLP. 2011. The polydispersity of αB-crystallin is rationalized by an interconverting polyhedral architecture. *Structure* **19**:1855–1863. doi:10.1016/j.str.2011.09.015

Bartelt-Kirbach B, Slowik A, Beyer C, Golenhofen N. 2017. Upregulation and phosphorylation of HspB1/Hsp25 and HspB5/αB-crystallin after transient middle cerebral artery occlusion in rats. *Cell Stress and Chaperones* **22**:653–663. doi:10.1007/s12192-017-0794-9

Bassnett S. 2002. Lens organelle degradation. *Experimental Eye Research* **74**:1-6. doi:10.1006/exer.2001.1111

Bassnett S. 2009. On the mechanism of organelle degradation in the vertebrate lens. *Experimental Eye Research* **88**:133–139. doi:10.1016/j.exer.2008.08.017

Bassnett S, Duncan G. 1985. Direct measurement of pH in the rat lens using ion-sensitive microelectrodes. *Experimental Eye Research* **40**:585-590. doi:10.1016/0014-4835(85)90080-6

Baughman HER, Clouser AF, Klevit RE, Nath A. 2018. HspB1 and Hsc70 chaperones engage distinct tau species and have different inhibitory effects on amyloid formation. *Journal of Biological Chemistry* **293**:2687–2700. doi:10.1074/jbc.M117.803411

Baughman HER, Pham T-HT, Adams CS, Nath A, Klevit RE. 2020. Release of a disordered domain enhances HspB1 chaperone activity toward tau. *PNAS* **117**(6):2923-2929. doi:10.1073/pnas.1915099117

Billman GE. 2020. Homeostasis: the underappreciated and far too often ignored central organizing principle of physiology. *Frontiers in Physiology* **11**:200. doi:10.3389/fphys.2020.00200

Bloemendal H, de Jong W, Jaenicke R, Lubsen NH, Slingsby C, Tardieu A. 2004. Ageing and vision: structure, stability and function of lens crystallins. *Progress in Biophysics and Molecular Biology* **86**:407-485. doi:10.1016/j.pbiomolbio.2003.11.012

Boatz JC, Whitley MJ, Li M, Gronenborn AM, van der Wel PCA. 2017. Cataract-associated P23T γD-crystallin retains a native-like fold in amorphous-looking aggregates formed at physiological pH. *Nature Communications* **8**:15137. doi:10.1038/ncomms15137

Bova MP, Mchaourab HS, Han Y, Fung BK-K. 2000. Subunit exchange of small heat shock proteins. *Journal of Biological Chemistry* **275**:1035–1042. doi:10.1074/jbc.275.2.1035

Bova MP, Yaron O, Huang Q, Ding L, Haley DA, Stewart PL, Horwitz J. 1999. Mutation R120G in αB-crystallin, which is linked to a desmin-related myopathy, results in an irregular structure and defective chaperone-like function. *PNAS* **96**:6137-6142.

Brodehl A, Gaertner-Rommel A, Klauke B, Grewe SA, Schirmer I, Peterschröder A, Faber L, Vorgerd M, Gummert J, Anselmetti D, Schulz U, Paluszkiewicz L, Milting H. 2017. The novel αB-crystallin (CRYAB) mutation p.D109G causes restrictive cardiomyopathy. *Human Mutation* **38**:947–952. doi:10.1002/humu.23248

Carra S, Alberti S, Arrigo PA, Benesch JL, Benjamin IJ, Boelens W, Bartelt-Kirbach B, Brundel BJJM, Buchner J, Bukau B, Carver JA, Ecroyd H, Emanuelsson C, Finet S, Golenhofen N, Goloubinoff P, Gusev N, Haslbeck M, Hightower LE, Kampinga HH, Klevit RE, Liberek K, Mchaourab HS, McMenimen KA, Poletti A, Quinlan R, Strelkov SV, Toth ME, Vierling E, Tanguay RM. 2017. The growing world of small heat shock proteins: from structure to functions. *Cell Stress and Chaperones* **22**:601–611. doi:10.1007/s12192-017-0787-8

Chan MP, Dolinska M, Sergeev YV, Wingfield PT, Hejtmancik JF. 2008. Association properties of βB1- and βA3-crystallins: ability to form heterotetramers. *Biochemistry* **47**:11062–11069. doi:10.1021/bi8012438

Chen J, Callis PR, King J. 2009. Mechanism of the Very Efficient Quenching of Tryptophan Fluorescence in Human γD- and γS-Crystallins: The γ-crystallin fold may have evolved to protect tryptophan residues from ultraviolet photodamage. *Biochemistry* **48**:3708–3716. doi:10.1021/bi802177g

Chen W, Smeekens JM, Wu R. 2016. Systematic study of the dynamics and half-lives of newly synthesized proteins in human cells. *Chemical Science* **7**:1393–1400. doi:10.1039/C5SC03826J

Chesler M. 2003. Regulation and modulation of pH in the brain. *Physiological Reviews* **83**:1183-1221. doi:10.1152/physrev.00010.2003

Chin JW, Martin AB, King DS, Wang L, Schultz PG. 2002. Addition of a photocrosslinking amino acid to the genetic code of Escherichia coli. *PNAS* **99:**11020-11024. doi:10.1073/pnas.172226299

Ciechanover A, Kwon YT. 2015. Degradation of misfolded proteins in neurodegenerative diseases: therapeutic targets and strategies. *Experimental & Molecular Medicine* **47**:e147. doi:10.1038/emm.2014.117

Clark AR, Egberts WV, Kondrat FDL, Hilton GR, Ray NJ, Cole AR, Carver JA, Benesch JLP, Keep NH, Boelens WC, Slingsby C. 2018. Terminal regions confer plasticity to the tetrameric assembly of human HspB2 and HspB3. *The Journal of Molecular Biology* **430**:3297-3310. doi:10.1016/j.jmb.2018.06.047

Clark AR, Lubsen NH, Slingsby C. 2012. sHSP in the eye lens: crystallin mutations, cataract and proteostasis. *The International Journal of Biochemistry & Cell Biology* **44**(10):1687-1697. doi:10.1016/j.biocel.2012.02.015

Clark AR, Naylor CE, Bagnéris C, Keep NH, Slingsby C. 2011. Crystal structure of R120G disease mutant of human αB-crystallin domain dimer shows closure of a groove. *Journal of Molecular Biology* **408**:118-134. doi:10.1016/j.jmb.2011.02.020

Clouser AF, Baughman HER, Basanta B, Guttman M, Nath A, Klevit RE. 2019. Interplay of disordered and ordered regions of a human small heat shock protein yields an ensemble of 'quasi-ordered' states. *eLife* **8**:e50259. doi: 10.7554/eLife.50259

Datskevich PN, Nefedova VV, Sudnitsyna MV, Gusev NB. 2012. Mutations of small heat shock proteins and human congenital diseases. *Biochemistry Moscow* **77**:1500–1514. doi:10.1134/S0006297912130081

Delaglio F, Grzesiek S, Vuister GW, Zhu G, Pfeifer J, Bax A. 1995. NMRPipe: a multidimensional spectral processing system based on UNIX pipes. *Journal of Biomolecular NMR* **6**:277–293. doi:10.1007/BF00197809

Delbecq SP, Jehle S, Klevit RE. 2012. Binding determinants of the small heat shock protein, αB-crystallin: recognition of the 'IxI' motif. *EMBO Journal* **31**:4587-4594. doi:10.1038/emboj.2012.318

Delbecq SP, Klevit RE. 2013. One size does not fit all: the oligomeric states of αB crystallin. *FEBS Letters* **587**:1073–1080. doi:10.1016/j.febslet.2013.01.021

Delbecq SP, Klevit RE. 2019. HSPB5 engages multiple states of a destabilized client to enhance chaperone activity in a stress-dependent manner. *Journal of Biological Chemistry* **294**:3261–3270. doi:10.1074/jbc.RA118.003156

Derham BK, Harding JJ. 2002. Effects of modifications of α-crystallin on its chaperone and other properties. *Biochemical Journal* **364**:711–717. doi:10.1042/bj20011512

Dimauro I, Antonioni A, Mercatelli N, Caporossi D. 2018. The role of αB-crystallin in skeletal and cardiac muscle tissues. *Cell Stress and Chaperones* **23**:491–505. doi:10.1007/s12192-017-0866-x

Dorman G, Prestwich GD. 1994. Benzophenone photophores in biochemistry. *Biochemistry* **33**:5661–5673. doi:10.1021/bi00185a001

Eng JK, Jahan TA, Hoopmann MR. 2013. Comet: an open-source MS/MS sequence database search tool. *Proteomics* **13**:22–24. doi:10.1002/pmic.201200439

Fichna JP, Potulska-Chromik A, Miszta P, Redowicz MJ, Kaminska AM, Zekanowski C. 2017. A novel dominant D109A CRYAB mutation in a family with myofibrillar myopathy affects αB-crystallin structure. *BBA Clinical* **7**:1-7. doi:10.1016/j.bbacli.2016.11.004

Fardeau M, Godet-Guillain J, Tome FMS, Collin H, Gaudeau S, Boffety C, Vernant P. 1978. Une nouvelle affection musculaire familiale, définie par l'accumulation intra-sarco-plasmique d'un matériel granulo-filamentaire dense en microscopie électronique. *Revue Neurologique* **134**:411-425.

Foster A. 2000. Vision 2020: the cataract challenge. *Community Eye Health Journal* **13**(34).

Ghahramani M, Yousefi R, Krivandin A, Muranov K, Kurganov B, Moosavi-Movahedi AA. 2020. Structural and functional characterization of D109H and R69C mutant versions of human αB-crystallin: The biochemical pathomechanism underlying cataract and myopathy development. *International Journal of Biological Macromolecules* **146**:1142-1160. doi:10.1016/j.ijbiomac.2019.09.239

Ghosh JG, Clark JI. 2005. Insights into the domains required for dimerization and assembly of human αB crystallin. *Protein Science* **14**:684–695. doi:10.1110/ps.041152805

Goloubinoff P. 2016. Mechanisms of protein homeostasis in health, aging and disease. *Swiss Medical Weekly*. doi:10.4414/smw.2016.14306

Guttman M, Weis DD, Engen JR, Lee KK. 2013. Analysis of overlapped and noisy hydrogen/deuterium exchange mass spectra. *Journal of the American Society for Mass Spectrometry* **24**:1906–1912. doi:10.1007/s13361-013-0727-5

Haslbeck M, Weinkauf S, Buchner J. 2019. Small heat shock proteins: simplicity meets complexity. *Journal of Biological Chemistry* **294**:2121–2132. doi:10.1074/jbc.REV118.002809

Hashemi H, Pakzad R, Yekta A, Aghamirsalim M, Pakbin M, Ramin S, Khabazkhoob M. 2020. Global and regional prevalence of age-related cataract: a comprehensive systematic review and meta-analysis. *Eye* **34**:1357–1370. doi:10.1038/s41433-020-0806-3

Hochberg GKA, Benesch JLP. 2014. Dynamical structure of αB-crystallin. *Progress in Biophysics and Molecular Biology* **115**:11-20. doi:10.1016/j.pbiomolbio.2014.03.003

Hochberg GKA, Ecroyd H, Liu C, Cox D, Cascio D, Sawaya MR, Collier MP, Stroud J, Carver JA, Baldwin AJ, Robinson CV, Eisenberg DS, Benesch JLP, Laganowsky A. 2014. The structured core domain of αB-crystallin can prevent amyloid fibrillation and associated toxicity. *PNAS* E1562-E1570. doi:10.1073/pnas.1322673111

Hoopmann MR, Zelter A, Johnson RS, Riffle M, MacCoss MJ, Davis TN, Moritz RL. 2015. Kojak: efficient analysis of chemically cross-linked protein complexes. *The Journal of Proteome Research* **14**:2190–2198. doi:10.1021/pr501321h

Horwitz J. 1992. α-Crystallin can function as a molecular chaperone. *PNAS* **89**:10449-10453.

Horwitz J, Bova MP, Ding L-L, Haley DA, Stewart PL. 1999. Lens a-crystallin: function and structure. *Eye* **13**:403-408.

Huang Q, Ding L, Phan KB, Cheng C, Xia C, Gong X, Horwitz J. 2009. Mechanism of cataract formation in αA-crystallin Y118D mutation. *Investigative Ophthalmology & Visual Science* **50**:2919. doi:10.1167/iovs.08-3070

Ingolia TD, Craig EA. 1982. Four small Drosophila heat shock proteins are related to each other and to mammalian α-crystallin. *PNAS* **79**:2360-2364.

Janowska MK, Baughman HER, Woods CN, Klevit RE. 2019. Mechanisms of small heat shock proteins. *Cold Spring Harbor Perspectives in Biology* **11**:a034025. doi:10.1101/cshperspect.a034025

Jehle S, van Rossum B, Stout JR, Noguchi SM, Falber K, Rehbein K, Oschkinat H, Klevit RE, Rajagopal P. 2009. αB-Crystallin: a hybrid solid-state/solution-state NMR investigation reveals structural aspects of the heterogeneous oligomer. *Journal of Molecular Biology* **385**:1481–1497. doi:10.1016/j.jmb.2008.10.097

Jehle S, Vollmar BS, Bardiaux B, Dove KK, Rajagopal P, Gonen T, Oschkinat H, Klevit RE. 2011. N-terminal domain of αB-crystallin provides a conformational switch for multimerization and structural heterogeneity. *PNAS* **108**:6409–6414. doi:10.1073/pnas.1014656108

Jiaox X, Khan SY, Irum B, Khan AO, Wang Q, Kabir F, Khan AA, Husnain T, Akram J, Riazuddin S, Hejtmancik JF, Riazuddin SA. 2015. Missense mutations in CRYAB are liable for recessive congenital cataracts. *PLoS ONE* **10**:e0137973. doi:10.1371/journal.pone.0137973

Johnson, B. A. (n.d.). Using NMRView to visualize and analyze the NMR spectra of macromolecules. In Protein NMR Techniques (pp. 313–352). *Humana Press* https://doi.org/10.1385/1-59259-809-9:313

Jolly C. 2000. Role of the heat shock response and molecular chaperones in oncogenesis and cell death. *Journal of the National Cancer Institute* **92**:1564–1572. doi:10.1093/jnci/92.19.1564

Kaiser CJO, Peters C, Schmid PWN, Stavropoulou M, Zou J, Dahiya V, Mymrikov EV, Rockel B, Asami S, Haslbeck M, Rappsilber J, Reif B, Zacharias M, Buchner J, Weinkauf S. 2019. The structure and oxidation of the eye lens chaperone αA-crystallin. *Nature Structural and Molecular Biology* **26**:1141–1150. doi:10.1038/s41594-019-0332-9

Kato K, Shinohara H, Goto S, Inaguma Y, Morishita R, Asano T. 1992. Copurification of small heat shock protein with αB crystallin from human skeletal muscle. *Journal of Biological Chemistry* **267**(11):7718-7725. doi:10.1016/S0021-9258(18)42574-4

Keller A, Nesvizhskii AI, Kolker E, Aebersold R. 2002. Empirical statistical model to estimate the accuracy of peptide identifications made by MS/MS and database search. *Analytical Chemistry* **74**:5383–5392. doi:10.1021/ac025747h

Klevit RE. 2020. Peeking from behind the veil of enigma: emerging insights on small heat shock protein structure and function. *Cell Stress and Chaperones* **25**:573–580. doi:10.1007/s12192-020-01092-2

Koteiche HA, Mchaourab HS. 2006. Mechanism of a hereditary cataract phenotype: mutations in αA-crystallin activate substrate binding. *Journal of Biological Chemistry* **281**:14273-14279. doi:10.1074/jbc.M512938200

Kumar LVS, Rao CM. 2000. Domain swapping in human alpha A and alpha B crystallins affects oligomerization and enhances chaperone-like activity. *Journal of Biological Chemistry* **275**(29):22009-22013. doi: 10.1074/jbc.M003307200

Lamark T, Johansen T. 2012. Aggrephagy: selective disposal of protein aggregates by macroautophagy. *International Journal of Cell Biology* **2012**:1–21. doi:10.1155/2012/736905

Lampi KJ, Wilmarth PA, Murray MR, David LL. 2014. Lens β-crystallins: The role of deamidation and related modifications in aging and cataract. *Progress in Biophysics and Molecular Biology* **115**:21–31. doi:10.1016/j.pbiomolbio.2014.02.004

Leem CH, Lagadic-Gossmann D, Vaughan-Jones RD. 1999. Characterization of intracellular pH regulation in the guinea-pig ventricular myocyte. *The Journal of Physiology* **517**:159–180. doi:10.1111/j.1469-7793.1999.0159z.x

Li H, Yu Y, Ruan M, Jiao F, Chen H, Gao J, Weng Y, Bao Y. 2022. The mechanism for thermal-enhanced chaperone-like activity of α-crystallin against UV irradiation-induced aggregation of γD-crystallin. *Biophysical Journal* **121**:2233-2250. doi:10.1016/j.bpj.2022.05.032

Liang JJ, Liu B-F. 2006. Fluorescence resonance energy transfer study of subunit exchange in human lens crystallins and congenital cataract crystallin mutants. *Protein Science* **15**:1619–1627. doi:10.1110/ps.062216006

Lynnerup N, Kjeldsen H, Heegaard S, Jacobsen C, Heinemeier J. 2008. Radiocarbon dating of the human eye lens crystallines reveal proteins without carbon turnover throughout life. *PLoS ONE* **3**:e1529. doi:10.1371/journal.pone.0001529

Ma Y, Hendershot LM. 2004. ER chaperone functions during normal and stress conditions. *Journal of Chemical Neuroanatomy* **28**:51–65. doi:10.1016/j.jchemneu.2003.08.007

MacCoss MJ, McDonald WH, Saraf A, Sadygov R, Clark JM, Tasto JJ, Gould KL, Wolters D, Washburn M, Weiss A, Clark JI, Yates JR. 2002. Shotgun identification of protein modifications from protein complexes and lens tissue. *PNAS* **99**(12):7900–7905. doi:10.1073/pnas.122231399

Maciejewski MW, Schuyler AD, Gryk MR, Moraru II, Romero PR, Ulrich EL, Eghbalnia HR, Livny M, Delaglio F, Hoch JC. 2017. NMRbox: a resource for biomolecular NMR computation. *Biophysical Journal* **112**:1529-1534. doi:10.1016/j.bpj.2017.03.011

Mainz A, Peschek J, Stavropoulou M, Back KC, Bardiaux B, Asami S, Prade E, Peters C, Weinkauf S, Buchner J, Reif B. 2015. The chaperone αB-crystallin uses different interfaces to capture an amorphous and an amyloid client. *Nature Structural and Molecular Biology* **22**:898–905. doi:10.1038/nsmb.3108

Masson GR, Burke JE, Ahn NG, Anand GS, Borchers C, Brier S, Bou-Assaf GM, Engen JR, Englander SW, Faber J, Garlish R, Griffin PR, Gross ML, Guttman M, Hamuro Y, Heck AJR, Houde D, Iacob RE, Jørgensen TJD, Kaltashov IA, Klinman JP, Konermann L, Man P, Mayne L, Pascal BD, Reichmann D, Skehel M, Snijder J, Strutzenberg TS, Underbakke ES, Wagner C, Wales TE, Walters BT, Weis DD, Wilson DJ, Wintrode PL, Zhang Z, Zheng J, Schriemer DC, Rand KD. 2019. Recommendations for performing, interpreting and reporting hydrogen deuterium exchange mass spectrometry (HDX-MS) experiments. *Nature Methods* **16**:595–602. doi:10.1038/s41592-019-0459-y

Mathias RT, Riquelme G, Rae JL. 1991. Cell to cell communication and pH in the frog lens. *Journal of General Physiology* **98**: 1085-1103. doi:10.1085/jgp.98.6.1085

Michiel M, Duprat E, Skouri-Panet F, Lampi JA, Tardieu A, Lampi KJ, Finet S. 2010. Aggregation of deamidated human βB2-crystallin and incomplete rescue by α-crystallin chaperone. *Experimental Eye Research* **90**:688–698. doi:10.1016/j.exer.2010.02.007

Mishra S, Wu S-Y, Fuller AW, Wang Z, Rose KL, Schey KL, Mchaourab HS. 2018. Loss of αB-crystallin function in zebrafish reveals critical roles in the development of the lens and stress resistance of the heart. *Journal of Biological Chemistry* **293**:740–753. doi:10.1074/jbc.M117.808634

Moran SD, Zhang TO, Decatur SM, Zanni MT. 2013. Amyloid fiber formation in human γD-crystallin induced by UV–B photodamage. *Biochemistry* **52**:6169–6181. doi:10.1021/bi4008353

Moreau KL, King JA. 2012. Cataract-causing defect of a mutant γ-crystallin proceeds through an aggregation pathway which bypasses recognition by the α-crystallin chaperone. *PLoS ONE* **7**:e37256. doi:10.1371/journal.pone.0037256

Moreau KL, King JA. 2012b. Protein misfolding and aggregation in cataract disease and prospects for prevention. *Trends in Molecular Medicine* **18**:273–282. doi:10.1016/j.molmed.2012.03.005

Mühlhofer M, Peters C, Kriehuber T, Kreuzeder M, Kazman P, Rodina N, Reif B, Haslbeck M, Weinkauf S, Buchner J. 2021. Phosphorylation activates the yeast small heat shock protein Hsp26 by weakening domain contacts in the oligomer ensemble. *Nature Communications* **12**:6697. doi:10.1038/s41467-021-27036-7

Muranova LK, Strelkov SV, Gusev NB. 2020. Effect of cataract-associated mutations in the N-terminal domain of αB-crystallin (HspB5). *Experimental Eye Research* **197**. doi:10.1016/j.exer.2020.108091

Muranov KO, Poliansky NB, Chebotareva NA, Kleimenov SYu, Bugrova AE, Indeykina MI, Kononikhin AS, Nikolaev EN, Ostrovsky MA. 2019. The mechanism of the interaction of α-crystallin and UV-damaged βL-crystallin. *International Journal of Biological Macromolecules* **140**:736-748. doi:10.1016/j.ijbiomac.2019.08.178

Mymrikov EV, Riedl M, Peters C, Weinkauf S, Haslbeck M, Buchner J. 2020. Regulation of small heat-shock proteins by hetero-oligomer formation. *Journal of Biological Chemistry* **295**:158–169. doi:10.1074/jbc.RA119.011143

Mymrikov EV, Seit-Nebi AS, Gusev NB. 2012. Heterooligomeric complexes of human small heat shock proteins. *Cell Stress and Chaperones* **17**:157–169. doi:10.1007/s12192-011-0296-0

Pande A, Pande J, Asherie N, Lomakin A, Ogun O, King J, Benedek GB. 2001. Crystal cataracts: human genetic cataract caused by protein crystallization. *PNAS* **98**:6116–6120. doi:10.1073/pnas.101124798

Pedersen JT, Heegaard NHH. 2013. Analysis of protein aggregation in neurodegenerative disease. *Analytical Chemistry* **85**:4215–4227. doi:10.1021/ac400023c

Perez-Riverol Y, Csordas A, Bai J, Bernal-Llinares M, Hewapathirana S, Kundu DJ, Inuganti A, Griss J, Mayer G, Eisenacher M, Pérez E, Uszkoreit J, Pfeuffer J, Sachsenberg T, Yılmaz Ş, Tiwary S, Cox J, Audain E, Walzer M, Jarnuczak AF, Ternent T, Brazma A, Vizcaíno JA. 2019. The PRIDE database and related tools and resources in 2019: improving support for quantification data. *Nucleic Acids Research* **47**:D442–D450. doi:10.1093/nar/gky1106

Perng MD, Wen SF, van den Ijssel P, Prescott AR, Quinlan RA. 2004. Desmin aggregate formation by R120G αB-crystallin is caused by altered filament interactions and is dependent upon network status in cells. *Molecular Biology of the Cell* **15**:2335-2346. doi:10.1091/mbc.e03-12-0893

Peschek J, Braun N, Franzmann TM, Georgalis Y, Haslbeck M, Weinkauf S, Buchner J. 2009. The eye lens chaperone α-crystallin forms defined globular assemblies. *PNAS* **106**:13272–13277. doi:10.1073/pnas.0902651106

Peschek J, Braun N, Rohrberg J, Back KC, Kriehuber T, Kastenmüller A, Weinkauf S, Buchner J. 2013. Regulated structural transitions unleash the chaperone activity of αB-crystallin. *PNAS* **110**:E3780-E3789. doi:10.1073/pnas.1308898110

Preis W, Bestehorn A, Buchner J, Haslbeck M. 2017. An alternative splice variant of human αA-crystallin modulates the oligomer ensemble and the chaperone activity of α-crystallins. *Cell Stress and Chaperones* **22**:541–552. doi:10.1007/s12192-017-0772-2

Price JC, Guan S, Burlingame A, Prusiner SB, Ghaemmaghami S. 2010. Analysis of proteome dynamics in the mouse brain. *PNAS* **107**:14508–14513. doi:10.1073/pnas.1006551107

Rajagopal P, Tse E, Borst AJ, Delbecq SP, Shi L, Southworth DR, Klevit RE. 2015a. A conserved histidine modulates HSPB5 structure to trigger chaperone activity in response to stress-related acidosis. *eLife* **4**:e07304. doi:10.7554/eLife.07304

Rajagopal P, Liu Y, Shi L, Clouser AF, Klevit RE. 2015b. Structure of the α-crystallin domain from the redox-sensitive chaperone, HSPB1. *Journal of Biomolecular NMR* **63**:223–228. doi:10.1007/s10858-015-9973-0

Reinle K, Mogk A, Bukau B. 2022. The diverse functions of small heat shock proteins in the proteostasis network. *Journal of Molecular Biology* **434**:167157. doi:10.1016/j.jmb.2021.167157

Rosenzweig R, Nillegoda NB, Mayer MP, Bukau B. 2019. The Hsp70 chaperone network. *Nature Reviews Molecular Cell Biology* **20**:665–680. doi:10.1038/s41580-019-0133-3

Sacconi S, Féasson L, Antoine JC, Pécheux C, Bernard R, Cobo AM, Casarin A, Salviati L, Desnuelle C, Urtizberea A. 2012. A novel CRYAB mutation resulting in multisystemic disease. *Neuromuscular Disorders* **22**:66-72. doi:10.1016/j.nmd.2011.07.004

Scheidt T, Carozza JA, Kolbe CC, Aprile FA, Tkachenko O, Bellaiche MMJ, Meisl G, Peter QAE, Herling TW, Ness S, Castellana-Cruz M, Benesch JLP, Vendruscolo M, Dobson CM, Arosio P, Knowles TPJ. 2021. The binding of the small heat-shock protein αB-crystallin to fibrils of α-synuclein is driven by entropic forces. *PNAS* **118**(38). doi:10.1073/pnas.2108790118

Schmid PWN, Lim NCH, Peters C, Back KC, Bourgeois B, Pirolt F, Richter B, Peschek J, Puk O, Amarie OV, Dalke C, Haslbeck M, Weinkauf S, Madl T, Graw J, Buchner J. 2021. Imbalances in the eye lens proteome are linked to cataract formation. *Nature Structural and Molecular Biology* **28**:143–151. doi:10.1038/s41594-020-00543-9

Selivanova OM, Galzitskaya OV. 2020. Structural and functional peculiarities of α-crystallin. *Biology* **9**:85. doi:10.3390/biology9040085

Serebryany E, King JA. 2014. The βγ-crystallins: Native state stability and pathways to aggregation. *Progress in Biophysics and Molecular Biology* **115**:32–41. doi:10.1016/j.pbiomolbio.2014.05.002

Serebryany E, Takata T, Erickson E, Schafheimer N, Wang Y, King JA. 2016. Aggregation of Trp > Glu point mutants of human gamma-D crystallin provides a model for hereditary or UV-induced cataract. *Protein Science* **25**:1115–1128. doi:10.1002/pro.2924

Serebryany E, Yu S, Trauger SA, Budnik B, Shakhnovich EI. 2018. Dynamic disulfide exchange in a crystallin protein in the human eye lens promotes cataract-associated aggregation. *Journal of Biological Chemistry* **293**:17997–18009. doi:10.1074/jbc.RA118.004551

Shiels A, Hejtmancik JF. 2019. Biology of inherited cataracts and opportunities for treatment. *Annual Review of Vision Science* **5**:123–149. doi:10.1146/annurev-vision-091517-034346

Slingsby C, Wistow GJ, Clark AR. 2013. Evolution of crystallins for a role in the vertebrate eye lens. *Protein Science* **22**:367–380. doi:10.1002/pro.2229

Sluchanko NN, Beelen S, Kulikova AA, Weeks SD, Antson AA, Gusev NB, Strelkov SV. 2017. Structural basis for the interaction of a human small heat shock protein with the 14-3-3 universal signaling regulator. *Structure* **25**:305-316. doi:10.1016/j.str.2016.12.005

Sprague-Piercy MA, Wong E, Roskamp KW, Fakhoury JN, Freites JA, Tobias DJ, Martin RW. 2020. Human αB-crystallin discriminates between aggregation-prone and function-preserving variants of a client protein. *BBA General Subjects* doi:10.1016/j.bbagen.2019.129502

Srivastava OP, Srivastava K, Chaves JM, Gill AK. 2017. Post-translationally modified human lens crystallin fragments show aggregation in vitro. *Biochemistry and Biophysics Reports* **10**:94-131. doi:10.1016/j.bbrep.2017.01.011

Street D, Bangsbo J, Juel C. 2001. Interstitial pH in human skeletal muscle during and after dynamic graded exercise. *The Journal of Physiology* **537.3**:993-998.

Su S, Liu P, Zhang H, Li Z, Song Z, Zhang L, Chen S. 2011. Proteomic analysis of human age-related nuclear cataracts and normal lens nuclei. *Investigative Ophthalmology & Visual Science* **52**:4182. doi:10.1167/iovs.10-7094

Takalo M, Salminen A, Soininen H, Hiltunen M, Haapasalo A. 2013. Protein aggregation and degradation mechanisms in neurodegenerative diseases. *American Journal of Neurodegenerative Disease* **2**(1):1-14.

Takemoto L, Sorensen CM. 2008. Protein–protein interactions and lens transparency. *Experimental Eye Research* **87**:496–501. doi:10.1016/j.exer.2008.08.018

Treweek TM, Rekas A, Lindner RA, Walker MJ, Aquilina JA, Robinson CV, Horwitz J, Der Perng M, Quinlan RA, Carver JA. 2005. R120G αB-crystallin promotes the unfolding of reduced α-lactalbumin and is inherently unstable. *The FEBS Journal* **272**:711–724. doi:10.1111/j.1742-4658.2004.04507.x

Tsiatsiani L, Akeroyd M, Olsthoorn M, Heck AJR. 2017. *Aspergillus niger* Prolyl endoprotease for hydrogen–deuterium exchange mass spectrometry and protein structural studies. *Analytical Chemistry* **89**:7966–7973. doi:10.1021/acs.analchem.7b01161

Ueda Y, Duncan MK, David LL. 2002. Lens proteomics: the accumulation of crystallin modifications in the mouse lens with age. *Investigative Ophthalmology & Visual Science* **43**(1):205-214

Ungelenk S, Moayed F, Ho C-T, Grousl T, Scharf A, Mashaghi A, Tans S, Mayer MP, Mogk A, Bukau B. 2016. Small heat shock proteins sequester misfolding proteins in near-native conformation for cellular protection and efficient refolding. *Nature Communications* **7**:13673. doi:10.1038/ncomms13673

Vérétout F, Tardieu A. 1989. The protein concentration gradient within eye lens might originate from constant osmotic pressure coupled to differential interactive properties of crystallins. *European Biophysics Journal* **17**:61–68. doi:10.1007/BF00257103

Vicart P, Caron A, Guicheney P, Li Z, Prévost M-C, Faure A, Chateau D, Chapon F, Tomé F, Dupret J-M, Paulin D, Fardeau M. 1998. A missense mutation in the αB-crystallin chaperone gene causes a desmin-related myopathy. *Nature Genetics* **20**:92–95. doi:10.1038/1765

Voth W, Jakob U. 2017. Stress-activated chaperones: a first line of defense. *Trends in Biochemical Sciences* **42**:899–913. doi:10.1016/j.tibs.2017.08.006

Wang X, Osinska H, Klevitsky R, Gerdes AM, Nieman M, Lorenz J, Hewett T, Robbins J. 2001. Expression of R120G–αB-crystallin causes aberrant desmin and αB-crystallin aggregation and cardiomyopathy in mice. *Circulation Research* **89**:84-91. doi:10.1161/hh1301.092688

Watson MJ, Harkewicz R, Hodge EA, Vorauer C, Palmer J, Lee KK, Guttman M. 2021. Simple platform for automating decoupled LC–MS analysis of hydrogen/deuterium exchange samples. *Journal of the American Society for Mass Spectrometry* **32**:597–600. doi:10.1021/jasms.0c00341

Webster JM, Darling AL, Uversky VN, Blair LJ. 2019. Small heat shock proteins, big impact on protein aggregation in neurodegenerative disease. *Frontiers in Pharmacology* **10**:1047. doi:10.3389/fphar.2019.01047

Weinreb O, van Boekel MAM, Dovrat A, Bloemendal H. 2000. Effect of UV-A light on the chaperone-like properties of young and old lens α-crystallin. *Investigative Ophthalmology & Visual Science* **41**(1):191-198.

Wistow G. 2012. The human crystallin gene families. *Human Genomics* **6**:26. doi:10.1186/1479-7364-6-26

Woods CN, Ulmer LD, Janowska MK, Stone NL, James EI, Guttman M, Bush MF, Klevit RE. 2022. HSPB5 disease-associated mutations have long-range effects on structure and dynamics through networks of quasi-ordered interactions. *BioRxiv [preprint]*. Accessed July 18, 2022.

Wu S-Y, Zou P, Mishra S, Mchaourab HS. 2018. Transgenic zebrafish models reveal distinct molecular mechanisms for cataract-linked αA-crystallin mutants. *PLoS ONE* **13**:e0207540. doi:10.1371/journal.pone.0207540

Zantema A, Verlaan-De Vries M, Maasdam D, Bol S, van der Eb A. 1992. Heat shock protein 27 and alpha B-crystallin can form a complex, which dissociates by heat shock. *Journal of Biological Chemistry* **267**:12936–12941. doi:10.1016/S0021-9258(18)42364-2

Żwirowski S, Kłosowska A, Obuchowski I, Nillegoda NB, Piróg A, Ziętkiewicz S, Bukau B, Mogk A, Liberek K. 2017. Hsp70 displaces small heat shock proteins from aggregates to initiate protein refolding. *EMBO Journal* **36**:783–796. doi:10.15252/embj.201593378

VITA

EDUCATION:

B.S. Biochemistry & Biology: Biomedical Science Concentration
University of Wisconsin – La Crosse, La Crosse, WI 2015

Ph.D. Biochemistry
University of Washington, Seattle, WA 2022

PUBLICATIONS:

Woods CN, Ulmer LD, Bush MF, Guttman M, Klevit RE. 2022. α-crystallin N-terminal region encodes chaperone activity against the lens client γD-crystallin [in preparation]

Woods, CN, Ulmer LD, Janowska MK, Stone NL, James EI, Guttman M, Bush MF, Klevit RE. 2022. HSPB5 disease-associated mutations have long-range effects on structure and dynamics through networks of quasi-ordered interactions [under review, eLife]

Serebryany E, Chowdhury S, **Woods CN**, Thorn DC, Watson NE, McClelland AA, Klevit RE, Shakhnovich EI. 2022. A native chemical chaperone in the human eye lens. *eLife* https://doi.org/10.7554/eLife.76923

Janowska MK, Baughman HER, **Woods CN**, Klevit RE. 2019. Mechanisms of small heat shock proteins. *Cold Spring Harbor Perspectives in Biology* **11**(10). DOI:10.1101/cshperspect.a034025

Wimmer MR, **Woods CN**, Adamczak KJ, Glasgow EM, Novak WRP, Grilley DP, Weaver TM. 2015. Sequential unfolding of the hemolysin two-partner secretion domain from *Proteus mirabilis*. *Protein Science*, **24**(11):1841-1855. DOI: 10.1002/pro.27

PRESENTATIONS:

Poster, Cold Spring Harbor Labs: Protein Homeostasis in Health & Disease (Virtual) 2020

Poster and Flash Talk, Gordon Research Conference of Stress Proteins in Growth, Development and Disease 2019

Poster, 31st Annual Protein Society 2017

Poster, 19th Annual Meeting – ASBMB 2015

Poster, Seven Rivers Undergraduate Research Symposium 2014